ELECTRICAL RESISTIVITY OF SILVER FOILS

UNDER SHOCK-WAVE COMPRESSION

Jerry J. Dick

WSU SDL 74-01

February 1974

ELECTRICAL RESISTIVITY OF SILVER FOILS

UNDER SHOCK-WAVE COMPRESSION

ABSTRACT

Resistance changes in silver foils were monitored during uniaxial shock compression. Foils of 15 to 25 micrometers thickness were subjected to pressures of 25 to 120 kilobars. Calculations based on the Debye model of a solid generate a reference curve of isothermal resistivity versus hydrostatic pressure which, when a single parameter is adjusted, agrees with the 0 to 30 kilobars Bridgman results. The shock isothermal resistivity is significantly higher than the hydrostatic value for the same pressure; deviation is attributed to resistivity of lattice imperfections generated by the plastic deformation associated with uniaxial shock compression. The amount of deviation of the resistivity depends on initial purity of the silver. The deviation may also have a slight dependence on state of anneal of the foil. Lattice defect concentrations deduced from the resistivity deviations increase as the three-halves power of strain. Using published values for resistivity per vacancy in silver, computed vacancy concentrations at 100 kilobars are about 10^{-3}. A dislocation model for defect

production in shock deformation is reviewed. A particular
model involving stress relaxation is introduced to explain the
observed effect of specimen purity on shock-induced resistivity
change.

TABLE OF CONTENTS

LIST OF TABLES

LIST OF ILLUSTRATIONS

I. INTRODUCTION

A traditional good way of studying material behavior is
to monitor some material property while varying a thermodynamic
parameter, such as temperature or pressure, and compare results
to theoretical predictions. Temperature is varied more often
than pressure because it is easier to modify and control, while
electrical resistivity is a material property often studied
since it is relatively easy to measure.

Measurements of resistance of crystalline materials as
a function of pressure can tell us something about properties
of the ideal lattice and of the lattice imperfection. Changes
in the ideal lattice which will affect resistivity include
changes in electron band structure and changes in electron
coupling with the lattice vibration spectrum; theory exists for
comparison with experimental results (Paul, 1963; Bridgman,
1952). Changes in number and types of imperfections will affect
electron scattering and hence resistivity. Lattice imperfection
changes are often monitored by precise measurement of resistiv-
ity changes of materials which have been rapidly quenched from
temperatures near the melting point while maintaining the system
at a high hydrostatic pressure. Activation volume of formation,
identifying the dominant type of defect present, and equilibrium
concentrations of vacant lattice sites (vacancies) as a function
of pressure are obtained (Emrick, 1972; Emrick and McArdle,

1969; Huebener, 1965). We see then that measuring resistivity while varying pressure is important to understanding material behavior.

Effects of material history on resistance changes due to transient high pressure generated by shock waves have been noted but there has been no systematic attempt to compare results with static high pressure results or to theory so that properties of lattice defects under dynamic pressure might be studied. Dynamic data are expected to be different from static data due to generation of lattice imperfections by plastic deformation by uniaxial shock compression. In a truly hydrostatic compression of an isotropic solid there is no plastic deformation, only a change in lattice parameter. Evidence for the defect generation in shock experiments on metals is found in a number of metallurgical and annealing studies which have been done on metals which have been shocked for a short duration and relieved back to atmospheric pressure (Kressel and Brown, 1968; Mahajan, 1970; van Wely, 1968). While many of the defects generated by the shock wave will have annihilated or migrated out before examination, these studies indicate some of the effects of different shock strengths and initial conditions on the point and line imperfection densities and configurations generated. The generation of these imperfections will affect resistance changes observed in a shocked metal.

Shock-induced resistance changes have been measured for copper, iron, nickel, and ytterbium, as well as manganin alloy (Ginsberg and Grady, 1972; Styris and Duvall, 1970). Fractional

resistance change for a given pressure level is generally greater for shock compression than for hydrostatic compression. Agreement among results of different experimenters is not good. Material history has been shown to be important but few attempts have been made to do experiments on well-characterized material. Good experiments require good shock-impedance match between metal and anvil, geometry that assures uniaxial compression, elimination of perturbations by electrical leads, and well-characterized initial condition of the metal. In addition, careful analysis is necessary to subtract out the thermal effects occurring in shock compression so that comparison can be made to hydrostatic experiments and theories.

In the present experiments, electrical resistance changes in silver foils were monitored during uniaxial compression by shock waves; foils were 15 to 25 micrometers thick. Electrical resistance of silver under hydrostatic compression has been measured by Bridgman (1952), but no previous studies on silver resistance under shock compression have been published.

Pressure levels in the silver ranging from 25 to 120 kilobars (1 bar = 1 atmosphere) were generated by high-velocity impact; shock duration was 0.5 microseconds. The voltage drop across the foil due to 150 amperes of current was monitored during this time. In several cases, foil fragments were recovered after the experiment and examined by microscopy and isothermal annealing studies.

The present work also involved several types of analysis. Using a Debye model of a solid, a method was developed for

computing isothermal resistivity as a function of volume. When
a single parameter is adjusted to experimental results, the com-
putation agrees closely with the experiments of Bridgman to
30 kbar. This method was also used to correct shock resistivity
data to isothermal conditions. The deviation between isothermal
data from uniaxial shock compression and calculated hydrostatic
results is attributed to the resistivity of lattice imperfec-
tions generated by plastic deformation in the shock wave. A
speculative model was developed to explain the high lattice
defect concentration found and its dependence on silver purity.

The purpose of this paper is to present experimental
results on shock resistivity of silver foils, to put the iso-
thermal analysis on a firm footing, to consider all possible
effects on the resistivity, and to establish the credibility of
the shock-generated defect concentrations deduced.

Presentation will begin with description of experimental
design and procedure. Then analyses needed to reduce acquired
data to meaningful forms are described. Results of the experi-
ments and data reduction are presented next, along with dis-
cussion of the physical content of the data. Finally, conclu-
sions and recommendations are presented.

In summary, by careful experimental design and sample
preparation, accurate, reproducible resistance measurements
during shock compression were accomplished. Shock isothermal
resistivity is found to be significantly higher than hydrostatic
resistivity at a given pressure. The deviation is attributed
to resistivity of point defects generated by uniaxial shock

compression. These results give the first quantitative indi-
cations of defect concentrations generated during shock com-
pression, and confirm what was qualitatively expected from
previous work. The results show higher defects concentrations
for more pure silver. The two shots on unannealed, cold-rolled
foil indicate a shock-induced defect concentration slightly
higher than that in annealed silver of the same purity.

II.   EXPERIMENTAL PLAN AND PROCEDURE

Design of the experiment to measure resistance changes
in metals due to shock compression involved (1) choice of a
particular metal for study, (2) developing a configuration of
impactor and target to ensure uniaxial compression of the metal,
(3) choosing a recording system for monitoring the resistance
changes, and (4) developing a specimen preparation sequence
which produced uniform, well-characterized samples.

A.   Choice of Material

In terms of doing a basic study of resistivity of a
metal under dynamic pressure, one wishes to choose a metal which
typifies metallic behavior and in as many ways as possible be-
haves according to simple theories.

Two requisites then were that it have no phase transi-
tions in the pressure range to be studied, and that it be
available in high purity. Another requisite is that the
experimental static pressure response of its resistivity should
behave at least qualitatively according to the predictions of a
Debye-Mott model (Mott, 1934) for changes due to compression in
the electron scattering by lattice vibrations. Preferably the
resistivity change under pressure should be large for ease in
accurate data gathering.

One might initially think that alkali metals would be
prime candidates. Aside from the fact that they are not easily

obtained and handled in high purity, they in general do not follow the Debye-Mott model. This may be understood as follows: Fermi surfaces of the alkali metals at room conditions are more or less spherical, but as pressure is applied the Fermi surfaces distort from spherical shape and at some volume make contact with the Brillouin zone faces. This distortion of the Fermi surface due to compression results in additional electron scattering, countering the decrease in scattering by lattice vibrations. On the other hand, Fermi surfaces of noble metals are already distorted and touching the Brillouin zone faces at room conditions. Thus while compression does cause more distortion of the Fermi surface, there is not such a drastic change in electron scattering as in the case of alkali metals. One might then expect that resistivity changes due to changes in scattering cross-section of lattice vibrations might dominate in noble metals under pressure. Then one might hope to understand any deviations of shock data from static data from the standpoint of simple models. Hence, the choice was narrowed to the noble metals, available in high purity, following Debye-Mott theory under static pressure and quite resistant to surface oxidation. Silver was chosen because it has a Debye temperature well below room temperature, simplifying many calculations, and there exists a readily available anvil material, Al_2O_3, with mechanical shock impedance U_s/V_o (U_s is shock wave speed and V_o is initial specific volume) close to that of silver; the silver foil will be sandwiched between two discs of the anvil material during the impact experiment.

B. Constraints on Experimental Configuration

Reliable shock resistance experiments require that resistance changes under shock compression result in accurately measurable voltage changes as recorded on oscilloscopes. For the bandwidth necessary for these experiments, the voltage sensitivity limit of oscilloscopes is typically one millivolt per division. That this limit is physical may be understood from the formula for thermal voltage noise,

$$\overline{E^2} = 4Rk_BT(f_2 - f_1)$$

where $f_2 - f_1$ is the frequency band width, R is circuit impedance, T is absolute temperature, and k_B is Boltzmann's constant. For R = 50 Ω, $f_2 - f_1 = 10^9$ Hz, T = 300°K, we find E_{rms} = 0.03 milli-volts. Since artifact voltage signals of the order of one millivolt are not unusual in shock experiments of the type considered here, it is desirable that the expected signal be at least 100 millivolts.

For experiments to be characterized by one-dimensional compression, the specimen should be in the form of a foil about 100 times wider than it is thick. Anomalous resistance changes due to two-dimensional deformation at the foil lateral edges will then be small compared to the total resistance change. Such effects arise when the foil edges are adjacent to a layer of material such as epoxy which reaches stress equilibrium with the anvil pieces more slowly than the specimen.

Since room temperature resistivity, ρ, of silver is 1.6 $\mu\Omega$cm, achieving the desired voltage levels will require high current I, long sample length L, and small sample cross-section A; i.e., $E = I \rho L/A$. Values for these experiments were

typically 154 amperes, 1.27 cm, and 4.1×10^{-4} cm^2, respectively, so that the resistance $R_o = 5$ mΩ and $E_o = 0.76$ volts. The change in voltage under shock compression is given by $\Delta E = I \, \Delta(\rho \frac{L}{A})$ and in these experiments turned out to be as much as 20% of E_o.

Current density in the experiments was as high as 0.4×10^5 A/cm^2; this is still below the 10^6 A/cm^2 at which Bridgman (1921) observed non-ohmic effects in noble metal foils. To avoid ohmic heating of the specimen, current was supplied in pulses of 50 microsecond duration.

We want to measure bulk properties in the shock experiments so foils should not be so thin that a significant part of electron scattering is by the foil surfaces. Electron mean free path in silver at room temperature is 0.05 μm, less than 1/300 of the foil thickness. Consequently, surface scattering of electrons at room temperature will be an insignificant fraction of the total scattering, and the resistivity measured will be a bulk property. At 4.2°K, however, the mean free path will be 7 to 21 μm and surface scattering will be very important. Fuchs-Sondheimer theory would imply that surface scattering accounts for 20 to 35% of the resistivity at that temperature (Sondheimer, 1952).

The thin foils cannot be impacted directly but must be sandwiched in a suitable anvil material. The foil will not reach the final pressure state by a single shock but by shock-wave reverberations traversing it and being partially reflected at the foil-anvil interfaces. For simplicity, it is desirable

to reach the final state in as few wave transits as possible so that deviation from the state reached by a single shock to the final state is small. This requires that the shock impedance U_s/V_o be nearly the same in foil and anvil; in these experiments the silver foils were placed between synthetic sapphire (Al_2O_3 single crystal) anvils. The longitudinal elastic stress limit in uniaxial shock compression (Hugoniot elastic limit) in sapphire is about 120 kbar for the orientations used, placing an upper limit on pressures in these experiments, in order to avoid complications due to yielding and double waves in sapphire.

The high currents in the foil couple inductively with a moving metal plate. To avoid such induced voltages in the foil, it is necessary to use non-conducting impactors. Impactors chosen were fused quartz and sapphire. Both are good insulators and have well-characterized shock response.

C. Impact Arrangement

High pressures for the experiments are generated by high-velocity impact (Fowles, 1972). Figure 1 represents schematically the experimental configuration. The 4-inch diameter projectile is shown emerging from the launching tube. The non-metallic impactor, clamped to the projectile face is also shown. The aluminum projectile shoulder strikes a series of accurately spaced, electrically charged pins, shorting each in turn. The shorting signals from these pins are monitored in time on an oscilloscope, providing a measurement of velocity.
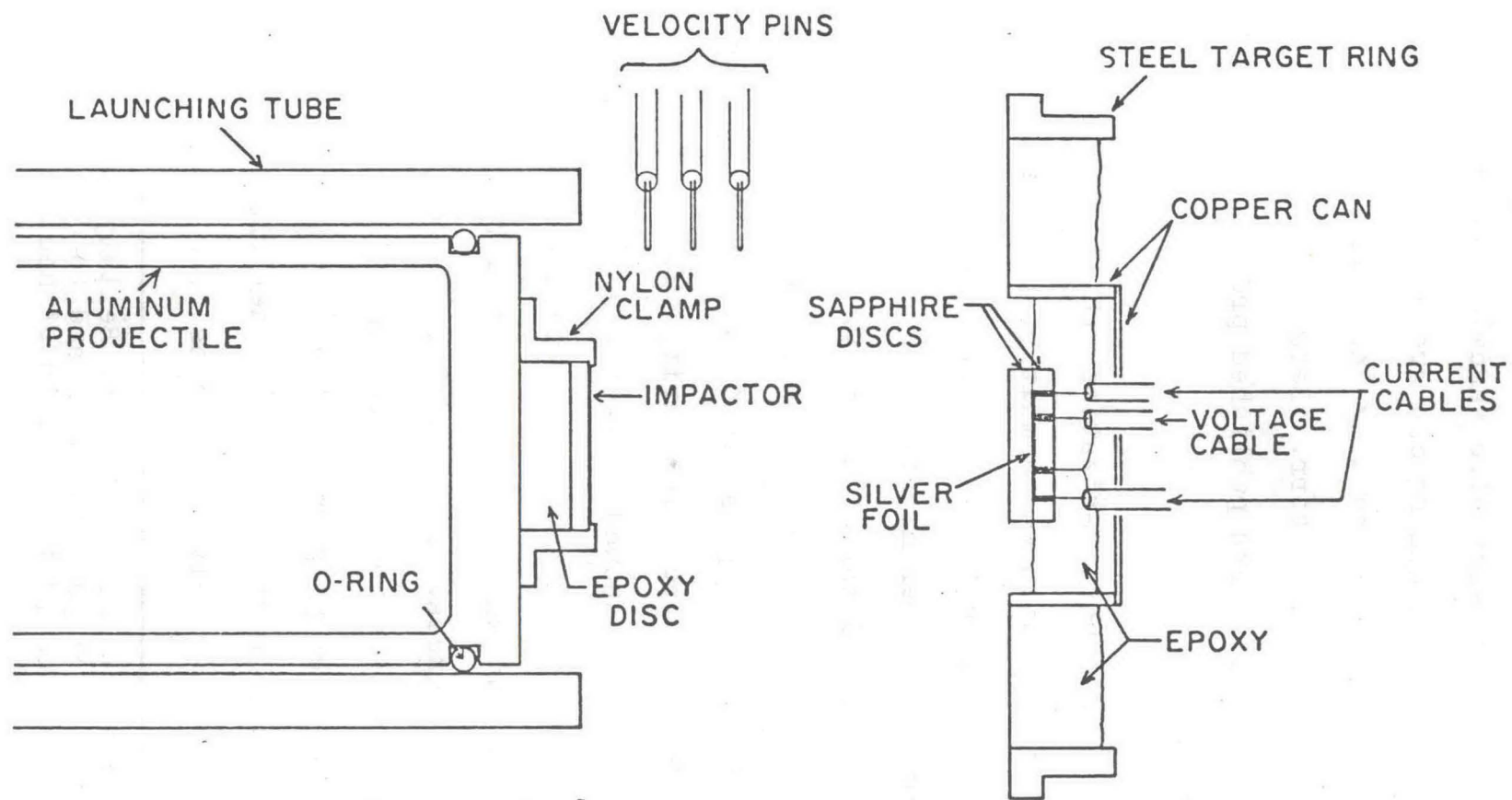
Fig. 1. Schematic diagram of impact configuration showing impactor and target assemblies.

Shorting of one of these pins is also used to trigger the current supply to the foil before impact. The target assembly consisting of the silver-sapphire sandwich, current and voltage cables and the copper shielding can are held in the target ring with epoxy plastic. Sample housing and launching tube volumes are evacuated to about 10^{-3} torr. Details of the projectile launching facility have been published previously (Fowles et al., 1970).[1]

D. Sample Characterization and Preparation

Sample preparation was a multistep process involving mechanical polishing, cutting to desired shape, thickness measurement, microscope examination, annealing, resistance ratio measurements, and target assembly.

The silver foils used in the initial experiments came from Material Research Corporation (MRC). They were cold-rolled into 2.5 cm wide strip from high purity (5N) silver stock. Microscope examination showed surface ridges and valleys due to the rolling process. Since valley to peak variation was about 5 μm on each side, it was necessary to polish the 25 μm foils to about 15 μm thickness. Additional cold-rolled foils (specified as 3N purity) were obtained from The Wilkinson Company (W3N). After specimen preparation the W3N silver purity as measured by residual resistance was higher than the MRC silver purity. The W3N, as received, surfaces were much smoother than

those of the MRC foils and required much less polishing; final
thickness after polishing was about 24 μm. Electro-deposited
silver foils from Goodfellow Metals Ltd. were also prepared.
However, density and resistance measurements showed portions of
the material to be as much as 30% porous. Shock resistance
experiments were not performed on this material.

Mean grain size of Wilkinson foils was about 35 μm,
whereas that of the Materials Research Corporation foils was
about 75 μm. Orientation of crystallites in cold-rolled metal
foils is not random; in silver the preferred orientation is with
(110) planes parallel to the rolling plane and the [1$\bar{1}$2]
direction parallel to the rolling direction (Barrett and
Massalski, 1966).

To polish the foils, a technique was needed to hold the
foil piece flat and rigid during polishing. The technique
developed was to bond the foil to a quartz glass plate with
phenyl salicylate. These glass plates, 6.3 cm in diameter,
were first bonded to aluminum plugs with Duco cement. Then the
plugs with attached plates were heated on a hot plate to 45° to
50°C. The phenyl salicylate was then placed on the glass where
it melted. Taking care to avoid dust particles, the piece of
silver foil, 2.5 cm by 5 cm, was laid on the plate. A Mylar
plastic sheet, a glass plate, and a brass plug weighing 700 grams
were placed in that order on the foil. The assembly was then
cooled to room temperature allowing the phenyl salicylate to
recrystallize. The Mylar sheet was next peeled off and excess
phenyl salicylate was scraped away.

Polishing was done on a Struers Company polishing wheel at 250 rpm; the plug was hand-held. The polishing sequence involved (1) 5 to 8 minutes using 3 μm alumina abrasive on billard cloth with distilled water as carrier; (2) about 2 minutes using 0.05 μm alumina on Microcloth (Buehler Ltd.). All parts were washed with detergent when switching abrasive grit size. Cloths were charged with abrasive by making a paste of distilled water and 2 to 3 heaping tablespoons of abrasive powder in a watch glass. This was then applied to the wet cloth with a finger. Care was taken to remove excess moisture from the cloth. After a polish was finished the foil was rinsed with distilled water and swabbed with cotton balls soaked in distilled water. It was then rinsed with ethanol and dried stain-free in a stream of warm air. The foil was removed by remelting the phenyl salicylate and then turned over; the polishing sequence was repeated on the second surface.

After both surfaces were polished, the foil was ready for cutting to the desired specimen shape and size (see Fig. 2a). A photo-etching technique was used to cut two specimens from each polished foil. The technique is reasonably simple to use and gives foils of accurate and reproducible dimensions. The technique is as follows: (1) the foil is coated with photo-resist solution and dried; (2) a negative template is placed over the foil and then the foil is irradiated with ultraviolet light (this sensitizes all photo-resist except that under the template); and (3) foil is placed in the photo-etch solution where chemical reaction erodes the parts of the
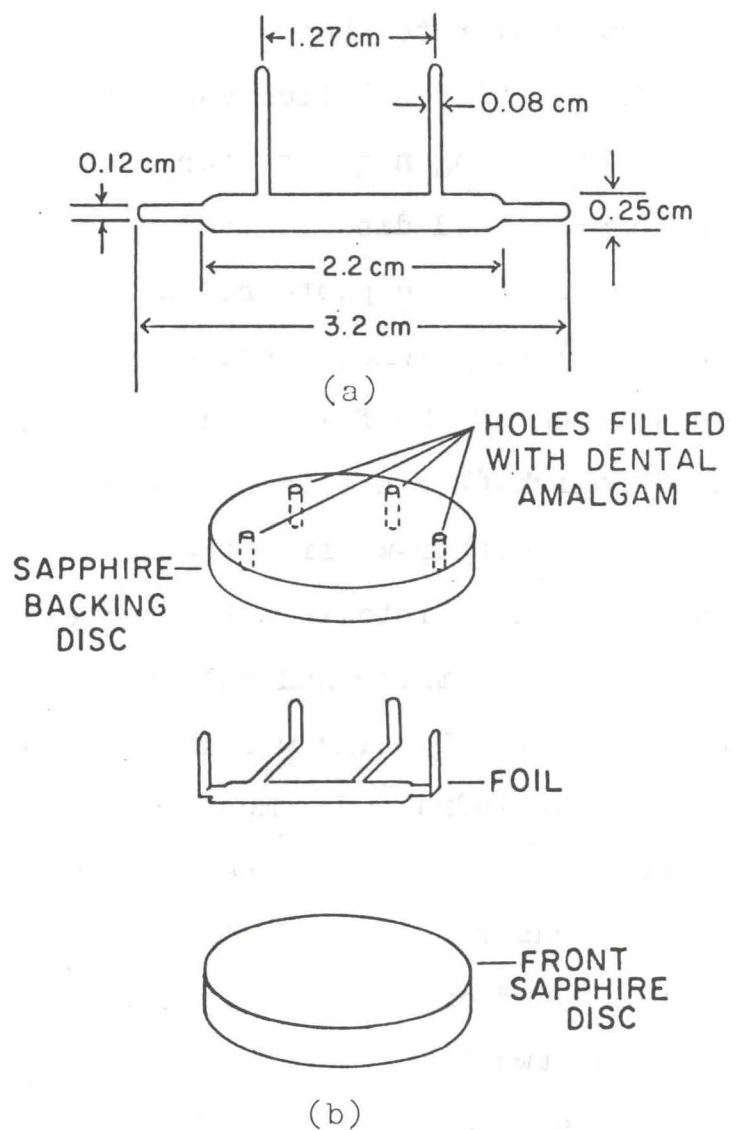
Fig. 2. Details of foil-anvil sandwich.
(a) Foil dimensions. (b) Sandwich, exploded view.

foil under the sensitized photo-resist, leaving the remaining foil in the template shape. The template was a Kodalith negative on an Estar base made by a 6:1 photo-reduction of a drawing. Shipley Company type AZ-111 photo-resist solution, AZ-303 developer, and a ferric nitrate photo-etch solution were used for silver. The photo-resist solution was first filtered by using over-pressure of nitrogen gas to force it through a Buchner funnel with a fritted disc of medium porosity. The silver foils were dipped in the photo-resist solution after being cleaned in trichlorethylene, acetone, and ethanol. (In order to enhance wetting of the foil, each foil was given a light chromic acid polish (Levinstein and Robinson, 1962) before dipping.) The foil was withdrawn from the solution at a rate of 3 to 10 inches per minute into air at a temperature of 70° to 90°C; a one-rpm electric motor and pulley arrangement was used for lifting the foil. Heating was accomplished by using two red-domed, 250-watt, infra-red lamps under a tent of aluminum foil. The foil was left in the warm air for 5 minutes for drying. Exposure was for 8 to 22 minutes by a 0.22 ampere, 115 VAC blacklight about 3 cm above the foil, half the time spent over each of the two templates. The foil lay on a black cloth; the templates were kept flat by a quartz glass plate (weighted with lead blocks) over the templates and foil. A 1:4 volume mixture of AZ-303 developer and distilled water developed the sensitized photo-resist coating in 2 to 3 minutes; solution temperature was about 30°C. For etching, the foil was floated on the etch solution by surface tension. The ferric nitrate

solution, 90 g of $FeNO_3$ in 100 cm^3 of distilled water, at 45°C, accomplished photo-etching in a few minutes while the solution was stirred constantly to remove gas bubbles from the reacting surface. After washing the cut specimen in distilled water, the photo-resist coating was dissolved with acetone.

Foil thickness was then measured mechanically using gage blocks and an electronic, dial depth gage. Typically a total of five measurements were made at various spots on the foil; thickness variation was ± 4%. Average thickness measured in this way agreed within 3% with the thickness calculated from measured resistance of the foil and handbook values for the silver resistivity. A repeat of several thickness measurements reproduced the average thickness within 2% or better.

Cut foils were examined and photographed under a microscope. Faint scratches from the polishing were usually visible at 100X magnification. Spots of tarnish and some areas where ridges due to rolling were still visible were noted; occasionally spots about 25 μm in diameter were visible where apparently a dust speck had allowed the photo-etch solution to start eroding the foil body. But overall, the foil surfaces were smooth and relatively stain-free.

Annealing of cut foils was accomplished at 800 ± 15°K for one to two hours in a vacuum better than 10^{-5} torr. Cooling took place at less than 100°K per hour. The anneal gives specimens a known thermal history and increases the crystal lattice perfection.

A measure of crystal perfection is specimen resistance at 4.2°K; at liquid helium temperature lattice vibrations are of such low amplitude that electron scattering is predominantly due to lattice imperfections, impurity atoms, and foil surfaces. Surfaces come into play since electron mean free path in silver at 4.2°K is a substantial fraction of foil thickness. Hence, a correction is necessary to get bulk resistance (Sec. II.E). Resistance across specimen potential leads was measured at room temperature, liquid nitrogen temperature, and at liquid helium temperature using 2 amperes of current and measuring the potential drop with a Keithley 148 Nanovoltmeter. Foil leads were clamped between copper blocks. Current reversal was used to nullify any thermal emf's. A total of four readings were taken at each temperature.

As mentioned previously, the W3N silver specimen purity, as measured by residual resistance, was higher than the MRC silver purity. Spectrographic analyses of foils which had been through the preparation sequence were consistent with this result. The spectrographic analyses also indicated that foil surfaces were probably contaminated by Al_2O_3 particles acquired during the polishing sequence.

Before assembling the silver-sapphire sandwich each foil was weighed, and foil width and distance between potential leads were measured. Weighing provides a very rough density check, providing a relative quality check among the foils used. Finally, short 28 gage silver wire leads were spot welded to the ends of the foil leads for ease of handling during assembly.

Starting with shot 73-040, the spot welds were augmented with a drop of silver paint.

E. Target Assembly

Target assembly involved bonding the silver specimen between sapphire anvil plates, potting the sandwich into a target holding ring, attaching electrical coaxial cables, and providing electrical shielding for the sample. Synthetic sapphire (single crystal Al_2O_3) discs 3.8 cm in diameter and 0.3 cm thick were purchased from Adolph Mellor Company. According to the supplier, the perpendiculars to the disc faces were oriented 50 to 90 degrees from the c-axis of the single crystals. Sapphire is hexagonal structure so that one might expect that shock-wave propagation would be anisotropic and mixed-mode. But it has been determined experimentally that shock waves propagate isotropically and in a pure longitudinal mode with an experimental error of ± 1% (Graham and Ingram, 1968). This is consistent with the experimental result that the elastic constants c_{11} and c_{33} happen to be of equal magnitude; its elastic response is symmetrical as a result.

The sapphire disc faces were parallel to within 2 to 10 μm. Faces were flat to within about 3 μm as observed with an optical flat and monochromatic light. As a check, the density of each sapphire disc was determined from weight measurements in air and water; the average value was 3.985 ± 0.005 g/cm^3. The backing piece had four 0.16 cm diameter holes for foil leads (Fig. 2b).

Assembly involved wetting all pieces (sapphire and foil) with vacuum-outgassed epoxy (Shell Epon Resin 815). Foil leads were bent over the edges of a glass microscope slide and then pulled through the holes in the sapphire backing piece. The slide was then removed, and the front sapphire disc placed over the foil. This assembly was placed on a flat plate and screw pressure applied to a small, Mylar-faced, aluminum block placed on the sapphire backing piece. Lead holes were cleaned of epoxy using toothpicks soaked in acetone. After two hours or more, the holes were filled with dental amalgam, which provided a better shock impedance match than epoxy for silver and sapphire. The sandwich was inspected after curing to verify that the foil lay flat and that there were no air bubbles near it. The assembled thickness of the sandwich was typically less than 3 μm thicker than the total thickness of the individual pieces. In 17 assemblies, the average increase in thickness was -0.5 ± 2.5 μm. The uncertainty is indicative of the accuracy of micrometer measurements. The sandwich was then potted inside a copper ring which in turn had been potted into a target holding-ring (Fig. 1). Next, a layer of aluminum was vacuum deposited on the target; this was done to provide a reflecting surface for optical alignment of the target on the end of the launching tube and to complete the electrical shielding with the copper ring and lid. Cables (RG-223/U) were attached and potted in place. Length of unshielded conductor from the plane of the foil to the coaxial cable was about 0.6 cm.

F.   Projectile

In the first three shots the impactors were made of 6061-T6 aluminum. Extraneous signals were observed due to inductive coupling between sample and the metal projectile face. The remaining shots were done with a fused quartz or a sapphire impactor clamped to an aluminum projectile (Fig. 1). Impact misalignment was measured only in the first two shots. Tilt values recorded were 0.25 and 0.28 milliradians. In the case of non-conducting impactors the projectile alignment was checked with an auto-collimating telescope. Impactor face was perpendicular to the launching tube axis within 0.1 to 0.3 milliradians. The sapphire target was also aligned optically to the tube axis. But the actual tilt on impact was not recorded, since the small-diameter, non-conducting impactors precluded such recording.

Impact alignment was tested with an aluminum disc clamped to the projectile in a manner similar to that used for the non-conducting impactors. Impactor misalignment before the shot was measured as 0.35 milliradians; tilt measured on impact was 0.35 milliradians. It should be noted that the projectile has enough clearance for a possible 0.5 milliradian wobble on impact. This is not usually observed, however.

As received, the fused quartz and sapphire impactor discs were typically flat to within about 2 μm across the area which generated the stress pulse in the foil. Late in the experiments it was discovered that clamping a disc to a projectile head distorted the disc out of flat as much as 8 μm; this

would contribute to deviation from planarity in the shock wave
generated by impact, degrading rise time by about the same
amount as a number of other existing experimental conditions
(Sec. IV.C). The distortion could also contribute to lateral
deformation as discussed in Appendix C.

G.   Recording System

The pulsed current source was a Pulsar Model 301 power
supply with three channels, each consisting essentially of a
90 microfarad capacitor, charged to 500 volts, in series with
8.3 ohms (Fig. 3). The three channels were triggered simulta-
neously 15 to 30 microseconds before impact. The current
attainable was limited by the transient current rating of the
silicon-controlled rectifiers which switch the current on and
off. Current pulses were limited to 50 microseconds duration,
preventing sample heating during preshot pulsing.

One oscilloscope recorded the initial voltage step as
well as voltage change across the foil upon shock compression.
Two other oscilloscopes recorded only the voltage change due to
shock compression. This was achieved by suppressing the initial
voltage step using a differential comparator amplifier. The
oscilloscopes used were 580 series and 7000 series Tektronix,
Inc. models; system rise time was 4 to 5 nanoseconds. Oscillo-
scope traces were recorded on Polaroid film.

Time calibration was achieved using a Tektronix, Inc.
2901 Time Mark Generator. Voltage calibration was done by
recording pulses of known voltage on the oscilloscopes. These
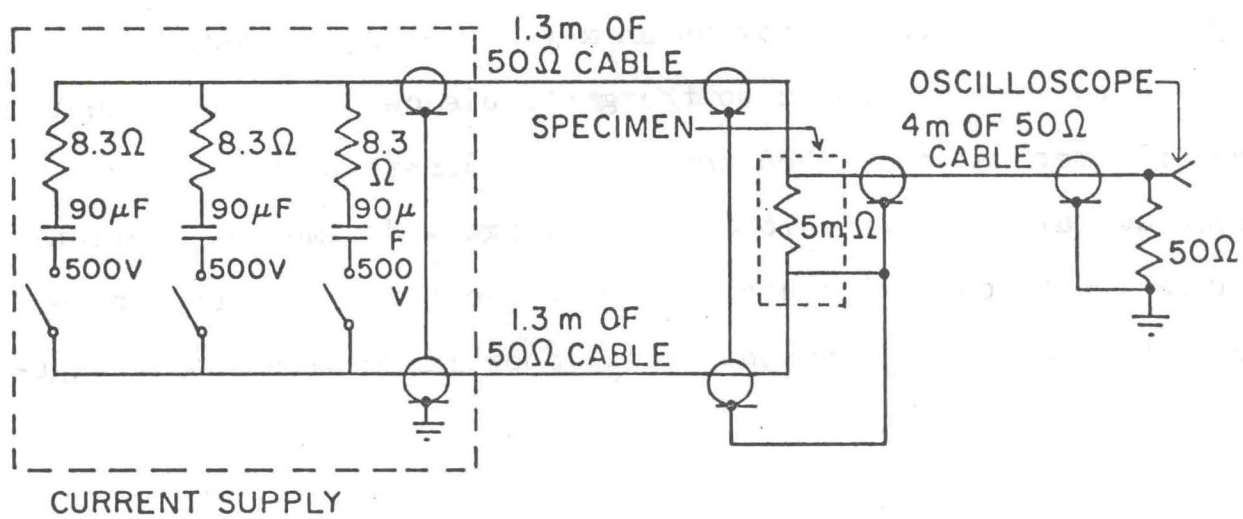
Fig. 3.   Electronic measuring system.

pulses came from a pulsed constant current source in series with a 10 ohm load resistor at the target position. Voltage across the resistor was first monitored by a digital voltmeter (NLS Series X-3) with the current source in a continuous mode. Then in single-pulse mode the voltage step was recorded on the oscilloscope. Calibration was usually completed within one hour after the shot.

Data reduction of shot traces and calibration traces began by reading the photos on an x-y traveling microscope. Each photo was referenced to the graticule center so that shot and calibration photos had the same coordinate origin. Shot trace coordinate pairs along with voltage and time calibration values within each time division were fed into a computer program which converted the shot-trace coordinate pairs to voltage-time pairs.

III. THEORY-ANALYSIS

Flow of the analysis is displayed in Fig. 4. From the experiment one obtains impactor velocity and a voltage-time profile of the shock response of the silver resistance. Known Hugoniot curves of silver and sapphire, and impactor velocity are used to compute the pressure-volume state in silver (Fowles, 1972). (Computation is based on the Rankine-Hugoniot jump conditions for steady shocks.) Then the shock resistivity of silver is computed. Using a P-V-T equation of state for silver fitted to experimental data, shock temperature is also calculated. Theory of a Debye solid is coupled with hydrostatic experiments on silver resistivity versus pressure to give an expression for the dependence of the temperature coefficient of resistivity on volume and to extrapolate the dependence of silver resistivity on hydrostatic pressure to 120 kbar. Then shock resistivity is corrected to isothermal conditions and compared to hydrostatic resistivity. Any deviation between shock and hydrostatic results is of interest.

Other analyses include the effect of material strength, work of plastic deformation, effect of wave reverberations in the sandwich, and eddy current corrections made in results from experiments where metal impactors were used.

A consistent set of units for calculation is time in microseconds, length in centimeters, and mass in grams. Then
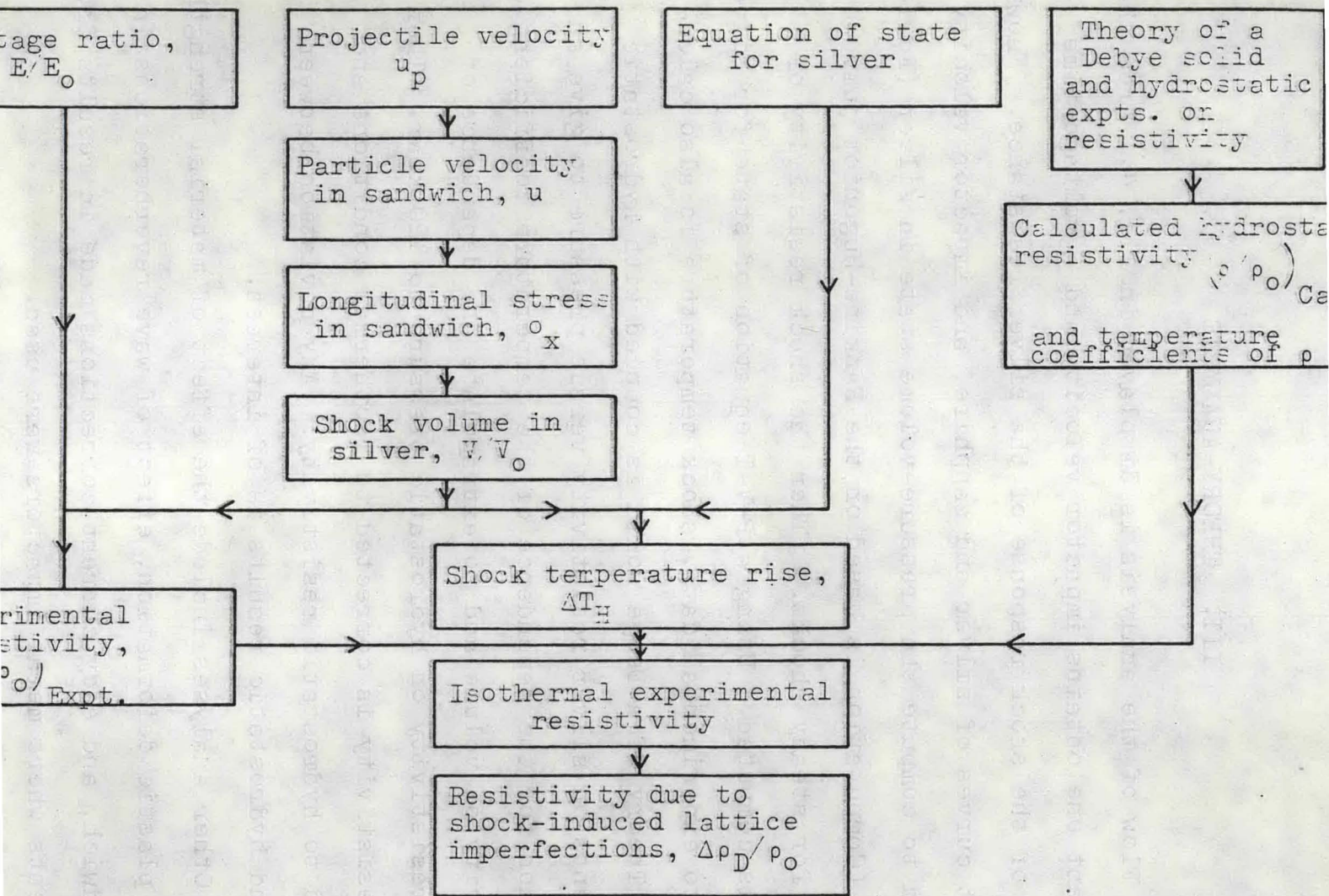
Fig. 4. Analysis flow chart.

pressures are in units of Mbar, volumes in cm^3/g, speeds in cm/µsec, and energies in Mbar cm^3/g.

A. Resistivity Theory and Analysis

To understand the resistivity change in a metal under shock compression, we first need an understanding of the effect of hydrostatic pressure on resistivity. It turns out that for a number of metals the main effect is a change in scattering of electrons by lattice vibrations. Changes in electronic band structure, the Fermi surface, and crystal structure can also be important.

1. Volume Dependence of Resistivity due to Lattice Vibrations

We can get a physical picture of the change in resistivity due to the lattice vibrations by using an Einstein model of a solid. In an Einstein model a solid consisting of N atoms is represented by 3N one-dimensional harmonic oscillators all vibrating with the same characteristic frequency, ω_E. The characteristic temperature θ_E is defined by

$$\hbar \omega_E = k_B \theta_E$$

($\hbar$ is Planck's constant and k_B is Boltzmann's constant). At high temperature where the classical equipartition theorem holds, the energy

$$E = k_B T = 2 \overline{V} = m \omega_E^2 \overline{x^2}$$

where here $\overline{V}$ is the mean potential energy and the virial theorem has been used. It is reasonable to expect that the cross-section of the vibrating atom for scattering electrons would be

proportional to the mean squared amplitude of vibration. This conclusion was first reached by Wien (Mott, 1934). Then

$$\rho \propto \overline{x^2} = \frac{k_B T}{m\omega_E^2} = \frac{\hbar^2}{mk_B} \frac{T}{\theta_E^2}$$

where θ_E will be dependent on the volume through ω_E. We find that the main volume dependence of resistivity may be expressed as

$$\left(\frac{\partial \ln \rho}{\partial \ln V}\right)_T = -2 \frac{\partial \ln \theta_E}{\partial \ln V}.$$

In the more complete Bloch-Gruneisen theory of resistivity, the resistivity is expressed as

$$\rho = \frac{K}{\theta_R} \left(\frac{T}{\theta_R}\right)^5 J\left(\frac{\theta_R}{T}\right)$$

where

$$J = \int_0^{\theta_R/T} \frac{x^3 dx}{(e^x - 1)(1 - e^{-x})}.$$

(See Ziman (1960) for a detailed treatment of this approach.) The quantity K depends on the crystal structure and other factors independent of T and θ. At temperatures large compared to θ_R, $J \propto \left(\frac{\theta_R}{T}\right)^4$ so that again we find $\rho \propto \frac{T}{\theta_R^2}$.

The Bloch-Gruneisen results are derived for a monovalent metal with a spherical Fermi surface, a Debye model for the lattice vibrations, and a deformation potential model for the change of potential of both ions and electrons as an ion moves off a lattice site in its thermal motion.

If we equate θ_R to θ_D then $\frac{d\ln\theta}{d\ln V}$ can be related to thermodynamic quantities; this was first noted by Gruneisen in 1926. The result is

$$-\frac{d\ln\theta}{d\ln V} = \frac{V\alpha'}{C_V K_T} = \gamma(V) \tag{1}$$

where $\gamma(V)$ is the Gruneisen parameter, α' the volume coefficient of thermal expansion, K_T the isothermal compressibility and C_V the constant volume specific heat (Lennsen and Michels, 1935).

Values for the characteristic temperatures are obtained by fitting experimental data to the equations, using θ as an adjustable parameter to get the best fit. Values for θ_R come from fits to resistivity-temperature data and θ_D from heat capacity-temperature data (Gschneidner, 1964).

Let us consider the assumption $\frac{d\ln\theta_R}{d\ln V} = \frac{d\ln\theta_D}{d\ln V}$. Ziman (1960) notes that Bloch resistivity theory is derived assuming scattering by longitudinal phonons only. So for a solid fitting the Bloch model we would expect $\theta_R = \theta_L$ which might be quite different from θ_D. The fact that θ_R is within 1% of θ_D for silver ($\theta_R = 223°K$, $\theta_D = 225°K$) may imply that shear waves participate in electron scattering processes to the same extent that they do in thermal processes. Therefore, the assumption $\frac{d\ln\theta_R}{d\ln V} = \frac{d\ln\theta_D}{d\ln V}$ has some plausibility in the case of silver, and for the lattice vibration contribution

$$\left(\frac{d\ln\rho}{d\ln V}\right)_T = -2\frac{d\ln\theta}{d\ln V} = 2\gamma(V).$$

Several attempts have been made to get the pressure dependence of resistivity from wave-mechanical calculations. Lennsen and Michels (1935) started from Nordheim's formula for resistivity based on a rigid ion model for the potential field around a vibrating ion. For nearly free electrons they derived

$$\left(\frac{\partial \ln \rho}{\partial \ln V}\right)_T = 2 \gamma(V) - 1 \qquad T \gg \theta \; ;$$

For $T \sim \theta$ this is modified to

$$\left(\frac{\partial \ln \rho}{\partial \ln V}\right)_T = \left(2 + \frac{\theta^2}{9T^2}\right) \gamma - 1 \; .$$

Using a tight-bonding approximation they derived

$$\left(\frac{\partial \ln \rho}{\partial \ln V}\right)_T = \left(2 + \frac{\theta^2}{9T^2}\right) \gamma + 1 \; .$$

According to Paul (1963), the rigid ion model is hard to justify physically, but it does give pressure dependences similar to that of other calculations. (See also review articles by Dugdale (1969) and Lawson (1956).)

2. A Semi-empirical Approach

Since an exact calculation is not practical (Ziman, 1965), a semi-empirical approach may be the best. Start from the expression $\rho = \alpha(V)T = A(V)\dfrac{T}{\theta^2(V)}$ (2)

where A is a catch-all parameter for the volume dependence of the band structure, Fermi geometry, Fermi energy, and details of the electron-phonon interaction and $\alpha(V)$ is the temperature coefficient of resistivity. Then,

$$\left(\frac{\partial \ln \rho}{\partial \ln V}\right)_T = 2\,\gamma(V) + \frac{d\ln A}{d\ln V} \, .$$

Now $\left(\frac{d\ln A}{d\ln V}\right)_{V=V_o}$ can be evaluated at atmospheric pressure from experimental values for $\left(\frac{\partial \ln \rho}{\partial \ln V}\right)_{T,\,V=V_o}$ and $\gamma(V_o)$. Then

$$\frac{\rho(V,T)}{\rho(V_o,T)} = \frac{\alpha(V)}{\alpha(V_o)} = \left(\frac{V}{V_o}\right)^B \exp\left[2\int_{V_o}^{V} \frac{\gamma(V')}{V'} \, dV'\right]$$

$$= \left(\frac{V}{V_o}\right)^B \left(\frac{\theta(V)}{\theta(V_o)}\right)^{-2} \qquad (3)$$

where $B \equiv \left(\frac{d\ln A}{d\ln V}\right)_{V=V_o}$. In this work it has been assumed that $\frac{d\ln A}{d\ln V}$ is a constant.

Dugdale (1961) used Bridgman's pressure derivatives for the resistance and found $B = -0.9$ for silver. Goree and Scott (1966) also measured isothermal pressure derivatives of the resistivity of silver. They subtracted the pressure derivative of impurity resistivity to get the perfect lattice pressure derivative

$$\left(\frac{\partial \ln \rho_L}{\partial P}\right)_{T,\,P=1\ \text{atm}} = -4.2 \times 10^{-6}/\text{bar}$$

(see Sec. III.A.3). Using Goree and Scott's derivative, a value of $B = -0.64$ was found; this value of B was used for generating ρ on a hydrostat. (In finding $\gamma(V_o) = 2.43$, ambient values of $\beta_T = 1.005 \times 10^6$ bar, $\alpha' = 57.1 \times 10^{-6}/°\text{K}$, and $C_V = 2.25$ bar cm^3/g were used.) Note that $\left(\frac{V}{V_o}\right)^B$ where $B < 0$ tends to increase the resistivity while $(\theta/\theta_o)^{-2}$ decreases the resistivity on compression.

For comparison, let us examine some of the electron scattering effects which are lumped in A(V). First consider how changing the Fermi energy influences the resistivity. (For free electrons

$$E_F = \frac{\hbar^2 k_F^2}{2m} \propto V^{-2/3}$$

where m is electron mass and k_F is electron wave number at the Fermi energy.) For nearly free electrons, Mott and Jones (1936) find the resistivity

$$\rho = \frac{3 \pi^2 \hbar^2}{e^2} \frac{1}{(\tau^2 k^2 \frac{dE}{dk})_{k=k_F}} .$$

(τ is electron relaxation time, e is electron charge.) Then $\rho \propto k_F^{-b} \propto V^{b/3}$ giving a logarithmic derivative of $\frac{b}{3}$, a constant. If b > 0, this will decrease the resistivity on com- pression, opposite to the behavior of A(V); b = 3 for free electrons.

We have accounted for the lattice vibration spectrum with a Debye model. This assumes isotropy of the vibrations. Anisotropy and changes in anisotropy of the elastic constants with pressure might be expected to affect resistivity. However, Dugdale (1965) notes that large volume dependence of the anisotropy of elastic constants in gold does not appear to have a major effect on pressure dependence of its resistivity.

We would also like to get some idea of changes in resistivity with pressure due to changes in the electron Fermi surface in reciprocal lattice space. For free electrons in an isotropic metal a simple formula for conductivity is

$$\sigma = n e^2 \, \frac{\tau}{m} = n e^2 \, \frac{\ell}{p_F} = n e^2 \, \frac{\ell}{\hbar k_F}$$

where ℓ is conduction electron mean free path, p_F is electron momentum at the Fermi surface, and n is conduction electron density. Since the area of a spherical Fermi surface is

$$S = 4 \pi k_F^2 = 4 \pi (3 \pi^2 n)^{2/3}$$

we may write

$$\sigma = \frac{e^2 \ell}{12 \pi^3 k} \, S \; .$$

From this we can assert that $\rho \propto S^{-1}$ for free electrons in isotropic metals. When a metal is hydrostatically compressed, the Brillouin zone and Fermi surface in reciprocal space expand, implying a decrease in resistivity.

Let us use the above resistivity relation to gain understanding in cases where the Fermi surface is not spherical. For instance, noble metal Fermi surfaces (Fig. 5) have necks which contact the Brillouin zone boundary, reducing the Fermi surface from that of an equivalent spherical Fermi surface. This reduced area would imply increased resistivity. (Electrons in the neck contact areas are Bragg reflected, and hence do not conduct.)

Experimental measurements to 25 kbar of the silver Fermi surface show increasing distortion with increasing pressure. (Templeton, 1966). (See Brandt, Itskevich, and Minina (1972) for a review of such work.) For the belly cross-section, A_1, $\frac{d \ln A_1}{dP} = 0.503 \times 10^{-3}$/kbar; for the neck cross-section, A_2, $\frac{d \ln A_2}{dP} = 4.40 \times 10^{-3}$/kbar for the range

34
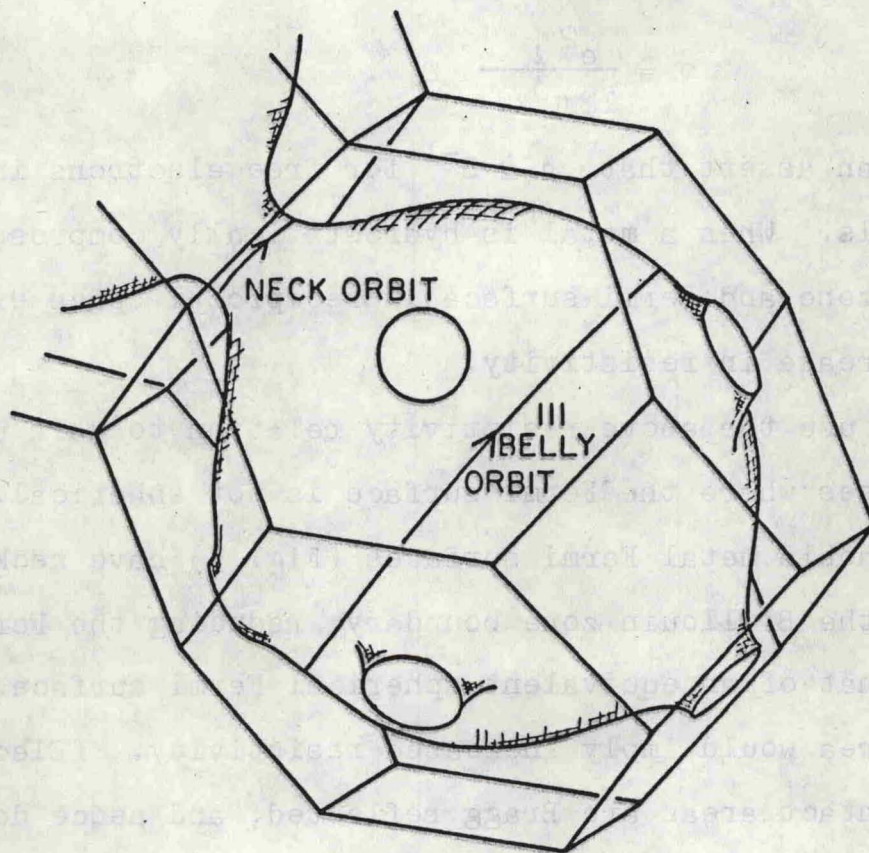
Fig. 5. Noble metal Fermi surface and
first Brillouin zone. (After Dugdale (1965).)

0 to 25 kbars. The belly cross-section derivative is comparable to a nearly-free electron calculation of $\frac{d\ln A_F}{dP} = 0.602 \times 10^{-3}/$ kbar (Brandt et al., 1972). The total neck cross-section increases at a faster rate than the belly cross-section. Extrapolation to 100 kbar implies a 40% increase in neck cross-section as compared to a 5% increase in belly cross-section. This is compared to a 6% increase calculated from a nearly free electron model. From handbook values of sizes of neck and belly cross-sections one finds that although the total neck cross-section goes from 4.0 to 5.4% of the net Fermi surface area, the net Fermi surface area itself increases by about 3.4% in going from ambient pressure to 100 kbar. From our simple model, $\rho \propto S^{-1}$, we would expect a decrease in resistivity with pressure. This is opposite to the direction of the effect predicted by Dugdale (1961) at low temperatures where electron scattering by long wave length phonons is enhanced by neck distortion. The present calculations also contradict the volume dependence of the lumped parameter A(V) in the semi-empirical approach which will be used in the present work.

For $\rho \propto S^{-1}$

$$\left(\frac{\partial \ln \rho}{\partial \ln V}\right)_T = \frac{d\ln S}{dP} B_T + \text{ other terms}$$

where β_T is the isothermal bulk modulus, we know that $\frac{d\ln S}{dP}$ is nearly constant to 25 kbar. But β_T is about 30% larger at 100 kbar than at 1 atmosphere, so that $\frac{d\ln S}{d\ln V} = \frac{d\ln S}{dP} \beta_T$ is by no means constant.

It should be noted that the effect of uniaxial tension on the Fermi surface of silver has been measured (Shoenberg and Watts, 1967). The neck cross-section increases strongly,

$$\frac{d\ln A_2}{d\sigma} = 15 \times 10^{-3}/\text{kbar}$$ while the belly cross-section decreases,

$$\frac{d\ln A_1}{d\sigma} = -0.3 \times 10^{-3}/\text{kbar}.$$ A 2 kbar elastic limit corresponds to a neck cross-section change of 3%, a small effect compared to the 40% hydrostatic effect at 100 kbar.

In some cases electronic transitions can occur on compression (Drickamer, 1965). A lower lying electron energy band may be raised above or overlap the conduction band, changing the electronic properties. No such effects have been observed in noble metals.

From all these considerations, lumping these volume dependences into a parameter A(V) in Eq. (2) such that $\frac{d\ln A}{d\ln V} =$ constant over the compression range studied here should be a fair assumption, as long as the dominant volume dependence of the resistivity is contained in the volume dependence of the characteristic temperature, $\theta(V)$.

3. Volume Dependence of Impurity Resistivity

It would be desirable to account for the pressure derivative of the impurity resistivity ρ_i for each purity of silver used. Goree and Scott (1966) found that a silver specimen which was twice as pure as another specimen had an impurity pressure derivative one-half as large. Using this proportionality we can find the approximate impurity pressure derivatives

for the silver purities used. For their more pure silver

$$\frac{R_{4.2°K}}{R_{293°K}} = 0.00714 \text{ and } \frac{1}{\rho_{4.2°}} \frac{d\ \rho_{4.2°}}{dP} = 2.4 \times 10^{-6}/\text{bar.}$$

For MRC silver we find $\frac{d\ell n\ \rho_i}{d\ell n\ V} = -1.4$ using $\frac{R_{4.2°}}{R_{298°}} =$

0.00412; for W3N silver we find $\frac{d\ell n\ \rho_i}{d\ell n\ V} = -0.8$ using

$\frac{R_{4.2°}}{R_{298°}} = 0.00240$. Let us assume that the logarithmic volume

derivative of the impurity resistance is a constant C so that

$$\frac{\rho_i(V)}{\rho_i(V_o)} = \left(\frac{V}{V_o}\right)^C .$$

Also assume the approximate validity of Matthiessen's rule

$\rho = \rho_L + \rho_i$ where ρ_L is the perfect lattice resistivity.
Then

$$\frac{\rho(V,T)}{\rho(V_o,T)} = \frac{\rho_L(V,T)}{\rho_L(V_o,T)} \left[1 + \frac{\rho_i(V_o)}{\rho_L(V_o,T)} \frac{\left(\frac{V}{V_o}\right)^C}{\rho_L(V,T)/\rho_L(V_o,T)}\right] \Big/$$

$$\left(1 + \frac{\rho_i(V_o)}{\rho_L(V_o,T)}\right) .$$

Computation can proceed by assuming

$$\frac{\rho_i(V_o)}{\rho_L(V_o,T)} = \frac{R_{4.2°}}{R_{298°}} .$$

Results at 120 kbar, for the foils used, are within 0.3% of
those obtained by ignoring impurity resistivity volume depend-
ence. Hence, this impurity effect was ignored in data analysis
of the present work.

4. Final Resistivity Analysis

Up to now we have assumed $\rho = \alpha T$ for the electrical resistivity. Experimentally metals do not exactly have resistivity proportional to absolute temperature; rather, the constant pressure resistivity is given by $\rho = \alpha T + \beta$. So, to adjust theory to reality, assume $\rho = \alpha(V)T + \beta(V)$ where $\alpha(V) = A(V)/\theta^2(V)$ as before and $\beta(V)$ is an empirical parameter. From data of Kos (1973) for silver $\alpha(V_o) = 0.005988$ $\mu\Omega cm/°K$ and $\beta(V_o) = -0.16$ $\mu\Omega cm$ for the 150-300°K range. At room temperature $\beta/\alpha T = -0.09$.

We now need to express the volume dependence of resistivity for the above case; ignore impurity resistivity for the time being, and assume $\alpha(V) = A(V)/\theta^2(V)$ as derived in the previous analysis (Eq. (2)). Some estimate of the volume dependence of β is needed.

For estimating the volume dependence of β, the Gruneisen-Borelius relation for resistance,

$$\frac{R_T}{R_\theta} = h\frac{T}{\theta} - (h-1) \quad (h = 1.17)$$

will be used (Gerritsen, 1956). This is an empirical relation for isotropic metals accurate in the range $0.2 < T/\theta < 1.2$. (For silver it is accurate at least to $T/\theta = 1.5$.) If we ignore thermal expansion $\frac{\rho_T}{\rho_\theta} = \frac{R_T}{R_\theta}$, and $\rho_T = h\frac{T}{\theta}\rho_\theta - (h-1)\rho_\theta$ ($h = 1.17$) in the form $\rho = \alpha T + \beta$. For silver $\rho_\theta = 1.18$ $\mu\Omega cm$ implies $\beta = -0.17$ $\rho_\theta = -0.20$ which is close to the exact value of -0.16 for silver from Kos' work. Actually silver resistivity is described better using $h = 1.14$.

Now $\beta(V)$ can be found from

$$\beta = (1-h)\rho_\theta = (1-h)(\alpha\theta + \beta)$$

$$\beta(V) = \frac{(1-h)}{h} \alpha(V) \theta(V)$$

Finally, the hydrostat is given by

$$\frac{\rho(V,T)}{\rho(V_o,T)} = \frac{\alpha(V)}{\alpha(V_o)} \frac{\left(1 + \frac{1-h}{h}\frac{\theta(V)}{T}\right)}{\left(1 + \frac{1-h}{h}\frac{\theta(V_o)}{T}\right)} \tag{4}$$

This implies that at 120 kbar α/α_o (Eq. (3)) is multiplied by 0.977.

For the resistivity change due to the shock temperature rise, the form used was

$$\frac{\Delta\rho_T}{\rho_o} \equiv \frac{\rho(V,T) - \rho(V,T_o)}{\rho(V_o,T_o)} = \frac{\alpha(V)}{\alpha(V_o)}\left(\frac{T}{T_o}-1\right) \Big/$$

$$\left(1 + \frac{\beta(V_o)}{\alpha(V_o)T_o}\right)$$

(T_o is 298°K and V and T are volume and temperature in the shocked state.)

The isothermal shock resistivity one wishes to compare to the hydrostatic resistivity (Eq. (4)) is

$$\frac{\rho(V,T_o)}{\rho(V_o,T_o)} = \frac{\rho(V,T) - \Delta\rho_T}{\rho(V_o,T_o)} \,.$$

From the shot one obtains $\rho(V,T)/\rho(V_o,T_o')$ where T_o' is ambient temperature. This varied from 295.6° to 298.4°K. The relation needed is

$$\frac{\rho(V,T)}{\rho(V_o,T_o)} = \frac{\rho(V,T)}{\rho(V_o,T_o')} \frac{\rho(V_o,T_o')}{\rho(V_o,T_o)}$$

where

$$\frac{\rho(V_o, T_o')}{\rho(V_o, T_o)} = 1 + a(T_o' - T_o)$$

($a = 0.00408/°K$). The above forms for isothermal resistivity were used in analyzing the data.

5. Resistance to Resistivity Transformation

What is measured in the experiment is the resistance ratio, R/R_o. For a slab geometry resistance is related to resistivity by $R = \rho L/A$, where L is the length and A is the cross-sectional area. In the shock wave experiment the compression is in one dimension only so that L is unchanged and A is decreased. Hence,

$$\frac{\rho}{\rho_o} = \frac{R}{R_o} \frac{A}{A_o} = \frac{R}{R_o} \frac{V}{V_o}$$

since $V/V_o = (AL)/(A_oL)$.

In a hydrostatic compression, however, all dimensions decrease by the same proportion. So

$$\frac{\rho}{\rho_o} = \frac{R}{R_o} \frac{A}{A_o} \frac{L_o}{L}.$$

But

$$A/A_o = (L/L_o)^2 = (V/V_o)^{2/3}. \text{ Finally, then}$$

$$\frac{\rho}{\rho_o} = \frac{R}{R_o} \frac{L}{L_o} = \frac{R}{R_o} \left(\frac{V}{V_o}\right)^{1/3}.$$

6. Piezoresistance Effects

The effect of the piezoresistance tensor of isotropic elastic material in the present work was considered (Ginsberg, Grady and DeCarli, 1972; Barsis, Williams, and Skoog, 1971).

Resistance in tension and under hydrostatic compression needed for the analysis are known for silver (Bridgman, 1925). For a 1 kbar HEL in silver and considering the pressure range of these experiments, the effect was found to be unimportant, since at the HEL $\frac{\Delta R}{R_o}$ = -0.002 for uniaxial compression.

7. Resistivity-Pressure Data of Bridgman

Bridgman's measurements (1938) of silver resistivity versus hydrostatic pressure to 30 kbar at 30°C in isopentane are used for comparison to calculated and experimental silver resistivity in the present work. Bridgman's pressures were measured by a manganin coil, using the freezing point of mercury as a calibration point. A review of pressure calibration by Decker et al. (1972) states that Bridgman's scale was about 1% low. Accordingly, Bridgman's pressure values were corrected for use in the present study by multiplying by 1.0103; corrected pressures are believed accurate to 1/4% at 25 kbar according to the reviewers. Bridgman's work was done with only two electrical leads, but because of the high resistance of the silver coil (24 ohms) contact resistance should not have been a problem. In 1952 he measured the silver resistance between opposed anvils to 100 kbar, where the foil was embedded in silver chloride. This anvil work is not used because observed resistance changes cannot be reliably attributed to hydrostatic pressure effect due to plastic deformation and pressure-gradient effects. For the record, at 50 kbar, Bridgman's anvil results give ρ/ρ_o = 0.827

and 0.847 using revised pressure scales suggested by Bundy
(1973) and Jura (1973), respectively. In comparison, isothermal
hydrostatic resistivity calculated from Eq. (4) is 0.832 at
50 kbar.

B.   Equation of State

An equation of state (a P-V-T relation) for silver is
needed to calculate shock temperatures and the temperature coef-
ficient of resistivity in the compressed state. Correcting
resistivity-shock pressure data to isothermal conditions
requires both shock temperatures and temperature coefficients.
Temperature coefficients are also used in the model calculation
of the resistivity of silver under pressure (Sec. III.A.4).

The equation of state chosen was an analytic fit by
Zharkov and Kalinen (1971) to static and dynamic P-V data.
Their approach, the method of potentials, involves writing down
inter-ionic potentials which depend on distance between charged
particles in ways appropriate to the main interactions in the
solid. The undetermined coefficients are then found by empiri-
cal fit. The method of potentials includes the following
advantages:

1.   an equation of state in analytic rather than tabular
     form;

2.   more accuracy when extrapolating V or T and when dif-
     ferentiating the equation of state than if an
     arbitrary polynomial, for example, is fitted to
     experimental data.

It should be noted that the second statement is valid only if
the potential is selected properly (Zharkov and Kalinen, 1971).

At $0°K$, ignoring zero-point vibrations, the resultant internal potential energy for non-alkali metals is

$$E_p = a \exp[b(1-X^{1/3})] - cX^{-1/3}$$

where $X = V/V_o$, the dimensionless volume, and a, b, c are constants. The first term corresponds to repulsion due to overlap of electron shells on the ions. The second term accounts for Coulomb interaction and for exchange interaction among conduction electrons.

Thermal energy is accounted for in a quasi-harmonic approximation. A Debye model gives the Helmhotz energy as

$$F = E_p + Nk_BT \left\{ \frac{9}{8} \frac{\theta_D}{T} + 3 \ln\left[1-\exp\left(- \frac{\theta_D}{T}\right)\right] -D \frac{\theta_D}{T} \right\}$$

where $D(\frac{\theta_D}{T})$ is the Debye function,

$$D\left(\frac{\theta_D}{T}\right) = \frac{3T^3}{\theta_D^3} \int_0^{\theta_D/T} \frac{Z^3 dZ}{e^Z-1} \quad ,$$

N is the number of unit cells in the solid, and k_B is Boltzmann's constant. From $P = -\left(\frac{\partial F}{\partial V}\right)_T$ we have

$$P = P_p + \frac{\gamma}{V} Nk_B\left[\frac{9}{8} \theta_D + 3T\ D\left(\frac{\theta_D}{T}\right)\right]$$

where γ is the Gruneisen parameter (Eq. (1)) and the potential pressure is

$$P_p = A\ X^{-2/3} \exp[b(1-X^{1/3})] - K\ X^{-4/3} \quad .$$

Note that this is a Mie-Gruneisen equation of state,
$P = P_p(V) + \frac{\gamma}{V} E_T.$

We have a single experimental compression curve and two unknown functions $P_p(V)$ and $\gamma(V)$. One way to handle this is to express the Gruneisen parameter as a function of the potential pressure. The model chosen for this was the Dugdale-MacDonald formula,

$$\gamma(V) = - \frac{V}{2} \frac{\partial^2 (P_p V^{2/3})}{\partial V^2} \bigg/ \frac{\partial (P_p V^{2/3})}{\partial V} - \frac{1}{3} \;.$$

A constant δ may be added to make $\gamma(V)$ agree at room conditions with the thermodynamic value (Eq. (1)). In a review article on the Gruneisen equation of state, Royce (1971) concludes that the Dugdale-MacDonald formula is the best choice for non-alkali metals.

Two basic assumptions were made in using shock data to generate an equation of state:

1. Experimental values of P, V, E belong to states of thermal equilibrium.

2. The solid is considered a fluid with a hydrostatic shock pressure, ignoring strength effects.

In silver this seems reasonable as its Hugoniot elastic limit is estimated at 1.2 kbar (Sec. III.C).

In the classical limit $T \gg \theta_D$, the Debye function may be expanded to give

$$P = P_p(x) + \frac{3RT}{MV_0} \frac{\gamma}{X} \left[1 + \frac{1}{20} \frac{\theta_D^2}{T^2} \right]$$

where M is the gram molecular weight, R the gas constant, and V_0 the reference specific volume. Temperature is determined from

$$E = E_p(X) + \frac{3RT}{M} \left[1 + \frac{1}{20} \frac{\theta_D^2}{T^2} \right]$$

a quadratic equation for the temperature. (Energy is now expressed for one gram of solid.) Internal energy E on the Hugoniot curve is known from the Rankine-Hugoniot relation. For a single shock from the ambient state the relation is

$$E_H = E_o + \frac{1}{2} P_H V_o (1 - X) \quad .$$

Besides calculating temperatures we can now perform the integration necessary for the resistivity model calculation (Eq. (3)),

$$I(X) = \int_1^X \frac{\gamma(X')}{X'} \, dX' \quad .$$

The Dugdale-MacDonald formula gives

$$\gamma(X) = -\frac{X}{6} \frac{2AbX^{-\frac{1}{3}}\exp(b(1-X^{\frac{1}{3}})) + Ab^2\exp(b(1-X^{\frac{1}{3}})) - 10KX^{-\frac{4}{3}}}{-AbX^{\frac{2}{3}}\exp(b(1-X^{\frac{1}{3}})) + 2KX^{-\frac{1}{3}}} - \frac{1}{3} + \delta$$

(For silver, Zharkov and Kalinen give values of A = 0.31495 Mbar, b = 11.9180, K = 0.33299 Mbar, and δ = 0.163 for the equation of state fit to shock and static high pressure data.) The integration was done numerically by the extension of Simpson's rule (Booth, 1957). Results for the Debye temperature

$$\frac{\theta}{\theta_o} = \exp(-I(X))$$

were fitted to a polynomial

$$\frac{\theta}{\theta_o} = 4.0465 \, X^2 - 10.523 \, X + 7.4770 \quad .$$

Aside from dependence on volume, the phonon spectrum as characterized by θ_D may also be affected by lattice defects. The Debye temperature may change linearly with dilute solute concentration by up to 1% per atomic percent solute (Berry,

1972). Defects generated by quasi-static plastic deformation can be accounted for in a solid's thermal behavior by a decrease in θ_D of 0.4% for saturation defect concentration (Berry, 1972). For the defect concentration generated by shock deformation the change would be greater, however these effects were neglected in computations in this work using θ_D.

C. Strength Effects

To a first approximation in these experiments silver can be treated as a fluid in calculating the shock (P,V,T) state. However, one would like an estimate of the significance of material strength effects for silver shock states. Also, one needs the strength for calculation of the work of plastic deformation. This work is important in analyzing the behavior of shock defect resistivity.

If material strength is significant, a number of adjustments have to be made. For an isotropic solid one defines a mean pressure by

$$-\overline{P} = \frac{1}{3} (\sigma_x + \sigma_y + \sigma_z) = \frac{1}{3} (\sigma_x + 2\sigma_y)$$

where σ_x is the stress in the direction of shock propagation. (Tensile stresses and strains are taken as positive.) In addition, equation of state calculations must be revised, accounting for the solid's elastic strength. For an ideal elastic-plastic, isotropic solid the work of plastic deformation is expressed

$$dW_{PD} = V \sum_j s_j \, de_j^P \tag{5}$$

where the deviatoric stresses are defined by $s_j = \sigma_j + \overline{P}$ and for small strains deviatoric strains by

$$e_j = \epsilon_j - \frac{1}{3} \sum_k \epsilon_k \qquad (\epsilon_k \text{ is natural strain}).$$

Invoking the Lamé constants for an isotropic, linearly elastic solid, one finds

$$dW_{PD} = \frac{4}{3} V\tau(d\epsilon_x - \frac{d\tau}{\mu})$$ (6)

(Duvall, 1972). Here μ is a Lamé constant or the shear modulus and $\tau \equiv (\sigma_x - \sigma_y)/2$, the maximum resolved shear stress.

No measurements of the Hugoniot elastic limit (HEL) for silver have been published. For a solid whose yielding response under shock shows no relaxation phenomena (i.e., no strain rate effects) one can estimate the HEL from the static yield stress in tension Y. The von Mises or Tresca yield criterion in uniaxial strain is $-\tau = Y/2$. For the linearly elastic solid the HEL is given by

$$-\sigma_x = Y \frac{(1-\nu)}{(1-2\nu)} = P_x^{HEL}$$

where ν is Poisson's ratio and $P_x \equiv -\sigma_x$ (Duvall, 1972).

For commercially pure silver the Metals Handbook lists a yield stress in tension of 0.54 kbar. For Poisson's ratio it lists 0.37 for annealed silver and 0.39 for hard drawn. (Wise and Cox, 1961). Dawson's work (1965b) on 99.999% pure, annealed silver gives a value of yield stress of 0.42 kbar. Values of 0.5 kbar for Y and 0.37 for ν were used in computations.

We than find P_x^{HEL} = 1.2 kbar. Provided that no volume changes result from plastic strain, one can derive $-\overline{P} = \sigma_x + \frac{2}{3} Y$ (Fowles, 1961). For the equation of state calculations in this work, this correction to the pressure (0.3 kbar for silver) was neglected.

The agreement of HEL's calculated as above with experimental values is not very good. A comparison done by Duvall

(1961) for iron and steels show experimental values to be about
twice as large as calculated ones. Work in annealed mild steel
showed observed HEL's to be two to three times calculated values
(Jones, Nielson, and Benedick, 1962; Taylor and Rice, 1963).
Fowles' work (1961) on 2024 aluminum, both hardened and annealed,
found agreement to within the precision of the experiment.
Other work on Dural aluminum found experimental HEL's 50% higher
in hardened material and 150% higher in the annealed case
(Taylor and Whiffen, 1948). It should be noted that these HEL
values correspond to values after several millimeters of shock
propagation.

D. Work of Plastic Deformation

Assuming $-\tau = Y/2$ we may write Eq. (6) as

$$dW_{PD} = -\frac{2}{3} Y V(d\epsilon_x + dY/2\mu) \qquad (7)$$

If there is no work hardening so that yield strength in tension
is constant the plastic work is

$$W_{PD} = -\frac{2}{3} Y_0 V_1(\frac{V}{V_1} - 1)$$

where V_1 is the volume at the Hugoniot elastic limit. Work
hardening may be included by allowing yield strength in tension
to be a function of plastic work. Yield strength in tension
(condition of uniaxial stress) as a function of strain has been
published for silver by Dawson (1965). One can find the uni-
axial strain for equivalent plastic work by equating plastic
work as a function of strain in the two cases. The approximate
result is

$$\epsilon_x \approx -\frac{3}{2} \epsilon_s \qquad \text{(Fowles, 1961).}$$

(Here ϵ_S is the strain in the uniaxial stress case.) Now let

$$Y = Y_o + H \, (\epsilon_S - \epsilon_S^1)$$

where $H = 0.014$ Mbar from Dawson's data on silver.

Using $\epsilon_X = \ell n(V/V_o)$, we find

$$W_{PD} = -\frac{2}{3} V_1 (1 + \frac{H}{3\mu}) \left\{ C(\frac{V}{V_1} - 1) - \frac{2}{3} H \left[\frac{V}{V_1}(\ell n \frac{V}{V_o} - 1) - \ell n(\frac{V_1}{V_o} - 1) \right] \right\}$$

where $C \equiv Y_o + \frac{2}{3} H \, \epsilon_X^1$. Resulting work of plastic deformation in shocked silver as function of compression is shown in Fig. 6.

In addition to work hardening there is also an effect of hydrostatic pressure on yield strength. Deformation of single-crystal copper in torsion by Abey showed for a given strain $\frac{d\tau}{dP} = 3.8 \times 10^{-3}$ (Abey, 1973). A value of 1.55×10^{-2} for $\frac{d\tau}{dP}$ was used by Erkman and Duvall (1965) to get agreement between experimental and calculated rarefaction profiles for copper. However, Barker (1968) was able to fit measured stress-time profiles using only work hardening and Bauschinger effect. Abey's result implies an increase in τ of 0.4 kbar at $P = 100$ kbar for copper. This indicates the pressure effect on yield strength may be significant for shock deformation but probably is less than the work hardening effect. Since no pressure effect data were available for silver, the effect was not taken into account in computations in the present work.

E. Temperature Calculations

An equation of state was developed for calculating temperatures (Sec. III.C). An expression was given for
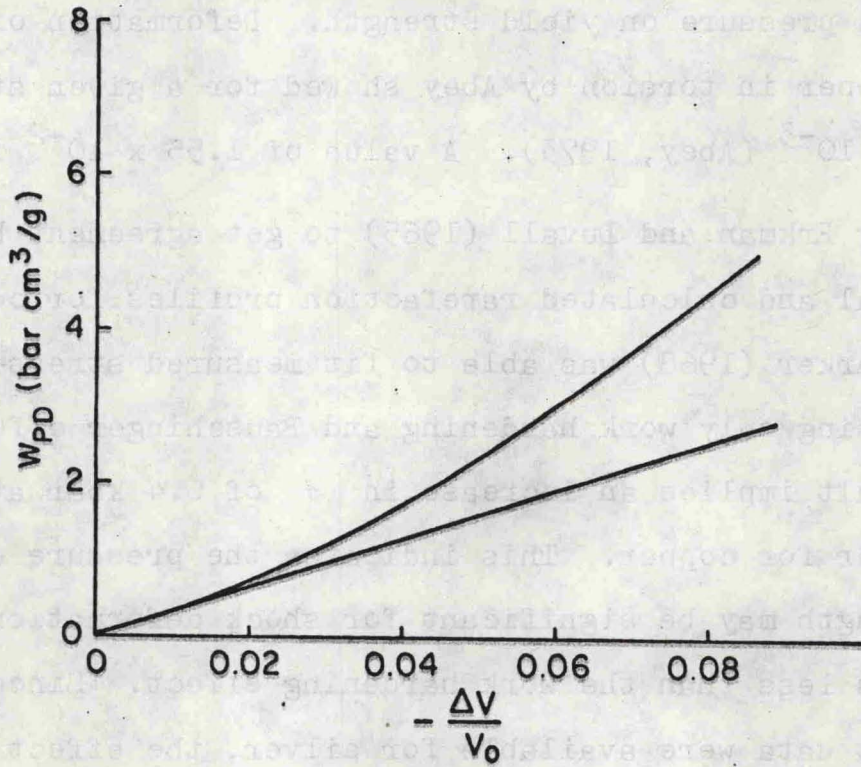
Fig. 6. Work of plastic deformation
versus compression. Upper curve includes
work hardening.

calculating temperatures reached by a single shock transition from the ambient state, treating the material as a fluid.

The actual temperature rise in the experiments will deviate from the above simple calculation for the following reasons:

1. The final state in the experiment is not reached by a single shock but by a series of shocks because of the sandwich configuration.

2. Since the material has strength, there will be heat generated by the irreversible work of plastic deformation.

3. Porosity, if present, will cause an additional temperature rise due to the extra work of compression done by the shock.

4. Heat flow from the adjacent epoxy (Sec. IV.J).

These temperature deviations, if significant, will affect results for shock isothermal resistivity and defect resistivity. The above contributions will be considered separately in following sections.

1. Reverberation Temperature Calculation

The sandwich configuration (anvil-foil-anvil) causes the final (P,V,T) state in the foil to be reached by a series of shock reverberations (Fig. 7). The amount of deviation from the state reached by a single shock depends on the mechanical shock impedance mismatch between foil and anvil (see Sec. I.A). (There may also be some small reverberation effects due to the thin, epoxy bonding layer.) For silver in sapphire, reverberation causes a smaller temperature rise than a single shock; the P-V state is not significantly affected. The smaller temperature rise by reverberation will affect the correction of shock
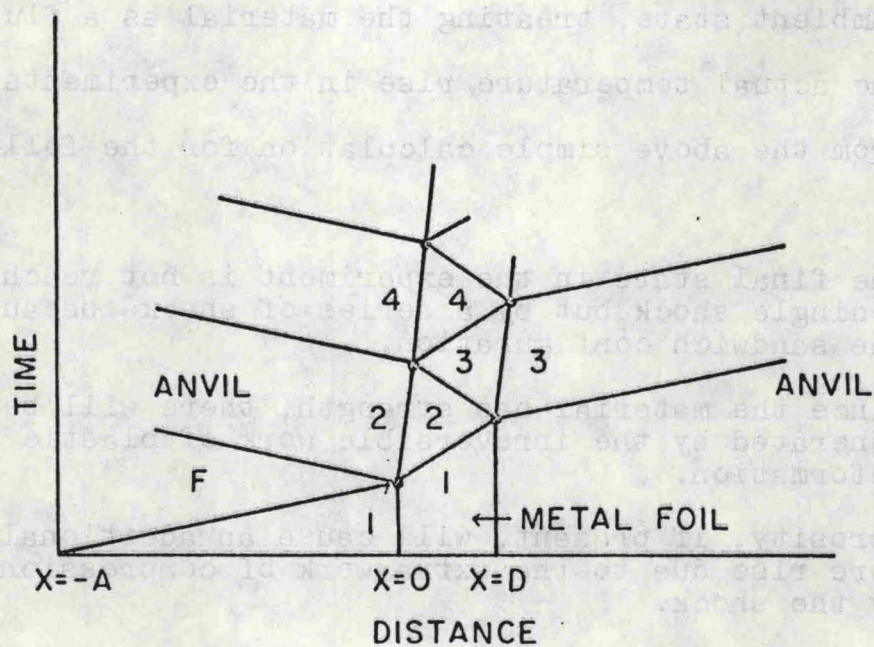
(a)
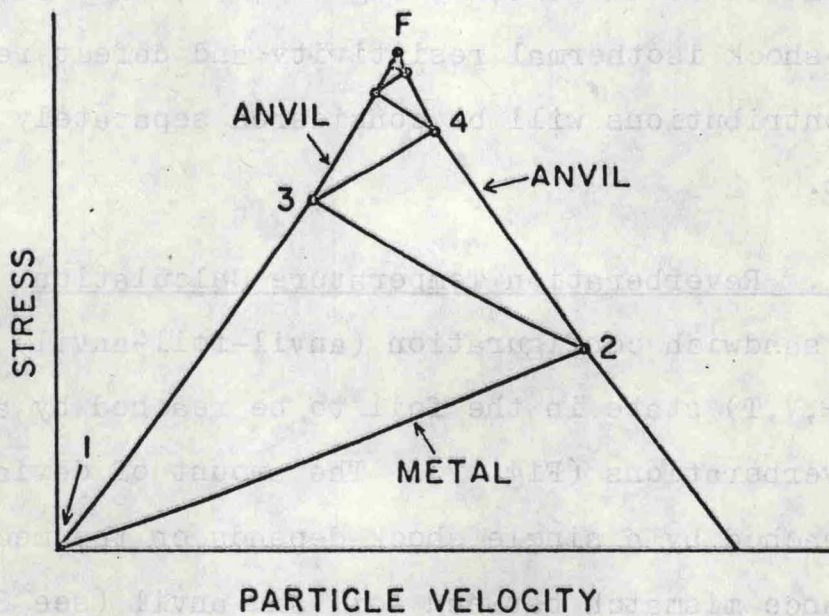
(b)

Fig. 7. Reverberation states in (t,x)
and (P,u) planes.

data to isothermal resistivity (Sec. III.A.4), making iso-
thermal resistivity, and hence defect resistivity, higher than
if one assumed single shock temperatures to be correct.

Continuity conditions for shocks at interfaces between
different materials require continuity of longitudinal stress
and particle velocity normal to the interface (Fowles, 1972).
So the pressure and particle velocity in silver are determined
by the shock state in sapphire. However, the final volume and
temperature in silver may have significant dependence on the
shock reverberation path as opposed to a single shock path to
the final state.

Calculations of the silver-sapphire interaction shows
that three wave transits are necessary to bring the silver to
within 0.1% of the final shock pressure for a 100 kbar shock.
In two transits it is within 0.3% and in one transit within 9%.
At 100 kbar the temperature change due to reverberation is 4%
lower than that due to a single shock. For comparison, tempera-
ture change at 100 kbar on the isentrope centered at the initial
state is about 20% lower than the single shock temperature
change.

The reverberation shock (P, u) states are found by the
method of characteristics in the (P, u) plane. Quadratic fits
$-\sigma$ or $P = A_i u + B_i u^2$ to the principal pressure-particle
velocity curves are used in the numerical solution. (The prin-
cipal Hugoniot curve through $P = 0$, $u = 0$ was used to generate
all characteristics.) For silver, $A_1 = 3.3384$ and $B_1 = 17.448$
and for sapphire, $A_2 = 4.44$ and $B_2 = 1.36$ (P is in Mbar and

u in cm/μsec). Fig. 7 sketches the states in the (P, u) and
(t, x) planes.

Solution of the simultaneous equations representing the
curve intersections in the (P, u) plane for even numbered states
is different from the solution for the odd numbered states.
For the nth even numbered state the quadratic equation to be
solved, $au^2 + bu + c = 0$, has coefficients

$$a = B_1 - B_2$$
$$b = A_1 + A_2 - 2B_1(u_{n-1} - u_R) + 2 B_2 u_p$$
$$c = -A_1(u_{n-1} - u_R) + B_1(u_{n-1} - u_R)^2 - A_2 u_p - B_2 u_p^2$$

and the positive branch of the quadratic solution is used.
Here u_p is twice the particle speed of the final state and u_R
is the solution of $B_1 u_R^2 + A_1 u_R - P_{n-1} = 0$. For the odd numbered
states,

$$a = B_1 - B_2$$
$$b = -A_1 - A_2 - 2 B_1(u_{n-1} + u_R)$$
$$c = A_1(u_{n-1} + u_R) + B_1(u_{n-1} + u_R)^2$$

and the negative branch is used.

To find volume and temperature of a reverberation state,
consider a shock from an arbitrary known initial state (P_{n-1},
V_{n-1}, T_{n-1}) to a final state (P_n, V_n, T_n). The Rankine-
Hugoniot relation is

$$E_n = E_{n-1} + \frac{1}{2} V_o(P_n + P_{n-1})(X_{n-1} - X_n)$$

where $X = V/V_o$.

Also

$$E_n = E_p(X_n) + \frac{3R}{M} T_n \left[1 + \frac{1}{20} \frac{\theta_n^2}{T_n^2}\right]$$

from the equation of state (Sec. III.B). Hence E_n can be eliminated between the equations and the equation for T_n becomes

$$T_n^2 - \frac{M}{3R}\left[E_{n-1} + \frac{1}{2} V_o(P_n + P_{n-1})(X_{n-1} - X_n) - E_p(X_n)\right]T_n + \frac{1}{20}\theta_n^2 = 0.$$

Now all (P_n, V_n, T_n) reverberation states can be calculated if u_p and T_o are given.

Using resistivity theory results (Sec. III.A.4), the resistivity change due to temperature rise is also calculated. Computations show that at 100 kbar the thermal resistivity change is 4% lower than for a single shock. The graph of shock isothermal resistivity versus pressure is not strongly affected by the correction, but the amount of resistivity change attributed to defects generated by the shock is about 20% higher on the MRC curve and 4.5% higher on the W3N curve after the multiple shock calculation for the data points.

2.   Temperature Rise Due to Plastic Deformation

Plastic deformation is an irreversible process. The entropy rise increases the thermal energy, which influences the temperature rise due to the shock wave.

Although the shock transition is achieved by irreversible processes, initial and final thermodynamic states are considered to be equilibrium states on the equation of state surface of the shocked substance. If entropy production can be

expressed as a function of volume, then temperature can be found from an integration of

$$T \, dS = C_V dT + \frac{\gamma}{V} T \, dV \tag{8}$$

along an equilibrium path (the Hugoniot curve) between initial and final states.

According to the theory of irreversible thermodynamics, define a local entropy $S(X_0, X_1, \ldots)$ with functional dependence on local extensive parameters $X_0, X_1, \ldots$ identical to its dependence in equilibrium thermodynamics (Callen, 1960). Then

$$dS = \sum_k F_k \, dX_k$$

where the F_k are local intensive parameters (entropy representation) having the same functional dependence on local extensive parameters as intensive parameters in equilibrium thermodynamics do.

In the shock transition there is entropy production due to plastic deformation and due to the hydrodynamic shock process itself (viscous dissipation) $dS = dS_1 + dS_2$ where

$$d \, S_1 = \frac{V}{T} \sum_j s_j de_j^p = \frac{V}{T} \left(\frac{4}{3} \tau \right) \left(d \, \epsilon_x - \frac{d\tau}{\mu} \right)$$

as in Eq. (5) and (6). An expression for dS_2 can be found using the Rankine-Hugoniot relation

$$dE = \frac{1}{2} \, dP_x (V_1 - V) - \frac{1}{2} (P_x + P_x^1) \, dV$$

where V_1 and P_x^1 are values at the Hugoniot elastic limit. Locally, for the hydrodynamic process

$$dS_2 = \frac{1}{T} \, dE + \frac{P_x}{T} \, dV$$

from the definitions of S and the intensive variables
(Callen, 1960), so that

$$dS_2 = \frac{1}{2} \; \frac{(P_x - P_x^1)}{T} \; \left[1 - \frac{V_1 - V}{P_x - P_x^1} \; \left(- \frac{dP_x}{dV}\right)\right] \quad dV.$$

Substituting dS in Eq. (8) and differentiating with respect to
volume results in an ordinary differential equation for tem-
perature

$$\frac{dT}{dV} + \frac{\gamma}{V} \, T = \frac{4}{3} \; \frac{\tau}{C_V} \; \left(1 - \frac{V}{\mu} \; \frac{d\tau}{dV}\right)$$

$$+ \frac{1}{2C_V} \; (P_x - P_x^1) \; \left[1 - \frac{V_1 - V}{P_x - P_x^1} \; \left(- \frac{dP_x}{dV}\right)\right]. \tag{9}$$

In order to get an estimate of temperature rise due to
plastic deformation, assume C_V and $G \equiv \gamma/V$ are constants.
Work hardening is included by

$$\tau = \tau_1 + \frac{H}{3} \, \ell n(V/V_1) \qquad \text{(Sec. III.D)}.$$

Then

$$T(V) = T(V_1) \; e^{G(V_1 - V)} + e^{-GV} \int_{V_1}^{V} e^{GV'} \; F(V') \; dV'$$

where $F(V)$ is the right hand side of Eq. (9). Integration was
done numerically by the extension of Simpson's rule. (The fit
of Rice, McQueen, and Walsh (1958) was used for $P_x(V)$ on the
Hugoniot curve.)

Calculation shows that the temperature rise in silver
due to work of plastic deformation is insignificant; at 110 kbar
the temperature rise is less than 0.1°C for $\tau_1 = -0.25$ kbar.

3.   Temperature Rise due to Porosity

Suppose a solid has some porosity and that shocked states of the porous solid are nearly on the Hugoniot curve of the full density solid. (We are assuming that the shock collapses the pores.) Work of pore collapse is approximately

$$W_P = -\frac{1}{2} P[(V-V_{P_0}) - (V - V_0)]$$

$$= \frac{1}{2} V_0 P \left(\frac{V_{P_0}}{V_0} - 1\right) ,$$

a linear function of pressure. (V_{P_0} is initial density of the porous solid and V_0 is initial density of the corresponding full-density solid.) The associated temperature rise will approximately be $\Delta T = W_P/C_V$. One percent porosity would give a 20°C temperature rise at 100 kbar in silver. Porosity greater than 0.1% would then noticeably affect resistance changes observed under shock.

Density measurements of the thin foils were not accurate enough to rule out such porosity. At the same time, the writer is not aware of reports of porosity in cold-rolled ductile metal foils. Transmission electron microscopy of cold-rolled foils shows no evidence of voids (Bailey and Hirsch, 1960). High densities of vacancies produced by deformation cause density changes of less than $10^{-3}\%$.

F.   Voltage Droop Correction

In the first experiments attempted, using aluminum impactors, the voltage drop across the potential leads of the silver foil decreased gradually beginning about 0.8 cm before

impact. This droop increased strongly with decreasing separa-
tion and then recovered substantially on impact. The droop was
eliminated by using non-metallic impactors so that all metallic
parts of the projectile were at least 1.2 cm from the impacting
surface.

It was concluded that voltage droop was due to inductive
coupling between the 150 ampere current in the foil and the
moving aluminum plate. Since the experimental configuration
did not have a simple symmetry, a calculation to check this was
not readily obtainable.

On the other hand, an approximate eddy current analysis
was used in order to subtract out the inductive voltage from the
voltage-time profile. Fritz and Morgan (1973) have done an
eddy current analysis with cylindrical symmetry for a metallic
plate moving in a static magnetic field. The essential result
is that for discrete accelerations interspersed with constant-
velocity, the induced emf is proportional to the relative
velocity of the moving plate and the magnetic field source.

A change in the induced emf at time of impact was
observed. This change is attributed to deceleration of the
projectile face. There will also be an induced emf change,
superimposed on the resistance change signal when the shock
arrives at the foil. Assuming a proportionality between induced
emf and relative speed, the induced emf superimposed on the
resistive signal was computed. (The proportionality constant
was obtained from the ratio of observed emf change to relative
speed change at impact.) The computed emf was subtracted from

the observed total signal. For shots 72-065, 72-068, and
72-069, the induced emf values subtracted were 17 mV, 13 mV,
and 23 mV, respectively. Non-metallic impactors were used in
all other shots.

IV.   RESULTS OF EXPERIMENTS AND DISCUSSION

Impact experiments were performed on 19 silver foils. Care was taken to prepare the foils in a uniform and well-characterized manner, and the experiment was designed so as to ensure a state of uniaxial shock compression in the silver. Data output of the impact experiments was in the form of voltage-time profiles which were used to get the resistivity of silver under shock compression. After correcting for resistivity change due to shock temperature rise, the data were compared to resistivity expected under hydrostatic pressure; from this comparison, shock-generated point defect concentrations were determined (Fig. 4). Dislocation models for production of these defects were considered and a particular model of stress relaxation was developed to explain the results of the present work.

In some cases post-shot recovery and examination of foil pieces by optical and electron microscopy was possible. An annealing study of the resistivity was also done on one of the recovered foil pieces.

This chapter gives a detailed discussion of the above results as well as analysis of errors and possible spurious effects.

A.   Summary of Impact Experiment Results

Data were obtained on the resistance changes in silver under shock compression in the pressure range from 27 to

119 kbar. Average initial temperature was 296.4 ± 0.7°K. The resistance change was found to be different for silver of two different purities; higher purity material had larger resistance changes. The resistance change also appeared to differ with annealing. Unannealed foils showed slightly higher resistance changes for a given shock pressure than did annealed foils of the same purity.

Shock results, after subtracting the resistivity changes due to shock temperature rise from the raw shock data (Sec. III.A.4), are significantly higher than hydrostatic results. The difference is attributed to generation of a high concentration of point defects by plastic deformation associated with uniaxial shock compression (see Table II). Both the amount of defects generated in all cases and the different amounts generated in different purity silver are difficult to understand. The higher defect resistivity observed in more pure silver is opposite to the results of quasi-static tensile deformation (Basinski and Saimoto, 1967).

Table I summarizes shot data. Experiments are presented in the order in which they were done. Shot number includes the year and the sequence number of the shot, in that year, for the facility. Foil type, state of anneal (A and UA signify annealed and unannealed, respectively), foil thickness, and resistance ratio follow. Resistance ratio is the ratio of foil resistance at liquid helium temperature and at room temperature, and gives a relative measure of impurity and imperfection content of the foils. Resistance ratios are also affected by scattering of

TABLE I. Results of impact experiments.

Shot No.	Foil Type	Foil Thickness (μm)	Foil Resistance Ratio $\dfrac{R_{4.2°K}}{R_{296°K}}$ X 10^3	Impactor Speed and Type[a] (mm/μsec)	Pressure (kbar)	Voltage Ratio ($\dfrac{E}{E_o}$ at 0.5 μsec)	Initial Rise Time (nsec)
72-065[b]	MRC-A[c]	16.5	3.57	0.637 Al	74.5	1.051	45
72-068[b]	MRC-A	15.6	4.17	0.853 Al	102.1	1.170	65
72-069	MRC-A	17.3	4.14	0.857 Al	103.5	1.073	35
73-009	MRC-A	14.7	4.31	0.390 S	87.1	1.049	37
73-010	MRC-A	14.3	4.38	0.392 S	87.5	1.058[d]	27
73-011	MRC-A	17.0	3.95	0.659 FQ	60.0	1.022	53
73-013	MRC-A	18.0	3.76	0.286 FQ	27.0	1.000	25
73-027	MRC-A	15.9	4.31	0.517 S	115.7	1.120	19
73-028	W3N-A	25.0	2.40	0.531 FQ	48.6	1.035	34
73-029	MRC-UA	16.1	6.85	0.562 FQ	51.8	1.032	36
73-034	MRC-UA	16.0	7.14	0.416 S	92.9	1.087	37
73-036	W3N-A	24.5	2.29	0.395 S	88.2	1.122	84
73-040	W3N-A	24.9	2.39	0.686 FQ	62.4	1.037	32
73-044	W3N-A	24.2	2.38	0.401 S	89.6	1.111	67
73-047	W3N-A	17.6	2.53	0.423 S	94.5	1.149 ± .013	..
73-050	W3N-A	24.0	2.25	0.524 S	117.3	1.185	34
73-051	MRC-A	16.9	4.46	0.525 S	117.5	.....	35
73-056	MRC-A	16.6	4.18	0.89 FQ	83	.....	..
73-059	MRC-A	17.2	4.48	0.530 S	118.6	1.139	34

[a] Al, FQ, and S stand for aluminum, fused quartz, and sapphire impactors, respectively.

[b] Anvils were of Lucalox.

[c] A ≡ annealed, UA ≡ unannealed.

[d] This value read after 0.14 μsec.

electrons at foil surfaces at 4.2°K. To correct them to bulk ratios using Fuchs-Sondheimer theory (Sondheimer, 1952) and a specular coefficient of 0.2 (Nagpal and Duggal, 1972), multiply MRC-A ratios by 0.77, MRC-UA ratios by 0.84, and W3N-A ratios by 0.75. The average bulk resistance ratios are 0.0032 for MRC-A, 0.0059 for MRC-UA and 0.0018 for W3N-A. Measured impactor speed and type and pressure deduced from the impactor and anvil Hugoniot curves (Fowles, 1972) are presented in columns five and six, while column seven gives the ratio of the voltage drop across the silver foil 0.5 microseconds after shock arrival to the pre-shock voltage drop. The last column is the rise time (10% to 90%) of the voltage jump on shock arrival at the foil.

The first two experiments, 72-065 and 72-068, were carried out using ceramic Al_2O_3 anvils; shot 72-069 used sapphire anvils. Although shots 72-068 and 72-069 were shocked to the same pressure and used silver foils cut from the same 3 cm X 5 cm piece of foil, the resistance change was significantly larger using ceramic anvils; apparently the ceramic anvils cause extraneous deformation of the foil. The remaining experiments used polished single crystal Al_2O_3 anvils.

To test whether observed, shock-induced changes in voltage droop across a foil were due to resistance change and not some artifacts, two experiments were carried out monitoring foils with no current flowing through them.

In the initial experiments (73-065, 73-068) two silver foils were put in each sandwich of Al_2O_3 ceramic (G. E. Lucalox);

foil elements were parallel and 1.2 cm apart. Both foils were
monitored in the same way but no external current was sent
through the passive foil. The passive foils exhibited a signal
of about 2 millivolts on shock arrival. This compares to more
than 70 millivolts from active foils carrying 150 amperes of
external current. The 2-millivolt signal is attributed to
inductive coupling. The passive foil was coupled to the high
current in the other foil via eddy currents in the moving metal
impactor. At any rate, we can conclude that the signal observed
on shock arrival at the foil in ensuing experiments is due to
current in that foil. By using Ohm's law we can with confidence
attribute the signal to the resistance change in the foil.

Table II presents the results of shot data analysis
according to Fig. 4. The experimental resistance ratio (col-
umn 1) $R/R_O = E/E_O$ is converted to resistivity (column 2) by

$$\frac{\rho}{\rho_O} = \frac{R}{R_O} \frac{V}{V_O} \qquad \text{(Sec. II.A.5).}$$

The shock temperature rise ΔT_H in column 3 is calculated as
described in Sec. III.E.1, and columns 4 and 5 give the resis-
tivity change due to temperature rise and isothermal shock
resistivity calculated from the results of Sec. III.A.4. The
last column gives the resistivity deviation between isothermal
shock resistivity and calculated hydrostatic resistivity
(Sec. IV.D).

TABLE II. Results of data analysis.

Shot No.	Resistance Ratio $\dfrac{R}{R_0}$	Resistivity Ratio $\left(\dfrac{\rho}{\rho_0}\right)_{\text{Expt.}}$	Temperature Rise ΔT_H (°C)	Thermal Resistivity Change $\dfrac{\Delta\rho_T}{\rho_0}$	Isothermal Resistivity Ratio $\dfrac{\rho(V,T_0)}{\rho(V_0,T_0)}$	Defect Resistivity $\dfrac{\Delta\rho_D}{\rho_0}$
72-065	1.051	0.992	~51	0.16	0.83	--
72-068	1.170	1.086	~74	0.21	0.88	--
72-069	1.073	0.995	71.6	0.190	0.797	0.072
73-009	1.049	0.982	58.6	0.160	0.813	0.058
73-010	1.058	0.990	58.9	0.161	0.820	0.066
73-011	1.022	0.974	39.3	0.113	0.853	0.039
73-013	1.000	0.977	17.6	0.052	0.917	0.013
73-027	1.120	1.031	81.8	0.211	0.810	0.106
73-028	1.035	0.995	31.3	0.094	0.895	0.052
73-029	1.032	0.990	33.4	0.099	0.884	0.049
73-034	1.087	1.014	63.1	0.170	0.834	0.090
73-036	1.122	1.050	59.4	0.162	0.879	0.126
73-040	1.037	0.987	40.8	0.117	0.862	0.053
73-044	1.111	1.039	59.9	0.170	0.870	0.120
73-047	1.149 ± .013	1.071	63.7	0.178	0.894	0.152
73-050	1.185	1.09	82.5	0.220	0.872	0.170
73-059	1.139	1.045	84.0	0.219	0.821	0.122

B. Error Analysis

Contribution to errors in the analysis are found in (1) determination of the shocked state (P,V,T), (2) recording and reading of foil resistance, and (3) assumptions for the model describing the temperature coefficient of resistivity as a function of pressure.

Errors in determination of the shock P-V state originate in the empirical Hugoniot curve and in projectile speed. Hugoniot data for silver has no values below 200 kbar. Hence, the portion of the curve used is an interpolation between the ambient state and data from 200 to 500 kbar. The Hugoniot curve used was from the Zharkov and Kalinen equation of state fit to shock data and to Bridgman's hydrostatic P-V data (Sec. III.B). Disagreement with the fit of Rice, McQueen and Walsh (1958) was 0.0005 and 0.002 in V/V_o at 40 and 120 kbar, respectively. Uncertainties in the projectile speed are about ± 0.002 mm/µsec. This uncertainty implies random uncertainty in the sapphire longitudinal stress state of ± 1 kbar.

The sapphire Hugoniot itself is well established below 120 kbar and should be accurate to within ± 0.5 kbar below 60 kbar and to within ± 1 kbar in the 60-120 kbar range. A fit by Ingram and Graham (1968) for the sapphire Hugoniot $P_x = 444u + 13.6u^2$ was used (u in mm/sec, P_x in kbar). (The Hugoniot data are for 0°, 60°, and 90° orientations relative to the c-axis.)

So the final pressure state in silver is accurate to within ± 1 kbar random errors and ± 0.5 to 1 kbar systematic

errors. The compressed volume state could be subject to a random error of ± 0.001 in V/V_o and a systematic error of up to ± 0.003.

It is worth noting that rough sapphire Hugoniot data were also obtained in the present work. In the sapphire-on-sapphire impacts, shock transit time through the impacted disc was monitored on the silver foil, voltage-time record. Transit time was marked by a 10 millivolt artifact blip on impact and the resistance change in the silver on shock arrival at the foil. The data have scatter reflecting the accuracy of the timing information. However, the data are consistent with the Hugoniot fit for sapphire of Ingram and Graham.

The ratio of shocked foil resistance to unshocked resistance is subject to errors in calibrating the voltage drop across the foil as recorded on an oscilloscope and in the reading of photos of oscilloscope traces. Also, current is not exactly constant--current droop amounts to about 0.15% per microsecond. The baseline for the voltage change was corrected for this current droop.

In the calibration procedure a digital voltmeter was used to monitor the amplitude of calibration voltage pulses recorded on oscilloscopes (Sec. II.G). Several times in the course of experimentation the accuracy of the digital voltmeter was checked against a potentiometer or against another high precision voltmeter; accuracy was within 0.2%.

Accuracy of reading a given photo record is quite good. By accident one record was unknowingly reread three weeks after

the first reading; voltage change readings agreed to within 0.1%. In some cases, however, two different oscilloscope records of the same voltage change ΔE disagreed by 3 millivolts or up to 5%.

The reference voltage level E_0 should be accurate to within 0.5%. Considering all elements of measurement, ΔE is accurate to about 5% and

$$\frac{E}{E_0} = 1 + \frac{\Delta E}{E_0} = \frac{R}{R_0}$$

is accurate to within 0.8% for the range studied.

Calculation of temperature in the shocked state is subject to systematic uncertainty. The thermodynamic calculation is generally accepted as valid for compressions of less than 20%. However, there has been no accurate experimental confirmation of the temperatures. Systematic uncertainties arise because the equation of state is fit to Hugoniot and hydrostatic compression curves; the fit is insensitive to thermal parameters. One can understand this by realizing that it would require a large temperature change to cause a 1% increase in volume at a given pressure; for silver it would take about 200°K temperature change from ambient conditions. Rice, McQueen, and Walsh (1958) state that calculated temperature increases should be accurate to within 10%. In fact, Rice, McQueen, and Walsh's calculated temperatures agree with those from the Zharkov and Kalinen equation of state to 60 kbar and diverge to a difference of 6% at 120 kbar of pressure (Fig. 8).
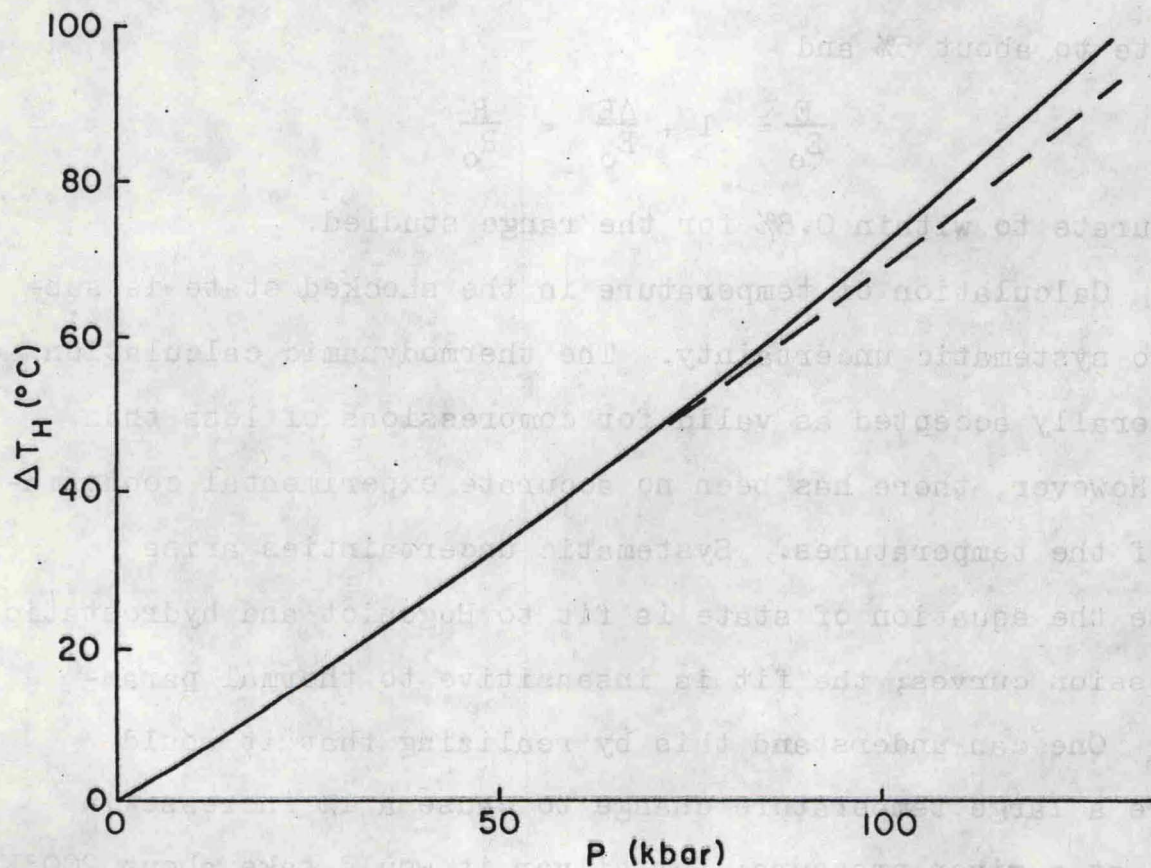
Fig. 8. Hugoniot temperature rise versus
pressure. ————, from Zharkov and Kalinen equation
of state; — — ——, from Rice, McQueen, and
Walsh (1958).

In correcting shock resistance to isothermal conditions the temperature coefficient of resistivity at a given volume (Eq. (3)) must also be calculated. This calculation also is used to extrapolate the hydrostatic pressure-resistivity data beyond 30 kbar (Eq. (4)). There are experimental data on the temperature coefficient of ressistivity as a function of pressure for iron (Clougherty and Kaufman, 1963). Calculated approximate coefficients,

$$\frac{\alpha}{\alpha_o} \approx \left(\frac{\theta}{\theta_o}\right)^{-2} \approx \exp\left[2\,\gamma_o\left(\frac{V}{V_o} - 1\right)\right],$$

(here we assumed γ/V = constant) are 0.4% higher at 50 kbar and 2.9% higher at 100 kbar than experimental results. (The iron data extend over a temperature range of 1000°C.) Bridgman has also measured temperature coefficients of resistance as a function of pressure, but there are contradictions in his work. In one set of experiments he measured resistance as a function of temperature at constant pressure and in a second set made measurements as a function of pressure at constant temperature. In the first set he measured resistance changes in noble metals over a 100°C temperature range at constant pressure of 0 to 12 kbar (Bridgman, 1958). The measured temperature coefficient of resistance is independent of pressure to within 1/4% (α/α_o = 1.00). Assuming $\rho = \alpha(V)T$, this work is inconsistent with Bridgman's other work on pressure dependence of resistance at constant temperature (30°C) where ρ/ρ_o = 0.956 at 12 kbar (Bridgman, 1938). That is to say, in the first work he found α/α_o = 1.00 at 12 kbar, in the latter work α/α_o = 0.956. (From

Eq. (3), α/α_o = 0.96.) This inconsistency remains if one uses

Eq. (4) for relating ρ/ρ_o and α/α_o. Based on the above dis-

cussions, accuracy of the calculated volume dependence of

resistivity for silver is not well known but may be about 3%

over the pressure range studied.

C. Voltage-Time Profiles

Voltage-time profiles for all impact-experiments are

presented in Appendix A. Examples of oscilloscope records of

the profiles are shown in Fig. 9.

The foils remain under uniaxial compression for 0.5 μsec

before a rarefaction wave from the rear sapphire-epoxy interface

(Fig. 1) arrives at the foil. Within another 0.5 μsec rarefac-

tions from the sapphire lateral edges also arrive.) The shock-

induced signal risetime is about 0.035 μsec. During the next

0.5 μsec the voltage level shows time-dependent structure.

Structure depends on pressure level, silver purity, and state of

anneal. That the structure is not random noise can be seen by

comparing the profiles of shots 73-026 and 73-044 (Fig. A.1 (c)

and (d)). The two shots had the same pressure level and were

the same foil type. Overall shape and bumps on the profiles do

roughly match.

Observed signal risetimes range from 19 to 85 nsec, 35

nsec being typical. Aside from the time it takes for foil

resistance to change in response to the shock transition, there

are a number of experimental conditions which also affect rise-

time. These conditions include shock impedance mismatch between
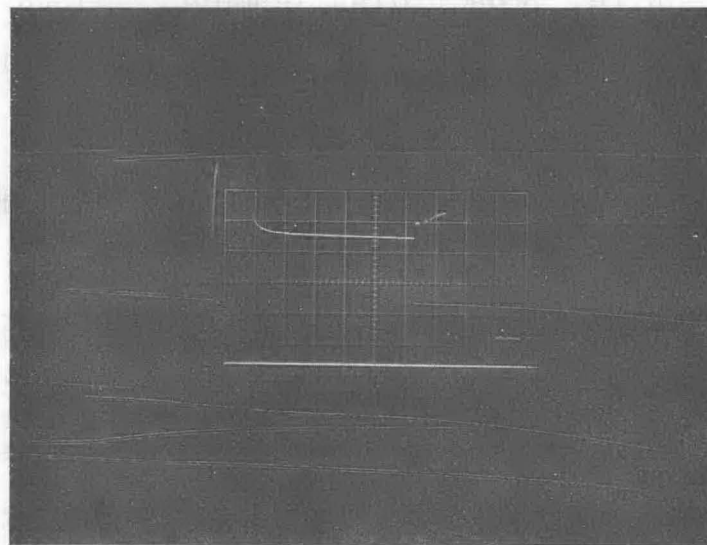
(a)
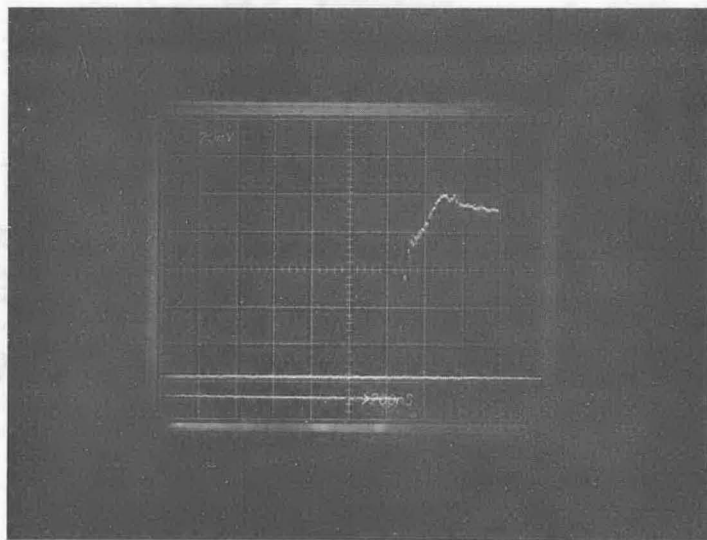
(b)

Fig. 9. Oscilloscope records. (a) Overall record from shot
73-027 showing E_O and ΔE; 0.2 V/div, 3.5 μsec/div. (b) Differ-
ential offset record from shot 73-050 showing ΔE vs. time;
0.02 V/div, 0.2 μsec/div.

silver and sapphire, impact misalignment, and the low-impedance epoxy layer adjacent to the foil edges. The foil reaches pressure equilibrium in about three shock transits across the foil (Sec. III.E.1); this takes 15 nsec. A typical impact misalignment of 0.3 milliradians would mean a time as long as 13 nsec for the shock front to cross the foil. These two time effects are additive. The pressure equilibration time of about 50 nsec for the epoxy adjacent to the foil edges will also degrade signal risetime. In conclusion, the above conditions are sufficient to account for observed risetime; response time of the resistance change is probably obscured.

In the W3N annealed foils the initial rise is followed by a gradual rise in voltage which peaks after 0.25 μsec and then decreases until arrival of the rarefaction wave. The MRC annealed foils typically show an initial overshoot and a following gradual voltage relaxation during the 0.5 μsec of observation. The highest pressure shots, 73-027 and 73-059 (Fig. A.1 (ℓ) and (m)), do not follow this pattern. In the MRC unannealed samples, the initial rise is followed by a gradual increase in the voltage level.

Very close agreement between W3N voltage-time profiles is evident in shots 73-036 and 73-044 at 88.2 and 89.6 kbar, respectively (Fig. A.1 (c) and (d)). The bumps in the profiles are qualitatively the same in size and time value. The two shots were done two weeks apart, and the silver foils used were polished, photo-etched, and annealed in different batches. While one cannot rule out the agreement as due to reproducible

artifacts of the experiment, it is tempting to ascribe the structure as due to time-dependent behavior of the silver resistivity. This behavior will be discussed in Sec. IV.I.

The last shot, 73-059 at 119 kbar (Fig. A.1 (m)) was done in order to see how closely a point on the MRC-annealed ρ versus P curve could be reproduced; all other MRC-annealed shots had been done before the W3N shots. So the last shot tested whether the difference between the W3N and MRC data could be due to subtle variations in experimental procedure over the course of time; the result was somewhat ambiguous. The data point for this shot agrees with other MRC data. As on the other shots, the point corresponds to the resistance level 0.5 μsec after the shock arrives at the foil. The overall voltage-time profile, however, is quite unlike the earlier MRC shot at 115 kbar. The earlier shot showed a fairly steady level for the 0.5 μsec while 73-059 peaks strongly at 0.2 μsec. Shot 73-059 is also unlike the W3N shot at 117 kbar, although the structure in the first 0.2 μsec has some similarity.

Shot 73-040 (Fig. A.1 (b)) was atypical in that there is a 10 nsec initial positive spike followed by a negative signal for 30 nsec; this is attributed to epoxy polarization signal. This shot had a wedge-shaped epoxy layer between the foil and sapphire pieces as thick as 15 μm, much thicker than that of the other shots where the epoxy signal would be too fast to be resolved.

Record 73-056 (Fig. A.1 (s)) is anomalous in that voltage levels are high and do not level off. Foil stretching

(lateral tensile deformation) due to non-planar impact could cause this. Appendix B discusses the resistance change due to stretching; resistance change should increase as time squared. Anomalous behaviors of 73-051 (Fig. A.1 (r)) and especially 73-056 are approximately of this form.

D. Isothermal Results

Because the shock process raises the silver temperature by an amount depending on shock strength, it is necessary to convert the shock resistance change data to isothermal resistivity before comparing it to hydrostatic experiments and theory. Conversion was done using calculations of temperature and temperature coefficient of resistance described in Chapter III.

Since the voltage-time profiles were not square pulses, some judgment was necessary in picking representative values for use in plotting data. The best-characterized point on the profile seemed to be at the end of the viewing window, 1/2 μsec after shock arrival at the foil. Since on many records a more or less steady level had been reached by this time, this value was used for computing ρ/ρ_o data points.

Isothermal resistivity of silver as a function of compression is shown in Fig. 10. All shock data lie well above the calculated hydrostat. The data point at 27 kbar lies slightly above Bridgman's hydrostatic results to 30 kbar. Shock results for different purity silver also differ among themselves. There may be a small effect of annealing prior to shocking in the data (Fig. 11) for the less pure silver.
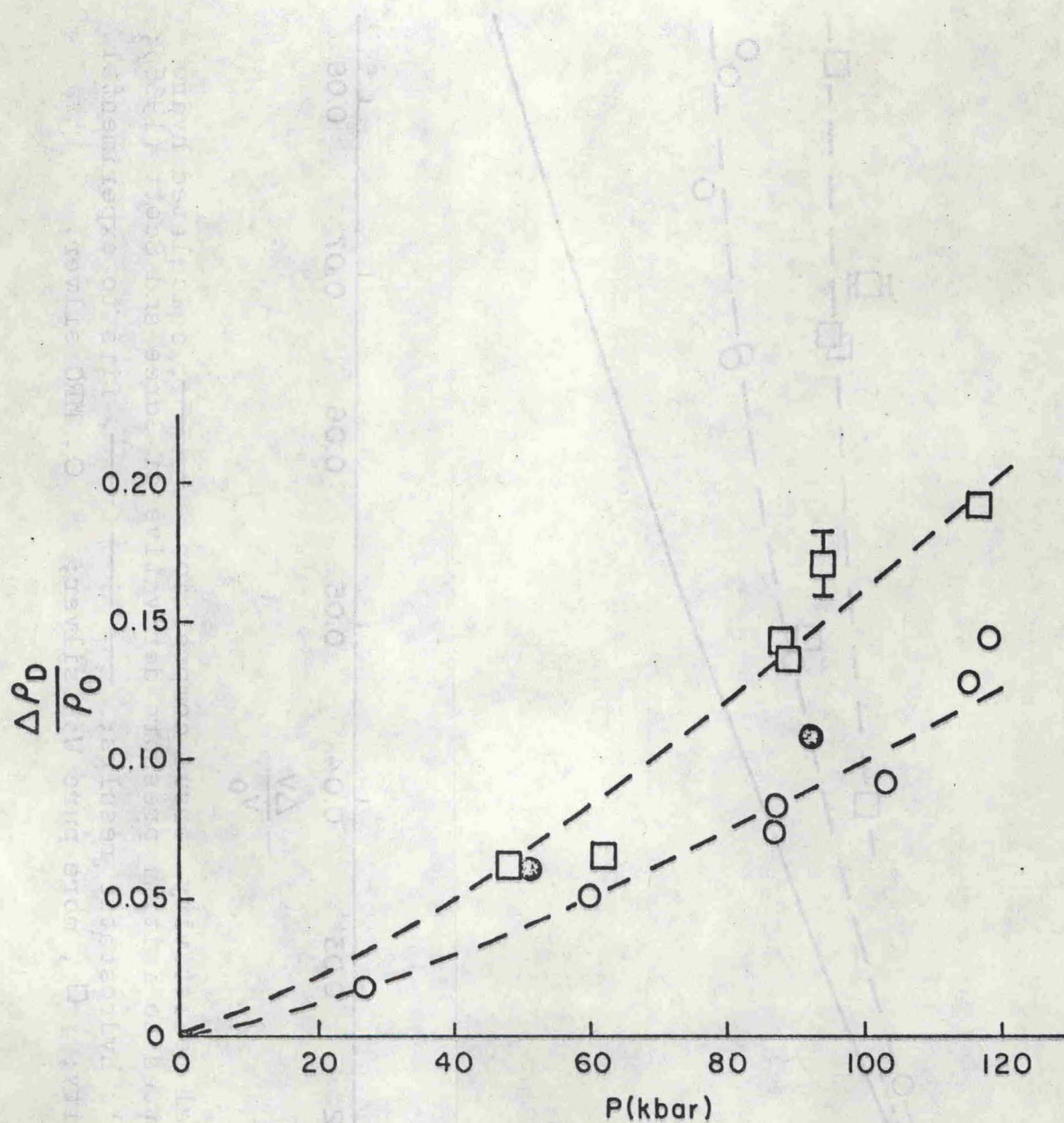
Fig. 10. Isothermal resistivity versus compression. ⸻, calculated hydr[...]
static resistivity fitted to initial pressure derivative of Goree and Scott (196[...]
⸺⸺⸺⸺, Bridgman's hydrostatic results; ⸺ ⸺ ⸺, fits to experiment[...]
[d]ata of different purity; □ , more pure W3N silver; O, MRC silver.

Fig. 11. Deviation resistivity versus pressure.
— — —, fits to experimental data of different
purity; □, more pure W3N silver; ○, annealed
MRC silver; ●, unannealed MRC silver.

Deviation of the shock isothermal resistivity from the hydrostatic results is attributed mainly to resistivity of lattice imperfections generated by plastic deformation associated with passage of the shock wave. Estimated uncertainties in temperature, temperature coefficients of resistivity, and hydrostatic resistivity extrapolation do not account for the difference. The deviation is given by

$$\frac{\Delta \rho_D}{\rho_o} = \frac{[\rho(V,T_o)]_{Expt.} - [\rho(V,T_o)]_{Calc.}}{\rho(V_o,T_o)} \quad ;$$

$[\rho(V,T_o)]_{Calc.}$ comes from Eq. (4). Examination of metals which have been shocked and relieved back to ambient conditions shows evidence of this increased lattice imperfection; evidence is found in changes in microstructure, changes in hardness, and results of annealing studies (O. Jones, 1970; A. Jones, Marden, and Isbell, 1970; Christou, 1971; Rose and Berger, 1968; van Wely, 1968; Kressel and Brown, 1967; Mahajan, 1970; present work, Sec. IV.K).

If we accept the above interpretation of the deviation, the number of defects generated by the shock is quite large. Fig. 11 shows the excess resistivity $\Delta \rho_D/\rho_o$ of the shock data as a function of pressure. At 100 kbar $\Delta \rho_D/\rho_o = 0.099$ for MRC silver and 0.158 for W3N silver. In comparison, shock conductivity data of Keeler and Royce (1971) for copper and iron result in $\Delta \rho_D/\rho_o = 0.12$ and 0.16, respectively. (They corrected their data for shock temperature rise but details of the calculation were not discussed (Duff, 1969).)

Theory and experiments indicate that vacancies are formed preferentially to interstitials in face-centered cubic (f.c.c.) metals (Nabarro, 1967; Rose and Berger, 1968; Christou, 1971; Kressel and Brown, 1967). Electron microscopy of shocked and recovered aluminum and nickel gives some evidence for prismatic dislocation loops formed by the collapse of vacancy clusters (van Wely, 1968; Rose and Berger, 1968).

Actually, imperfections produced by shock deformation will include vacancies, interstitials, dislocations, and possibly deformation twins. Besides evidence for predominance of vacancy production mentioned in the previous paragraph, production of vacancies appears to cause the most resistivity increase for a given amount of energy spent in defect production. Production of interstitials or dislocations to cause a given resistivity increment requires roughly two to three times as much energy as vacancy production. For the record, a resistivity increment of 0.15 $\mu\Omega$cm ($\Delta\rho_D/\rho_o \approx 0.1$) corresponds to a dislocation line density of 8×10^{11} cm/cm^3 in silver.

To find approximate defect concentrations, let us assume for simplicity that all the excess resistivity is due to vacancies. The vacancy concentration then is $x_V = \Delta\rho_D/\rho_V$ where ρ_V is the resistivity per vacancy. Since vacancy resistivity as a function of pressure is not available, we will use the vacancy resistivity at one atmosphere, $\rho_V = 1.3 \pm 0.7$ $\mu\Omega$cm/at.% for silver (Balluffi, Koehler, and Simmons, 1963). Since $\rho_o = 1.6$ $\mu\Omega$cm,

$$\chi_V = \frac{\Delta\rho_D}{\rho_0} \frac{\rho_0}{\rho_V} \approx 1.2 \times 10^{-2} \frac{\Delta\rho_D}{\rho_0} . \qquad (10)$$

At 100 kbar for MRC silver, computed vacancy concentration is about 10^{-3} vacancies/atomic site. (In computation we have assumed that at these high concentrations the resistivity of N defects is still N times the resistivity of a single defect (Martin and Paetsch, 1973).) Defect concentrations generated by severe torsion deformation or radiation damage below 20°K are also of this magnitude (Thom, 1972; Wagner, Dworshak, and Wombacher, 1971). Estimates of equilibrium vacancy concentration at the melting points of metals range as high as 10^{-2} (Kraftmakher and Strelkov, 1970). For the temperatures and pressures in shocked states of the present work, concentrations like 10^{-3} correspond to strongly nonequilibrium defect concentrations. It should be kept in mind that the shock temperature rise is roughly proportional to pressure so that defects generated by two different shock strengths reside in different thermal as well as pressure environments.

These shock experiments correspond to deformation experiments at cryogenic temperatures in that defects generated in both cases are not allowed to migrate to the surface. In the cryogenic case the constraint is low thermal energy of the solid; in the shock case it is short time scale of the experiments.

E. Dislocation Models

We are concerned with defect production at high strain rates where the strain is due to plastic deformation associated

with uniaxial shock compression. In seeking explanations of
defect production in terms of dislocation models, vacancy type
defects as opposed to interstitials will be considered to be
the dominant defect. As previously mentioned, experimental evi-
dence in face-centered cubic metals indicates vacancies are
produced in preference to interstitials.

The concept of vacancies being produced by moving dis-
locations was first proposed by Seitz (1952). Mechanisms for
this production include intense local heating due to dislocation
motion; approach of edge dislocation segments of opposite sign
on adjacent glide planes; and nonconservative motion (motion out
of the surface defined by a dislocation's line and Burgers
vector) of jogs on dislocations (Nabarro, 1967). It is gen-
erally accepted that the most important process for this dis-
cussion is the last one.

Short jogs are formed by intersection of a dislocation
by a second dislocation having a small Burgers vector (Hull,
1965). A dislocation on one glide plane becomes jogged in
passing through the network or forest of dislocations on another
glide plane. Jogs, having edge character, can move conserva-
tively only in the direction of the Burgers vector. For screw
dislocations, motion is not confined to that direction, so non-
conservative motion of jogs on screws will occur. The non-
conservative motion of these jogs being dragged along by a
moving dislocation generates vacancies or interstitials depend-
ing on the sign of the jog (Fig. 12).
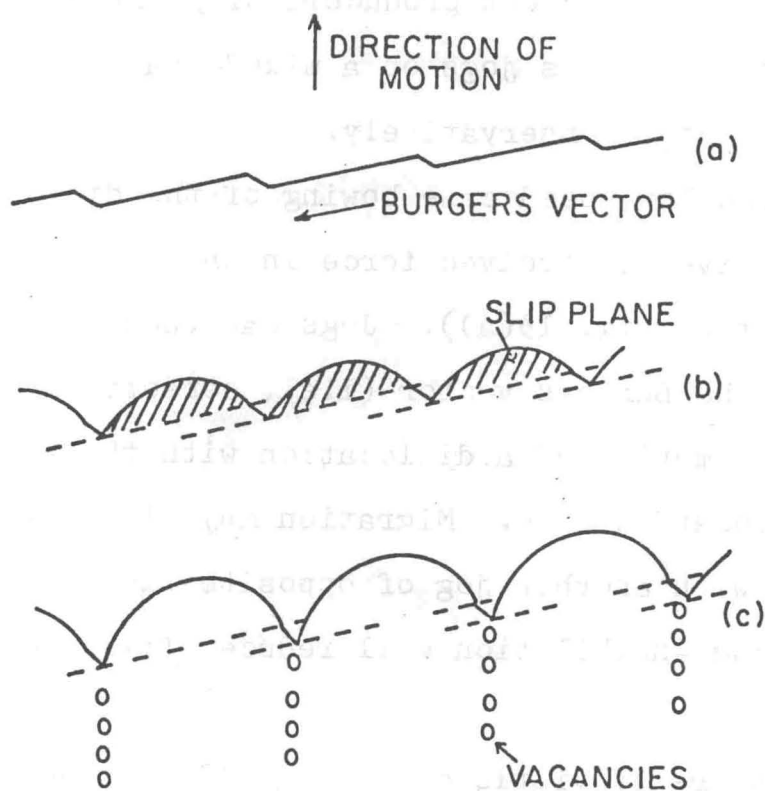
Fig. 12. Motion of a jogged screw
dislocation. (a) Straight dislocation under
zero stress. (b) Dislocation bowed out in the
slip plane between jogs due to applied shear
stress. (c) Motion of dislocation after reaching
critical stress, leaving trails of vacancies
behind the jogs. (After Hull (1965).)

Weertman (1961) has considered production of point defects by dislocations moving at relativistic speeds. For most dislocations the limit speed is the shear wave speed for that solid. He predicts that relativistic ($v > 0.95\ c_s$) dislocations will be much more efficient producers of point defects than slow ones; at low speeds jogs on a mixed-character dislocation may be able to move conservatively.

For the low-speed case bowing of the dislocation due to drag of jogs gives a resolved force in the direction of the Burgers vector b (Fig. 13(a)). Jogs can then move in the direction of the Burgers vector (i.e., conservatively) by combining overall motion of a dislocation with their own migration down the dislocation line. Migration may also lead to their annihilation with another jog of opposite sign. Both conservative motion and annihilation will reduce efficiency of defect production.

In the relativistic case (Fig. 13(b)) jogs would have to move at supersonic speeds in order to move in the direction of the Burgers vector. Furthermore, the reduced bowing of the dislocation line at high speeds (due to increased self-energy) will retard jog migration down the line. Therefore, one concludes that jogs on high-speed dislocations will have to move nonconservatively and produce a trail of point defects. According to Weertman, experimental observation in fast deformation of defect concentrations larger than found in slow deformation to the same strain will be confirmation of the presence of relativistic dislocations. At ordinary temperatures he

DIRECTION OF DISLOCATION MOTION

DIRECTION OF JOG MOTION

b

A

(a) SLOW DISLOCATION

DIRECTION OF JOG MOTION

b

A

VACANCIES
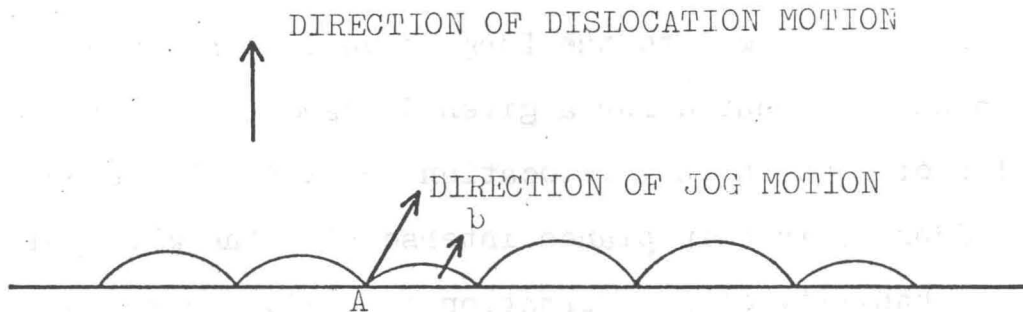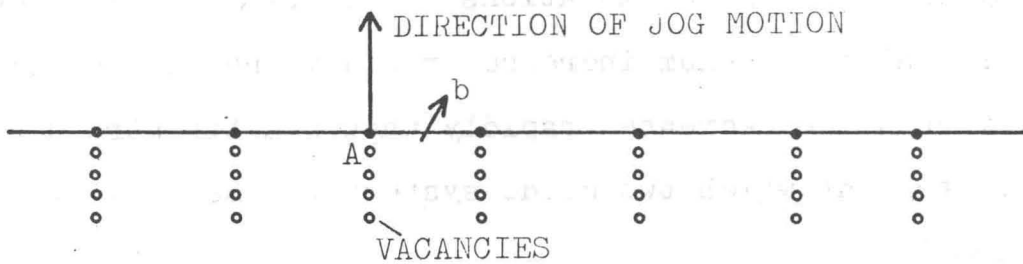
(b) FAST DISLOCATION

Fig. 13. Motion of jogged dislocations of mixed character at low and high speeds. (a) Low speed dislocation. (b) Dislocation speed approaching shear-wave speed.

estimates the stress on a dislocation required to bring it to relativistic speed to be about 1 kbar; this conclusion is supported by work by Granato (1973).

In summary, rate of formation of vacancies by dislocation motion will depend on concentration of jogs on the dislocation, jog speed normal to the Burgers vector, and mean number of vacancies created for a given distance of jog travel. Concentration of jogs on the dislocation in turn will depend on dislocation density in slip planes intersecting the glide plane and on the probability of jog formation in a given dislocation-dislocation interaction (Nabarro, 1967).

There is indirect experimental evidence for point defect formation by intersecting dislocations. Electrical resistance of single crystal molybdenum increases rapidly and mass density of potassium chloride decreases rapidly when plastic strain reaches the stage at which two glide systems become active. (Nabarro, 1967).

The above discussion indicates that theory of the rate of formation of vacancies as a function of plastic strain and strain rate will depend on the spatial and velocity distributions of dislocations. Nabarro (1967) cites two simple models based on these ideas which predict vacancy concentrations depending respectively on the three-halves and five-fourths power of strain. Saada (1961) has developed a model for defect production in tensile deformation valid for annealed f.c.c. metals. The concentration of point defects generated is given by

$$x_{pd} = \frac{H'}{E} \int_0^\epsilon \sigma(\epsilon')d\epsilon'$$

where E is the modulus of elasticity, ϵ is the relative elongation, σ is the stress applied, and H' is a numerical factor of the order of 1/3 (van den Beukel, 1969). If stress is linearly related to strain in the plastic region, then Saada's relation predicts that defect concentration depends quadratically on plastic strain (compare to Nabarro's models). The above models do not explicitly account for the effect of strain rate.

There are a number of empirical relations published for low strain rate deformation which suggest proportionality between

1. defect concentration and square of flow stress (Kovacs, Nagy, and Feltham, 1964; Gindin, Khotkevich, Neklyudov, Lebedev, and Bobonets, 1971);

2. defect concentration and dislocation density (Kovacs et al., 1964);

3. flow stress and square root of dislocation density (Kovacs et al., 1964; Briley and Hirsch, 1960);

4. stored energy and square of shear stress (Wolfenden, 1969; Nakada, 1965).

Relation 3 is also derived in work hardening theories for the rapid work hardening region (stage II) (Hirsch, 1967). The above relations can be incorporated into a single scheme if we assume a Saada-type relation, and linear relations between stress and strain, and between flow stress and square root of dislocation density.

Whether this scheme is descriptive of the high strain-rate deformation associated with shock waves is not known. At

least, coefficients of proportionality will probably be different from those at low strain rates. For the shock case the scheme implies

$$\chi_{pd} \propto \epsilon^2 - (\epsilon^1)^2 \approx \epsilon^2 = (\ln \frac{V}{V_o})^2 \quad ;$$

ϵ^1 is the uniaxial strain at the Hugoniot elastic limit. Fig. 14 shows that this relation gives a fair fit to the data. For W3N $\chi_V = 0.36 \, \epsilon^2$ and for MRC $\chi_V = 0.22 \, \epsilon^2$ using Eq. (10). A plot of $\ln(\Delta \rho_D / \rho_o)$ versus $\ln(-\epsilon)$ actually shows χ_{pd} is proportional to $\epsilon^{3/2}$ (as in one of Nabarro's models) rather than ϵ^2 (Fig. 15). For the expression $\chi_V = A(-\epsilon)^n$ the results for W3N foil are A = 0.14, n = 1.58, and for MRC foil are A = 0.051, n = 1.46.

It is of interest to calculate the defect concentration predicted for silver by Saada's relation. For silver H' = 0.28 (Dawson, 1965b), E = 0.71 Mbar and $\sigma \, d\epsilon^p$ is taken from Sec. III.C and III.D. For a final strain of -0.08 the relation predicts a defect concentration of 2×10^{-5}; about two orders of magnitude below values computed from the shock data. Hence, within the framework of our assumptions that all deviation resistivity is due to vacancies, and that shock yield stress can be computed from low strain-rate tensile data, Saada's relation is not valid at the high strain rates associated with shock compression.

F. Energy Balance

One important check on the assertion that deviation from the hydrostat is due to defect resistivity is energy balance.
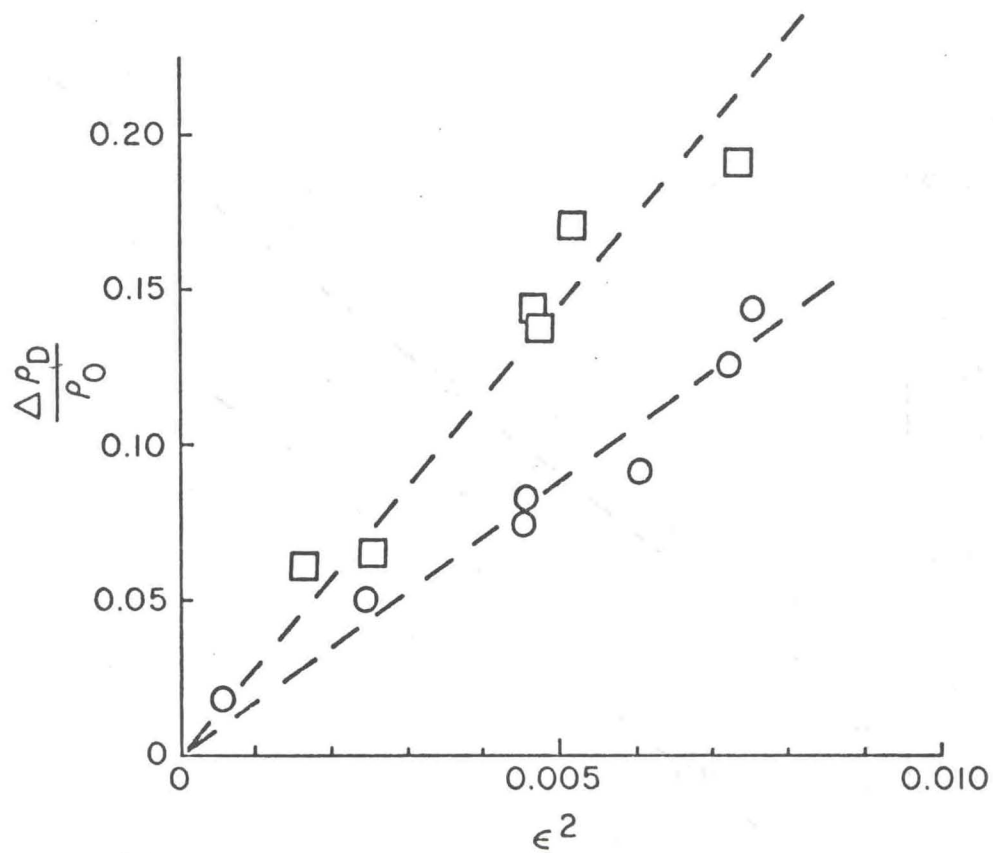
Fig. 14.   Deviation resistivity versus
square of strain.   □ , more pure W3N silver;
O , MRC silver.

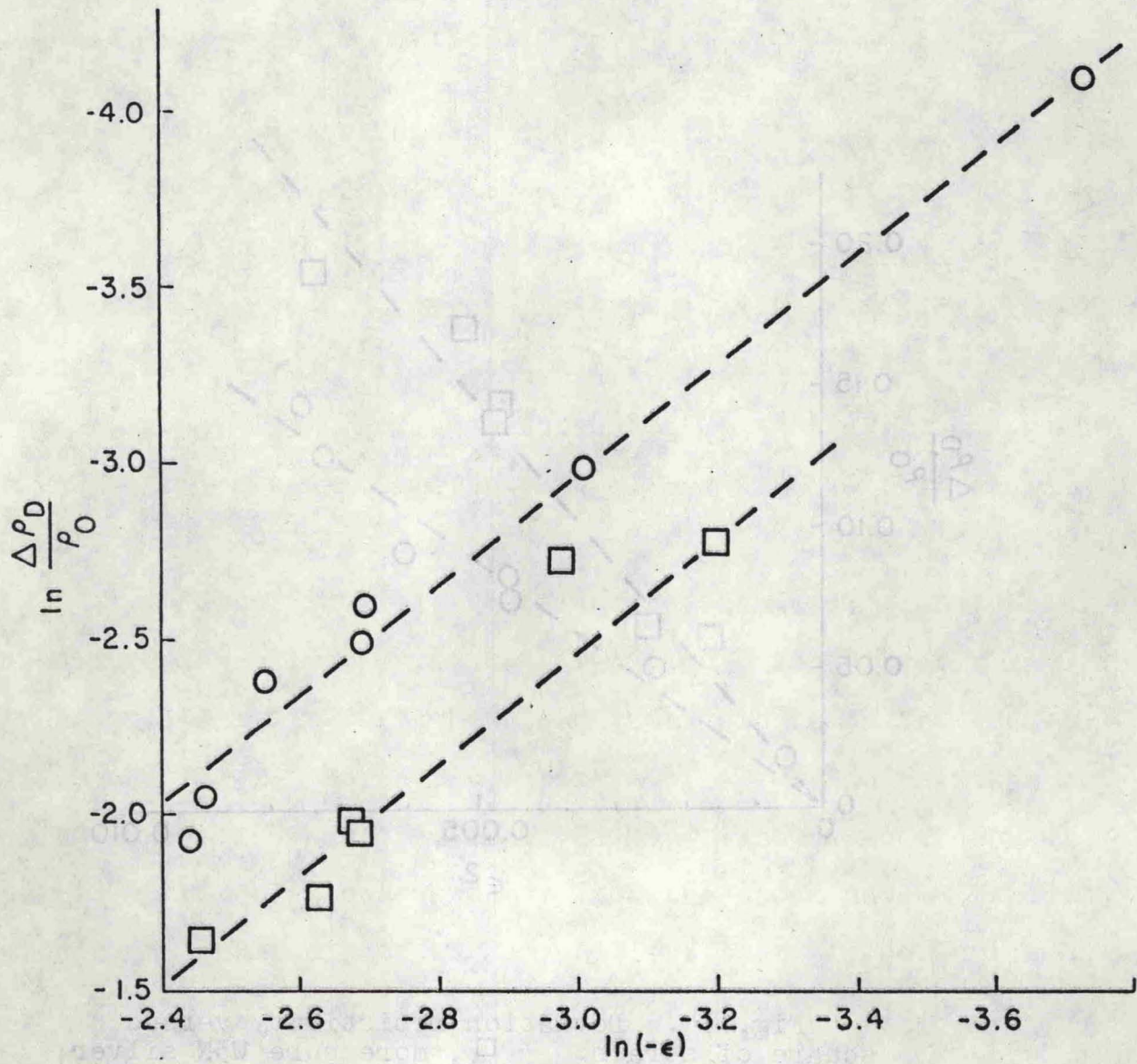Fig. 15. Logarithmic plot of deviation
resistivity versus strain. □ , more pure W3N
silver;   O, MRC silver.

Was enough plastic work done to generate the defect concentration asserted? At 100 kbar the elementary calculation of work of plastic deformation gives 3.9 bar cm^3/g (Fig. 6). At one atmosphere of pressure, vacancy formation energy in silver is 1.8×10^{-12} erg/vacancy (Koehler, 1969). As with vacancy resistivity, the dependence of monovacancy formation energy on pressure is not known. Using the one atmosphere value for formation energy implies an energy of formation of 11 bar cm^3/g for a monovacancy concentration of 10^{-3}. This energy is 2.8 times larger than the work of deformation calculated. An initial Hugoniot elastic limit of three or four kbar would be needed to balance work with formation energy of the vacancies, even if none of the plastic work were converted to heat. More work hardening would also help increase plastic work. Since the HEL used in calculating the plastic work was estimated from the yield stress in tension at low strain rate it could be in serious error. A number of materials have HEL's larger than values calculated from yield stress at low strain rate (Sec. III.C). In lithium fluoride the HEL after several millimeters of propagation was steady at as much as 100 times the static yield stress (Asay et al., 1972). In addition, the resolved shear stress in single crystal copper under shock loading is 20 times the quasi-static value (Jones and Mote, 1969).

A further difficulty is that a fraction of the work of deformation is dissipated as heat. In quasi-static deformation only 5 to 10% of plastic work is stored in the form of lattice imperfections (Williams, 1967). It should be noted that the

fraction of stored energy which is in the form of point defects
as opposed to dislocations and other imperfections may vary
from 3 to 70% depending on purity, strain, and temperature of
deformation (Clarebrough, Hargreaves, and Loretto, 1962). When
nickel and copper are shock loaded, the stored energy is twice
that obtained when the metals are quasi-statically deformed to
the same strain (Leslie, 1973). Kressel and Brown's annealing
study of shock-deformed and cold-rolled nickel (1967) showed
point defect concentrations and dislocation densities after
shocking to be much larger than for cold rolling near 0°C to
the same strain value. Flow stress and hence work may have been
different at the two strain rates, so that the difference in
fraction of energy stored is not known. Assuming conservatively
the 5 to 10% figures for stored energy fraction, an average HEL
of 10 to 20 kbar in the first 20 µm of shock propagation in
silver would be necessary to balance energy for a 100 kbar
shock.

An aspect of shock response of solids which is relevant
to the problem of energy balance is stress relaxation in
elastic-plastic solids. For a stress relaxing solid it has
been hypothesized that initial elastic stress in the solid at
the face where the shock enters the material is equal to the
total stress acting on the face, provided that the loading wave
has a very fast rise time (Asay et al., 1972). This means very
high initial stresses on the dislocations in their glide planes.
As the shock propagates into the material, the elastic stress
relaxes with time and distance to a steady state level

characteristic of the shock response of that solid. At the
same time the plastic strain is gradually accommodated by dis-
location glide, multiplication, nucleation, and by twinning.
If such behavior occurs in the first 20 μm of shock-wave propa-
gation in the silver used, it is not difficult to imagine an
average elastic stress over distance and time which is a size-
able fraction of a 100 kbar driving stress.

Note should be taken that some very pure metals are not
elastic-plastic in behavior but visco-plastic. They begin to
flow at a measurable rate as soon as a small stress is applied,
and the rate increases in proportion to stress until some rate
limit is reached. Gilman (1968) showed that this results in
very rapid plastic relaxation of shear stress. Whether this
occurs in the silver used here is not known.

G. Model for Effect of Purity
on Shock Resistivity

In this section a model based in stress relaxation
processes is developed for the purity effect on shock resis-
tivity. Fig. 10 shows the effect of purity on resistivity
results. A greater deviation from hydrostatic resistivity
occurs for the more pure silver (W3N). Resistance ratios be-
tween room temperature and 4.2°K indicate that W3N silver speci-
mens have an impurity concentration about 45% less than MRC
specimens. As mentioned in Sec. II.D, MRC silver was specified
as 5N and W3N silver as 3N pure by the supplier.

This effect of purity is opposite to low strain rate
deformation results where, when a purity effect is noted, there

is more resistivity change for lower purity material (Blewitt et al., 1955; Tanaka and Watanabe, 1972; Basinski and Saimoto, 1967).

Effect of purity has been noted in other shock experiments. Experiments in lithium fluoride showed tensile yield stress to increase smoothly with initial defect concentration (either impurity atoms or irradiation-induced point defects) (Asay et al., 1972). Shock experiments on the same materials showed precursor decay rate to have a minimum for an intermediate concentration of 210 ppm divalent impurities. It is asserted that dislocation mechanisms for plastic flow at very high strain rates are different at higher and lower defect concentrations. At concentrations higher than 210 ppm the dominant mechanism is considered to be heterogeneous nucleation of dislocations at impurity clusters. At lower concentration dislocation multiplication is the dominant deformation mechanism.

If we take these results over to silver we would expect higher elastic limit values after relaxation for the less pure silver (MRC). This would imply greater plastic work and hence higher defect concentrations for it, contrary to the present resistivity experiments.

A more fruitful way of looking at it is to speculate that W3N foil impurity concentration corresponds to the level for minimum precursor decay rate in silver. If we also suppose that significant relaxation is going on in the first 20 μm of travel, we will expect higher transient elastic stress levels in the W3N foils than in the MRC foils (Fig. 16). Let the
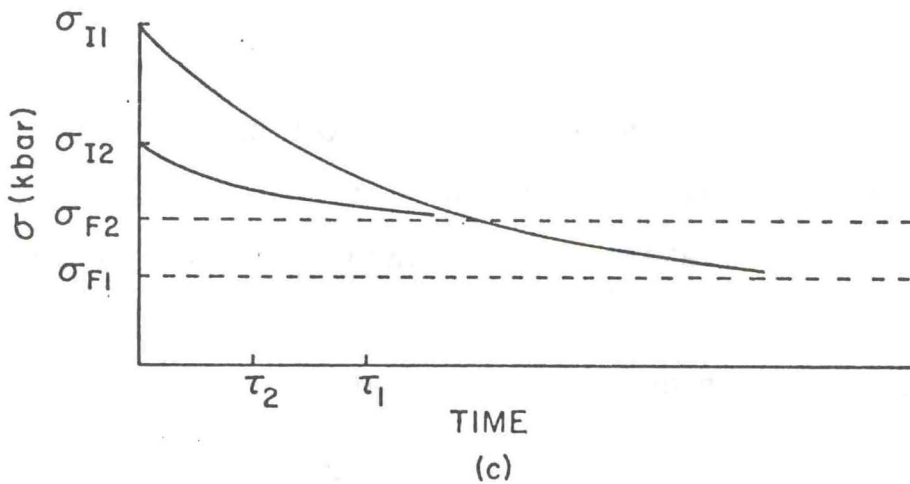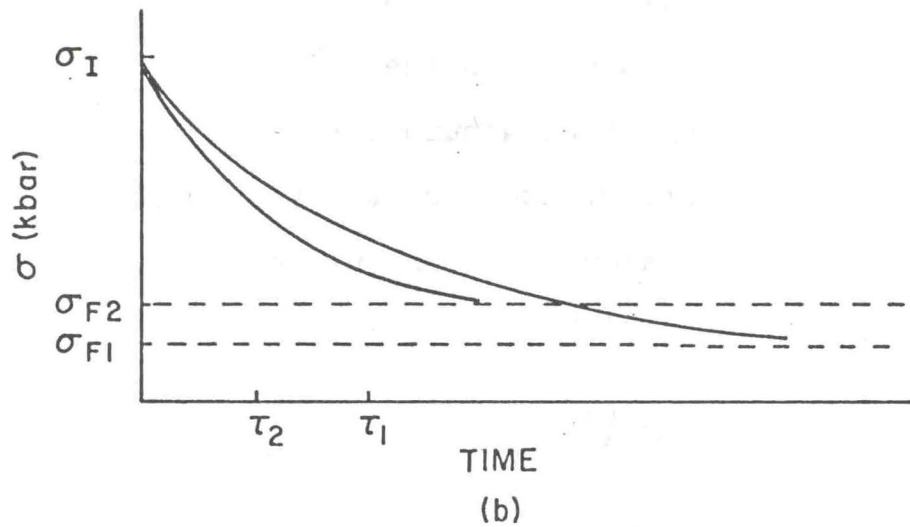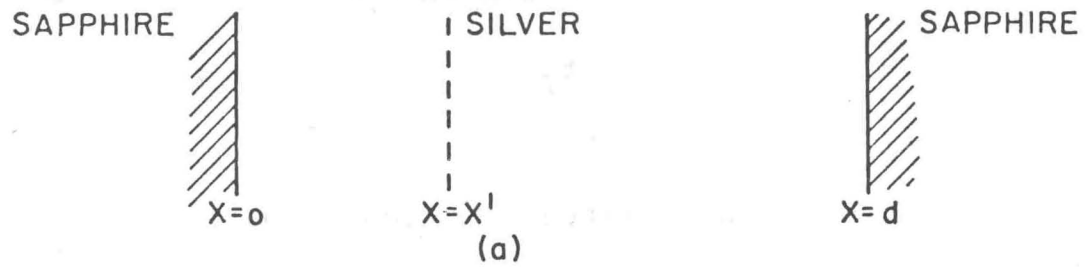
Fig. 16. Stress relaxation dependence on purity. (a) Sandwich configuration; shock wave propagates to the right. (b) Stress relaxation at x = 0; material 1 is more pure. (c) Stress relaxation at x = x'; material 1 is more pure.

strain be an explicit function of time t . Assuming a Saada-
type relation at a given position in the foil (Fig. 16a),
we have

$$\chi_{pd} = K \int_0^{t_f} \sigma(t) \frac{d\epsilon}{dt} dt \quad,$$

where K is some undetermined constant. (Defect concentration
will be a function of position because the peak elastic stress
decays as the wave propagates into the foil.) The following
sample calculation using these assumptions shows that computed
defect concentrations are greater for the W3N, more pure silver.

For the sample calculation let us model the relaxation
process at a given material point by

$$\epsilon = \epsilon_F \left(1 - e^{-\frac{t}{\tau}} \right)$$

and by

$$\sigma = \sigma_F + (\sigma_I - \sigma_F) e^{-\frac{t}{s}}$$

where τ and s are characteristic relaxation times for strain
and stress, respectively, ϵ_F is final strain, σ_I is initial
yield stress at that material point, and σ_F is the steady state
yield stress.

The result for defect concentration is

$$\chi_{pd} = K\sigma_F \epsilon_F \left[1 - \exp(-\frac{t_F}{\tau}) + \frac{rs}{s+\tau} \left(1 - \exp(-t_F(\frac{s+\tau}{s\tau})) \right) \right] \quad;$$

$r \equiv (\sigma_I/\sigma_F - 1)$. For times long compared to relaxation times
the result is

$$\chi_{pd} = K \sigma_F \epsilon_F (1 + \frac{rs}{s+\tau}). \tag{11}$$

Let us use Eq. (11) to calculate the relative defect concentration of W3N and MRC silver foils using hypothetical values of relaxation times and stress levels which are consistent with our assumptions. Let material 1 be the more pure W3N and material 2 be MRC silver. In accordance with our assumptions the following statements will hold:

1. Material 1 will have longer relaxation times than material 2.

2. At x' (Fig. 16 (a)) material 1 will have a larger value of σ_I and a smaller value of σ_F than material 2 (Fig. 16 (c)).

For simplicity, let $s = \tau$. Let $\tau_1 = 2\tau_2$, $\sigma_{F1} = 1.8$ kbar and $\sigma_{F2} = 3$ kbar in proportion to impurity concentration in the foils, and let $\sigma_{I1} = 7$ kbar and $\sigma_{I2} = 4.5$ kbar in accordance with their prescribed elastic precursor decay rates. (Keep in mind two processes: (1) peak elastic stress on the wave front decays as the wave propagates through the foil; (2) at a given material point the elastic stress decays in time until steady state is reached.) For any common final strain value

$$\epsilon_F = \ln(V/V_o),$$

at $x = x'$ we find

$$\frac{x_{pd}\ (1)}{x_{pd}\ (2)} = 1.17 \quad ;$$

the more pure silver has higher defect concentration in agreement with the experimental results. Higher values of σ_I increase the ratio. To compare to experiment, the ratio would need to be averaged over the foil thickness.

The model predicts the ratios of defect concentrations for different purities to be independent of final strain. Inspection of Fig. 11 shows that this agrees very well with experimental results; assuming proportionality between defect concentration and deviation resistivity, we find in the range 20 to 120 kbar

$$\frac{x_{pd}(W3N)}{x_{pd}(MRC)} = 1.64 \pm 0.05$$

from the curves fitted to the data. This constant ratio then is partial confirmation of the model. However, any model which predicts defect concentration proportional to the same power of strain for all purities will give the same result.

To recapitulate, the fundamental model assumptions are the following:

1. Elastic stress decays with distance of wave propagation and with time at a material point.

2. The more pure material has the lower elastic stress decay rate.

3. A Saada-type relation for defect production; defect concentration generated is approximately proportional to the work of plastic deformation.

The model is admittedly speculative and can only be tested by more experimentation.

It should be noted that if significant stress relaxation is actually present in the experiments, then equation of state calculations used to find P-V-T states will not be entirely correct. The equation of state analysis assumed steady state conditions in the shock process. The greatest correction would probably be on temperature calculations.

Another point that should be mentioned is that if during the experiments defect concentration and hence resistivity are functions of position in the foil, then the resistance measured is

$$R = \frac{L}{A} \quad \frac{1}{<\sigma>}$$

where $<\sigma>$ is the mean value of the electrical conductivity over the foil thickness and $<\sigma> = <\frac{1}{\rho}> \neq \frac{1}{<\rho>}$.

H. Effect of Anneal on Shock Resistivity

Part of the experimental program was to determine the effect of high-temperature annealing on the resistivity change of cold-rolled silver foil in response to shock waves. Two shots were done on unannealed MRC foil. Isothermal resistivity data for the unannealed foil are slightly higher than for annealed (Fig. 11). More data would be necessary to know if this deviation is real.

Since most point defects in silver will annihilate or diffuse to the surfaces at room temperature (Dawson, 1965), the main effect of high temperature anneal is removal of dislocations from the cold-rolled foil; impurity clustering could also take place. Density of dislocations removed by anneal was calculated from liquid helium temperature resistance measurements on MRC foil before and after anneal. Using published dislocation resistivity in silver (Basinski, Dugdale, and Howie, 1963)

$$\Delta\rho_D = (1.9 \times 10^{-13} \ \mu\Omega cm^3) \ \Lambda$$

(Λ is dislocation line density), the result was 2×10^{10} cm/cm^3.

This dislocation density is within reason for cold-rolled metals; $5 \times 10^{11}/cm^2$ is quoted by Hull (1965) for heavily cold-rolled metal.

Previous shock work shows a variety of effects of initial dislocation density on shock response. Work on single crystal copper shows that 3.5% prestrain reduces the initial elastic stress jump after 5 millimeters of shock propagation to near zero; a ramping precursor wave follows the jump (Jones and Mote, 1969). (The prestraining increased dislocation density to $10^9/cm^2$ from $10^6/cm^2$.) This ramping from zero stress is probably indicative of visco-plastic behavior (Gilman, 1968). Shock hardening of annealed nickel, on the other hand, was independent of prestrain, prestrained by cold rolling to as much as 80% reduction in thickness (Rose, Berger, and Inman, 1967). Also, a change of an order of magnitude in initial dislocation density did not significantly affect precursor decay in lithium fluoride (Asay et al., 1972).

Within the context of the model developed in Sec. IV.G, the lithium fluoride results would imply about the same defect concentration for annealed and unannealed silver. From the standpoint of the jog model discussed in Sec. IV.E, one might expect greater initial forest dislocation density in unannealed foil to result in more jogs and hence more defects. This is one possible explanation of the trend of the data.

I.   Discussion of Resistivity Time Dependence

In this section possible physical interpretations of the structure of the voltage-time profiles are discussed.

Observations in shock experiments indicate that in some materials stress relaxation or at least some deformation processes continue at a material point until times on the order of a microsecond after shock arrival (Jones, 1970; Barker, 1968). It is possible that the resistance-time structure observed for 1/2 microsecond in the present experiments may result from such processes. A gradual resistance increase after the main shock arrival was observed in unannealed MRC and annealed W3N silver (Fig. A.1). This could be explained by a reduced rate of defect production after the strain rate has decreased from its maximum value.

A gradual decrease in resistance as observed in annealed W3N silver after 1/4 microsecond and in annealed MRC silver for 1/2 microsecond (Fig. A.1) could be explained in terms of point defect annihilation and rearrangement; according to Martin and Paetsch (1973) the resistivity of a cluster of N vacancies or interstitials is given by

$$\rho(N) = \rho(1) \ N^A$$

where A = 0.7 to 0.9 and N < 100.

A problem with such an interpretation is that in 10^{-6} seconds no macroscopic diffusion can take place. Using a diffusion coefficient for silver at one atmosphere D = 1.6 x 10^{10} cm^2/sec (LeClaire, 1949), a diffusion distance of less than one lattice spacing is found: $x_{rms} = (Dt)^{1/2}$. At the same time we realize that a vacancy could make many jumps in 10^{-6} seconds, since the atomic vibration frequency is of the order of 10^{13}/sec, so that some clustering due to local migration

could still take place. Vacancy motion and clustering at high
concentrations of defects may be aided by stress fields asso-
ciated with the imperfections; this might be especially true in
the jog trails (Fig. 12).

In conclusion, there may be valuable information in the
time-dependent structure of the resistance change, but enough
ambiguity exists among the records to discourage attempts at
detailed conjecture on the physical meaning of the resistance-
time structure.

J.   Heat Flow Calculation and Discussion

There is significant heat flow into the silver foil
from the epoxy bonding layer during the impact experiment.
Epoxy being very compressible gets much hotter than silver when
shocked. The single shock temperature rise at 120 kbar in
epoxy is about 800°C (McQueen et al., 1970); silver temperature
rises about 90°C and sapphire temperature about 16°C. In these
experiments, where the shocked state is reached by wave rever-
berations, the epoxy temperature rise is approximately 370°C at
120 kbar.

The one-dimensional heat flow equation

$$\left(\frac{\partial u}{\partial t}\right)_x = k \left(\frac{\partial^2 u}{\partial x^2}\right)_t$$

was solved for three slabs, epoxy-silver-epoxy (u is tempera-
ture, t is time, x is position, and k is material diffusiv-
ity). Details of the solution are given in Appendix D. The
solution does indicate significant heat flow into the silver

from the epoxy in 0.5 microseconds. The sandwich reaches thermal equilibrium in about a millisecond.

Accurate estimates of the temperature rise are not possible because of incomplete knowledge of epoxy thickness and of variation of the thermal conductivity of epoxy with increasing pressure and temperature. Values for these two epoxy parameters are decisive in determining the temperature rise due to heat flow in silver.

Micrometer measurements of the sandwich thickness indicated a total epoxy thickness of -0.5 ± 2.5 μm, the uncertainty being indicative of the micrometer accuracy. This indicates a typical epoxy layer of less than 1.2 μm average thickness; perhaps about 0.6 μm is typical. One would not expect a thinner layer as the silver foil thickness measurements indicated a thickness nonuniformity of about $\pm$ 0.6 μm. Computation[2] shows temperature rise in silver in 0.5 microseconds is independent of epoxy layer thickness for thickness greater than about 1.5 μm. This is because of the poor thermal conductivity of the epoxy.

The behavior of the thermal conductivity of epoxy with pressure and temperature is not known. Experimental work on thermal conductivities of dielectric materials shows them to increase with increasing pressure (0 to 30 kbar) (Bridgman, 1958; Andersson and Backstrom, 1973). Similarly, increase in temperature increases thermal conductivity; melting or decomposition might change this behavior.

---

[2] The author acknowledges the assistance of J. Sy in getting a working computer program for this calculation.

Table III shows estimated results for the temperature rise and resistivity change in silver due to heat flow 1/2 microsecond after shock arrival, where the resistivity change is given by

$$\frac{\Delta\rho(HF)}{\rho_o} = \frac{\alpha(V)\Delta T_{HF}}{\rho_o} \quad .$$

TABLE III. Results of heat flow calculation. Temperature rise and resistivity change due to heat flow as a function of pressure for two different foil thicknesses. Epoxy layer thickness used in the calculation was 0.6 µm.

Foil Thickness (µm)		Pressure (kbar)				
		25	50	75	100	120
16	ΔT_{HF} (°C)	1.1	2.8	3.4	2.6	1.2
	$\dfrac{\Delta\rho(HF)}{\rho_o}$	0.004	0.009	0.010	0.007	0.003
24	ΔT_{HF} (°C)	0.7	1.9	2.5	2.3	1.7
	$\dfrac{\Delta\rho(HF)}{\rho_o}$	0.002	0.006	0.007	0.006	0.004

The MRC foils were about 16 µm thick while all W3N foils except one were about 24.4 µm thick. These estimated resistivity changes can account for some of the resistivity deviation between shock and hydrostatic results; as much as 22% in MRC silver and 9% in W3N silver. Correcting point defect resistivity accordingly would reduce total defect concentrations but would increase the concentration difference between MRC and W3N silver. Restated, defect concentrations due to shock compression

are reduced, but the effect of silver purity on defect concentrations is increased.

An experimental indication of heat flow effect may be present in shot 73-047 at 94 kbar. The W3N foil was thinned down to 17.6 μm from the 24.4 μm thickness of the other W3N foils; the isothermal resistivity data point without heat flow correction is indeed slightly high (Fig. 11). Heat flow correction according to Table 3.2 would bring the data point in line with the other W3N points.

It should be noted that, in addition to other uncertainties in the calculation, the differential equation used may not completely describe the physical situation. The differential equation is a diffusion equation and neglects thermal waves which may be generated by the steep temperature gradients. Morse and Feshbach (1953) note that a more correct description would be given by the differential equation

$$u_{xx} - \frac{1}{c^2} u_{tt} = a^2 u_t \ .$$

Solutions for this equation were not obtained.

K. Work on Recovered Silver Foil

Silver foils recovered after impact experiments were studied by observing resistance changes on annealing and by optical and electron microscopy.

Pieces of silver foil up to 0.8 cm long and 0.25 cm wide were recovered in air in four shots; the shots were 73-009, 73-010, 73-013 on MRC silver and 73-044 on W3N silver. The impactor-target assembly, decelerated by nylon rags, was

recovered with the silver and sapphire fragments trapped inside. Sapphire fragments were no larger than 0.2 cm. Significantly large areas of foil were found which had not been scarred by the final deceleration of the fragments. The silver was sub- jected to some lateral relief waves but most of the pressure was relieved by the rarefaction wave from the epoxy-sapphire interface behind the backing sapphire disc (Fig. 1 and 2). While the state of the recovered foils was affected by the relief and deceleration processes, it may give some clues to the nature of the shocked state.

A simple annealing study was made of the resistance of a foil piece recovered from shot 73-010 shocked to 87 kbar. The preshock value of the resistance ratio between liquid helium temperature and room temperature was 0.00438. As recovered, two different foil pieces gave postshock values of 0.0222 and 0.0220, five times larger than the preshock value. For shot 73-013 (27 kbar) the preshock value was 0.00376; the postshock value was 0.0178, 4.7 times as large.

The preshock resistance at 4.2°K should be due mainly to impurities. The difference between the postshock and pre- shock values should be due to lattice imperfections remaining after the shock process. For shot 73-010 the resistance-ratio difference is 0.0178; for 73-013, 0.0140.

A piece from 73-010 was subjected to anneals. The results are given in Table IV.

The table shows that annealing at less than 100°C caused almost no change in the imperfection resistance; if anything,

the resistance increased slightly. (The same behavior was noted in shocked copper (Leslie, 1973).) Rearrangement or dispersal of imperfections could cause this. Annealing at 200°C does remove two-thirds of the shock-induced resistivity. A 50°C anneal should remove all point defects created by plastic deformation (Dawson, 1965a). Evidently any point defects generated by shock compression were able to annihilate or migrate out after relief to one atmosphere in the impact experiment.

TABLE IV. Results of post-shock anneal.

Anneal Temperature (°C)	Time Duration (min)	$\frac{R_{4.2}}{R_{298}}$
Preanneal	....	0.0222
55- 58	17	0.0232
94- 97	10	0.0229
199-207	7	0.0064

So the annealing study indicates that the lattice imperfections in the recovered foil are mostly line imperfections, i.e., dislocations. A dislocation density of $6 \times 10^{10}/cm^2$ was therefore computed from the resistance change due to the 200°C anneal. In comparison, Rose and Berger (1968) found a dislocation density of $1.5 \times 10^{10}/cm^2$ by inspection of electron micrographs of aluminum shocked to 150 kbar.

Examination of recovered foils under an optical microscope at magnifications of 30 to 100 showed sets of lines locally parallel which were not present in unshocked foil.

These same lines were observed by scanning electron microscopy (Fig. 17). Similar lines have been observed in shocked nickel by Dieter (1961). Dieter identifies the lines as slip bands (clusters of closely spaced slip lines). In the present work as in the nickel work the slip bands are fragmented due to cross-slip. In both cases there is no evidence of deformation twins.

Average slip-band spacing in the nickel work was 2.7 ± 0.3 μm for all shock strengths (100 to 520 kbar). For the present work 1.4 ± 0.5 μm was a typical mean value for the observed spacing of primary slip bands. Some evidence of slip on secondary planes was observed with a spacing of about 8 μm (Fig. 17 (d)). Nickel shocked to 100 kbar showed no secondary slip, but at 460 kbar secondary slip was seen.

Dieter notes that the slip-band spacing in recovered nickel may be representative only of the residual strain following shock compression and relief. The slip-band spacing observed corresponds roughly to that expected from slow deformation to the residual strain value. Therefore, we conclude that the observed slip-band spacing in silver is probably typical of the final, relieved state and not of the compressed state.

For reasons not understood, recovered pieces from shots 73-010 and 73-044 showed only faint evidence of slip bands whereas the bands were prominent in the other two shots. Recall that 73-009 and 73-010 were both MRC foil shocked to 87 kbar.

(a)

(b)

(c)
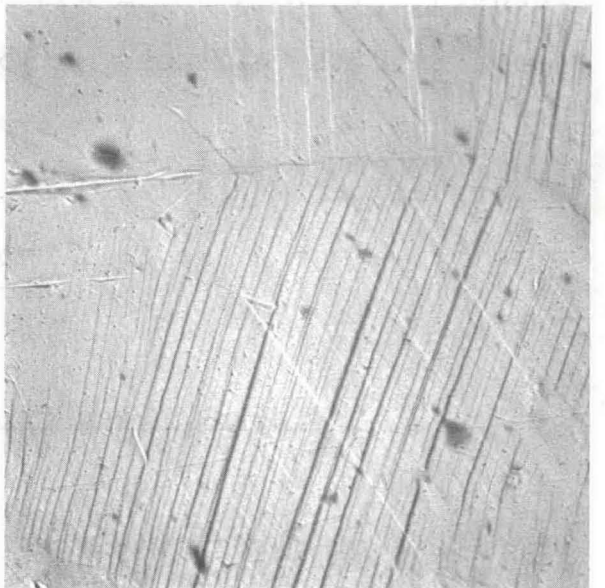
(d)

Fig. 17. Scanning electron micrographs (1000X) of shocked
and unshocked silver foil. (a) Unshocked W3N foil.
(b) Unshocked MRC foil. (c) Recovered foil from shot 73-013.
(d) Recovered foil from shot 73-009. Note evidence of cross-
slip, secondary slip, and grain boundaries.

L. Discussion of Details of Specimen State

Aside from the specimen characterization in terms of purity and anneal, there are a number of other aspects of the foil state prior to the impact experiment which should be discussed. Variations in the aspects discussed here are not believed to have significantly affected experimental results. See Appendix C also.

1. Effect of Foil Thickness Variation on Results

Average thickness of MRC foils was 16.2 μm while for all except one of W3N foils the average thickness was 24.4 μm. In order to check if the observed differences in experimental results between MRC and W3N type silver were due to the differences in foil thickness, a W3N foil was thinned down to 17.6 μm. This shot, 73-047, gave resistivity results consistent with the other thicker W3N foils. We conclude that the observed difference between the two foil types is not due to different thickness.

2. Effect of Specimen Handling on State of Anneal

Most of the experiments were done on annealed foils. The state of anneal was checked by measuring resistance at 4.2°K. The question arises whether the state of anneal was preserved during the handling involved in target assembly. Tests were made on two annealed MRC foils. To simulate assembly they were subjected to screw pressure between two glass plates wetted with acetone. One foil was also accidentally bent during this handling. Resistance at 4.2°K was the same before

and after handling within the 1% accuracy of measurement. We conclude that the state of anneal was not significantly affected by this handling.

Target preparation also involves some heating of the foil. Silver wires were spot-welded to the foil tabs, 1.2 cm from the sensitive part of the foil. Thermal transients accompany the weld. One hopes this transient is appreciably attenuated before it reaches the sensitive portion of the foil. After assembly, coaxial cables were soldered to the silver wires. (Solder melts at about 200°C.) Heat was applied to the silver wire twice, for about 2 seconds each time. The body of the silver foil is in contact with a heat reservoir consisting of sapphire discs and dental amalgam, so the foil should be heated to much less than 200°C, hopefully less than 50°C.

3. Condition of Foil Surfaces

Generation of dislocations at sources on the specimen surface has been shown to be important in quasi-static deformation of silver single crystals (Worzala and Robinson, 1967). This raises the question whether differences in surface condition could explain the differences in shock resistivity in the two silver foil types studied here. The surface state was rough and poorly defined from metallurgical and surface physics viewpoints (Fig. 17). Both foil types were prepared in nearly identical fashion except that the MRC foil, as received, had more initial surface roughness and therefore was mechanically polished for a longer time. No significant effect of surface preparation was found in the lithium fluoride precursor decay

studies (Asay et al., 1972). Deviation in surface preparation is not believed to be the cause of observed resistivity difference between foil types in the present work.

Surfaces on such soft metal with less roughness and less deformation could probably have been achieved using cerium oxide as the final polishing abrasive instead of the 0.05 μm alumina employed in this work. A non-mechanical polishing technique for mirror finishes developed by Henry, Hockey, and Mitchell (1970) might also have improved the surface condition.

4. Grain Size and Preferred Orientation

The mean grain sizes in the two types of silver foil used were significantly different. For annealed W3N foil, mean grain size was about 35 micrometers while for MRC foil, annealed and unannealed, it was about twice that. In both cases mean grain size seen on the foil surface was greater than the foil thickness; we then expect that a traverse of the foil thickness is usually confined to a single grain. For this reason, the difference in grain size is not expected to have a significant effect on defect production, dislocation glide, and dislocation generation. One can envision some effect on dislocations moving on glide planes at large angles to the shock direction; such dislocations might reach and interact with grain boundaries. Boundaries can cause dislocation pile-ups, followed by stress concentration and dislocation generation in the next grain. The effect would be more important in the smaller-grained W3N foil.

It should be noted that there is some effect of grain size on yield stress at low strain rates (Hall, 1970). A factor of two increase in grain size in silver causes an 8% decrease in yield stress. However, in shock experiments no effect of grain size on HEL after 19 millimeters of shock propagation was noted in Armco iron (Jones and Holland, 1968). An effect of grain size on precursor attenuation in the first millimeter or less of shock propagation is not ruled out by their work. Lithium fluoride work showed no effect of the number of subgrain boundaries on the precursor decay or HEL (Asay et al., 1972), whereas in copper there was an effect (Jones and Mote, 1969). Grain size is thus a possible but not likely source of the difference in defect resistivity between the two foil types.

This is an appropriate time to discuss preferred orientation of crystallites in cold-rolled foils. The topic has been reviewed by Barrett and Massalski (1966). For silver rolled at room temperature or below the texture is described by the (110) plane parallel to the rolling plane and the [1$\bar{1}$2] direction parallel to the rolling direction. Other crystallite orientations are present but with less frequency.

Rolling texture changes to a new texture on low-temperature annealing but becomes random with annealing above 800°C. After long annealing at 433° to 533°C (anneals in present work were one to two hours at 535°C) the orientation is the same as the original rolling texture.

Based on the above discussion, it is most likely that the silver foils used in the present work had a (110) [1$\bar{1}$2] texture.

Barrett and Massalski (1966) observed that in f.c.c. metals the predominant dislocation slip plane is the closest-packed (111) plane. Many metals alter their slip plane at high or low temperature or high strain rate. In copper, however, the same slip systems operate under shock as in quasi-static deformation (Jones and Mote, 1969). For crystallites with (110) planes parallel to the foil surfaces, three (111) planes will be at 45 degrees to the foil surface. The maximum resolved shear stress in uniaxial shock compression is approximately at 45 degrees to the foil surface, so that dislocations on (111) slip planes would be subjected to this maximum shear stress $(\sigma_x - \sigma_y)/2$. This leads us to observe that differences in crystallite preferred orientation in the two types of foil studied could lead to differences in defect production by the shock. No such differences in crystallite orientations are expected, however.

V.   CONCLUSIONS AND RECOMMENDATIONS

A.   Conclusions

Accurate and reproducible measurements of resistance changes in silver foils due to shock-wave compression were accomplished. These results were made possible by careful preparation of well-characterized specimens and by careful design of the impact experiment.   Experimental accuracy was sufficient to resolve an effect of silver purity on the electrical resistance or resistivity as a function of shock pressure. A smaller effect of annealing prior to shock loading also appears to be discernible. In some, but not all cases, the structure of voltage-time profiles obtained during the 1/2 microsecond of shock compression was reproducible. The structure of the voltage-time profiles appears to depend on purity and state of anneal of the foil and on pressure.

Comparison between shock and hydrostatic resistivity was used to deduce the point defect concentrations generated by the shock wave. Defect concentrations were found to be proportional to the three-halves power of strain; concentrations were higher than those found in slow deformation to the same strain. The high vacancy concentrations computed (as high as 2×10^{-3} at 120 kbar) are believed accurate to an order of magnitude. Dislocation models for the generation of point defects by plastic deformation in shock waves are useful in understanding the

present work. A speculative model involving stress relaxation effects was able to account for observed defect concentrations and to explain the purity effect.

Saada's model for point defect production in plastic deformation of f.c.c. metals was tested and found inadequate to explain magnitudes of defect concentrations found in the present work. However, a model of the Saada-type is still useful in interpreting present results.

Within the framework of Weertman's discussion of defect production in shock compression, the present results give evidence for the presence of dislocations moving at or near shear-wave speed.

Calculations involved in analyzing data have themselves provided some interesting results. A semi-empirical calculation of silver resistivity versus hydrostatic pressure has been established and used to extrapolate existing experimental data beyond 30 kilobars. Such calculations should prove useful in other high-pressure work. A contradiction was found in Bridgman's experimental results for the dependence of noble metal resistance on pressure and temperature; there is evidence of error in his conclusion that temperature coefficients of resistance are independent of pressure (0 to 12 kbar). Significant heat flow into the silver foils from epoxy bonding layers in 1/2 microsecond was indicated by solution of the boundary value problem for a composite sandwich with different initial temperatures in each material.

B.   Recommendations

Additional experiments of the type performed here should be done to test the range of validity of the above conclusions concerning defect generation by plane shock waves in metals. Theoretical work on perfect lattice and defect resistivity of metals under pressure would also be a contribution. Simultaneous study of elastic precursor stress and electrical conductivity as a function of thickness of a shocked metal would test the model proposed to explain the observed effects.

Measurements of resistance of a high-strength, elastic-plastic metal above and below its elastic limit would test current ideas concerning defect production by shock deformation.

More low-temperature shock experiments with recovery of the shocked metal at the low temperatures would be useful; then point defects produced would be trapped for post-mortem examination.

There are a number of studies using hydrostatic pressure which would contribute immensely to this type of work. Additional experimental work on temperature coefficients of resistivity as a function of hydrostatic pressure is needed to put the resistivity analysis on a firmer foundation. Data on epoxy thermal conductivity as a function of temperature and pressure would make the heat-flow calculation more meaningful.

REFERENCES

Abey, A. E., 1973, J. Appl. Phys., 44, 2087.

Andersson, P., Backstrom, G., 1973, J. Appl. Phys., 44, 2601.

Asay, J. R., Fowles, G. R., Duvall, G. E., Miles, M. H., Tinder, R. F., 1972, J. Appl. Phys., 43, 2132.

Bailey, J. E., Hirsch, P. B., 1960, Phil. Mag., 5, 485.

Balluffi, R. W., Koehler, J. S., Simmons, R. O., 1963, in Recovery and Recrystallization in Metals (Ed. L. Himmel) (Gordon and Breach, New York), p. 18.

Barker, L. M., 1968, in Behaviour of Dense Media under Dynamic High Pressures (Gordon and Breach, New York), pp. 483-504.

Barrett, C. S., Massalski, T. B., 1966, Structure of Metals (McGraw-Hill, New York).

Barsis, E., Williams, E., Skoog, C., 1971, J. Appl. Phys., 41, 5155.

Basinski, Z. S., Dugdale, J. S., Howie, A., 1963, Phil. Mag., 8, 1989.

Basinski, Z. S., Saimoto, S., 1967, Can. J. Phys., 45, 1161.

Berry, R. J., 1972, Phys. Rev. B, 6, 2994.

Blewitt, T. H., Coltman, R. R., Redman, J. K., 1955, in Report of the Conference on Defects in Crystalline Solids (The Physical Society, London), pp. 369-382.

Booth, A. D., 1957, Numerical Methods (Academic, New York).

Brandt, N. B., Itskevich, E. S., Minina, N. Ya., 1972, Soviet Phys. Usp., 14, 438.

Bridgman, P. W., 1921, Proc. Nat. Acad. Sci. U. S., 7, 299.

Bridgman, P. W., 1925, Proc. Am. Acad. Arts Sci., 60, 423.

Bridgman, P. W., 1938, Proc. Am. Acad. Arts Sci., 72, 157.

Bridgman, P. W., 1952, Proc. Am. Acad. Arts Sci., 81, 167.

Bridgman, P. W., 1958, <u>The Physics of High Pressure</u> (G. Bell and Sons, London).

Bundy, F. P. (private communication).

Callen, H. B., 1960, <u>Thermodynamics</u> (John Wiley and Sons, New York), p. 286.

Carslaw, H. S., Jaeger, J. C., 1959, <u>Conduction of Heat in Solids</u> (Oxford University, Oxford), pp. 319-326.

Christou, A., 1971, <u>Scr. Met.</u>, 5, 749.

Clarebrough, L. M., Hargreaves, M. E., Loretto, M. H., 1962, in <u>Recovery and Recrystallization in Metals</u> (Ed. L. Himmel) (Interscience, New York), p. 105.

Clougherty, E. V., Kaufman, L., 1963, in <u>High Pressure Measurements</u> (Eds. A. A. Giardini and E. C. Lloyd) (Butterworths, Washington), pp. 152-163.

Crosnier, J., Jacquesson, J., Migault, A., 1965, in <u>Fourth Symposium (International) on Detonation</u> (Office of Naval Research, Washington), pp. 627-638.

Dawson, H. I., 1965a, <u>Acta Met.</u>, 13, 453.

Dawson, H. I., 1965b, <u>Physica</u>, 31, 344.

Decker, D. L., Bassett, W. A., Merrill, L., Hall, H. T., Barnett, J. D., 1972, <u>J. Phys. and Chem. Ref. Data</u>, 1, 773.

Dieter, G. E., 1961, in <u>Response of Metals to High Velocity Deformation</u> (Eds. P. G. Shewmon and V. F. Zackay) (Interscience, New York), pp. 409-444.

Drickamer, H. G., 1965, in <u>Solid State Physics</u> (Eds. F. Seitz and D. Turnbull) (Academic, New York), Vol. XVII, pp. 1-133.

Duff, R. E., 1969, in <u>Properties of Matter under Unusual Conditions</u> (Eds. H. Mark and S. Fernbach) (Interscience, New York), p. 93.

Dugdale, J. S., 1961, <u>Science</u>, 134, 77.

Dugdale, J. S., 1965, in <u>Physics of Solids at High Pressures</u> (Eds. C. T. Tomizuka and R. M. Emrick) (Academic, New York), pp. 16-27.

Duvall, G. E., 1961, in <u>Response of Metals to High Velocity Deformation</u> (Eds. P. G. Shewmon and V. F. Zackay) (Interscience, New York), p. 193.

Duvall, G. E., 1972, in <u>Dynamic Response of Materials to Intense Impulsive Loading</u> (Eds. P. C. Chou and A. K. Hopkins) (Wright Patterson Air Force Base, Ohio), pp. 89-122.

Emrick, R. M., 1972, <u>Phys. Rev. B</u>, 6, 1144.

Emrick, R. M., McArdle, P. B., 1969, <u>Phys. Rev.</u>, 188, 1156.

Erkman, J. O., Duvall, G. E., 1965, in <u>Developments in Mechanics</u> (Eds. T. C. Huang and M. W. Johnson, Jr.) (John Wiley and Sons, New York), Vol. 3, Pt. 2, pp. 179-188.

Fowles, G. R., 1961, <u>J. Appl. Phys.</u>, 32, 1478.

Fowles, G. R., 1972, in <u>Dynamic Response of Materials to Intense Impulsive Loading</u> (Eds. P. C. Chou and A. K. Hopkins) (Wright Patterson Air Force Base, Ohio), pp. 405-480.

Fowles, G. R., Duvall, G. E., Asay, J., Bellamy, P., Feistmann, F., Grady, D., Michaels, T., Mitchell, R., 1970, <u>Rev. Sci. Instr.</u>, 41, 984.

Fritz, J. N., Morgan, J. A., 1973, <u>Rev. Sci. Instr.</u>, 44, 215.

Gerritsen, A. N., 1956, in <u>Encyclopedia of Physics</u> (Ed. S. Flugge) (Springer-Verlag, Berlin), Vol. XIX, p. 170.

Gilman, J. J., 1968, <u>Appl. Mech. Rev.</u>, 21, 767.

Gindin, I. A., Khotkevich, V. I., Neklyudov, I. N., Lebedev, V. P., Bobonets, I. I., 1971, <u>Phys. Metal. Metallog.</u>, 32, No. 1, 138.

Ginsberg, M. J., Grady, D. E., 1972, <u>Bull. Am. Phys. Soc.</u>, 17, 1100.

Ginsberg, M. J., Grady, D. E., DeCarli, P. S., 1972, Project No. PYU-1797, Quarterly Report (Stanford Research Institute, Menlo Park, Calif.).

Goree, W. S., Scott, T. A., 1966, <u>J. Phys. Chem. Solids</u>, 27, 835.

Graham, R. E., Ingram, G. E., 1968, in <u>Behaviour of Dense Media under High Dynamic Pressures</u> (Gordon and Breach, New York), pp. 469-582.

Granato, A. V., 1973, in <u>Metallurgical Effects at High Strain Rates</u> (Eds. R. W. Rohde, B. M. Butcher, J. R. Holland, and C. H. Karnes) (Plenum, New York), pp. 255-275.

Gschneidner, K. A., Jr., in <u>Solid State Physics</u> (Eds. F. Seitz and D. Turnbull) (Academic, New York), Vol. XVI, pp. 276-426.

Hall, E. O., 1970, Yield Point Phenomena in Metals and Alloys (Macmillan, London), pp. 37ff.

Henry, L. F., Hockey, B. J., Mitchell, J. W., 1970, Rev. Sci. Instr., 41, 1549.

Hirsch, P. B., 1967, Can. J. Phys., 45, 663.

Huebener, R. P., 1965, in Lattice Defects in Quenched Metals (Eds. R. M. J. Cotterill, M. Doyama, J. J. Jackson, and M. Meshii) (Academic, New York), pp. 569-589.

Hull, D., 1965, Introduction to Dislocations (Pergamon, Oxford).

Jones, A. H., Maiden, C. J., Isbell, W. M., 1970, in Mechanical Behaviour of Materials under Pressure (Ed. H. Ll. D. Pugh) (Elsevier, Amsterdam), pp. 680-747.

Jones, O. E., 1970, in Third International Conference on High Pressure--Engineering Solids under Pressure) (Inst. Mech. Engrs., London), pp. 75-86.

Jones, O. E., Holland, J. R., 1968, Acta Met., 16, 1037.

Jones, O. E., Mote, J. D., 1969, J. Appl. Phys., 40, 4920.

Jones, O. E., Nielson, F. W., Benedick, W. B., 1962, J. Appl. Phys., 33, 3224.

Jura, G. (private communication).

Keeler, R. N., Royce, E. B., 1971, in Physics of High Energy Density (Academic, New York), p. 121.

Koehler, J. S., 1969, in Vacancies and Interstitials in Metals (Eds. A. Seeger, D. Schumacher, W. Schilling, and J. Diehl) (North-Holland, Amsterdam), p. 175.

Kos, J. F., 1973, Can. J. Phys., 51, 1602.

Kovacs, I., Nagy, E., Feltham, P., 1964, Phil. Mag., 9, 797.

Kraftmakher, Ya. A., Strelkov, P. G., 1970, in Vacancies and Interstitials in Metals (Eds. A. Seeger, D. Schumacher, W. Schilling, and J. Diehl) (North-Holland, Amsterdam), pp. 59-78.

Kressel, H., Brown, N., 1967, J. Appl. Phys., 38, 1618.

Lawson, A. W., 1956, in Progress in Metal Physics (Eds. B. Chalmers and R. King) (Pergamon, London), Vol. VI, pp. 1-44.

LeClaire, A. D., 1949, in Progress in Metal Physics (Ed. B. Chalmers) (Interscience, New York), Vol. I, p. 371.

Lenssen, M. H., Michels, A., 1935, Physica, 2, 1091.

Leslie, W. C., 1973, in Metallurgical Effects at High Strain Rates (Eds. R. W. Rohde, B. M. Butcher, J. R. Holland, and C. H. Karnes) (Plenum, New York), pp. 571-586.

Levinstein, H. J., Robinson, W. H., 1962, Trans. AIME, 224, 1292.

Mahajan, S., 1970, Phys. Stat. Sol. (a), 2, 187.

Martin, J. W., Paetsch, R., 1973, J. Phys. F: Metal Phys., 3, 907.

McQueen, R. G., Marsh, S. P., Taylor, J. W., Fritz, J. N., Carter, W. J., 1970, in High-Velocity Impact Phenomena (Ed. R. Kinslow) (Academic, New York), p. 557.

Morse, P. M., Feshbach, H., 1953, Methods of Theoretical Physics (McGraw-Hill, New York), p. 865.

Mott, N. F., 1934, Proc. of Phys. Soc., 46, 680.

Mott, N. F., Jones, H., 1936, The Theory of Metals and Alloys (Oxford University, London).

Nabarro, F. R. N., 1967, Theory of Crystal Dislocations (Oxford University, London).

Nagpal, V. P., Duggal, V. P., 1972, Thin Solid Films, 9, 313.

Nakada, Y., 1965, Phil. Mag., 11, 251.

Paul, W., 1963, in High Pressure Physics and Chemistry (Ed. R. S. Bradley) (Academic, London), Vol. I, pp. 299-354.

Rice, M. H., McQueen, R. G., Walsh, J. M., 1958, in Solid State Physics (Eds. F. Seitz and D. Turnbull) (Academic, New York), Vol. VI, pp. 1-63.

Rose, M. F., Berger, T. L., 1968, Phil. Mag., 17, 1121.

Rose, M. F., Berger, T. L., Inman, M. C., 1967, Trans. AIME, 239, 1998.

Royce, E. B., 1971, in Physics of High Energy Density (Academic, New York), pp. 80-95.

Saada, G., 1961, Physica, 27, 657.

Seitz, F., 1952, Adv. Phys., 1, 43.

Shoenberg, D., Watts, B. R., 1967, Phil. Mag., 15, 1275.

Sondheimer, E. H., 1952, Adv. Phys., 1, 1.

Styris, D. L., Duvall, G. E., 1970, High Temp.--High Press., 2, 477.

Tanaka, K., Watanabe, T., 1972, Jap. J. Appl. Phys., 11, 1429.

Taylor, G. I., Whiffen, A. C., 1948, Proc. Roy. Soc., A194, 289.

Taylor, J. W., Rice, M. H., 1963, J. Appl. Phys., 34, 364.

Templeton, J. M., 1966, Proc. Roy. Soc., A292, 413.

Thom, F., 1972, Phys. Stat. Sol. (b), 49, K111.

van den Beukel, A., 1968, in Vacancies and Interstitials in Metals (Eds. A. Seeger, D. Schumacher, W. Schilling, and J. Diehl) (North-Holland, Amsterdam), pp. 427-479.

van Wely, F. E., 1968, in Behaviour of Dense Media under High Dynamic Pressures (Gordon and Breach, New York), pp. 337-342.

Wagner, H., Dworschak, F., Wombacher, P., 1971, in 1st European Conference on Condensed Matter (European Phys. Soc., Geneva), p. 68.

Weertman, J., 1961, in Response of Metals to High Velocity Deformation (Eds. P. G. Shewmon and V. F. Zackay) (Interscience, New York), pp. 205-247.

Williams, R. D., 1967, in Experimental Methods of Materials Research (Ed. H. Herman) (Interscience, New York), p. 252.

Wise, E. M., Cox, C. D., 1961, in Metals Handbook (Ed. T. Lyman) (American Society for Metals, Novelty, Ohio), Vol. I, p. 1182.

Wolfenden, A., 1969, Acta Met., 17, 585.

Worzala, F. J., Robinson, W. H., 1967, Phil. Mag., 15, 939.

Zharkov, V. N., Kalinen, V. A., 1971, Equations of State for Solids at High Pressures and Temperatures (Consultants Bureau, New York).

Ziman, J. M., 1960, in Electrons and Phonons (Oxford University, Oxford).

Ziman, J. M., 1965, in Physics of Solids at High Pressure
(Eds. C. T. Tomizuka and R. M. Emrick) (Academic, New
York), pp. 171-183.

APPENDIX A

VOLTAGE-TIME PROFILES

Fig. A.1. Voltage-time profiles are presented in the following order:

1. W3N annealed silver in order of increasing pressure, (a) to (f).

2. MRC annealed silver in order of increasing pressure, (g) to (m).

3. MRC unannealed silver, (n) and (o).

4. MRC annealed silver in Lucalox sandwiches, (p) and (q).

5. Anomalous records with MRC annealed silver, (r) and (s).
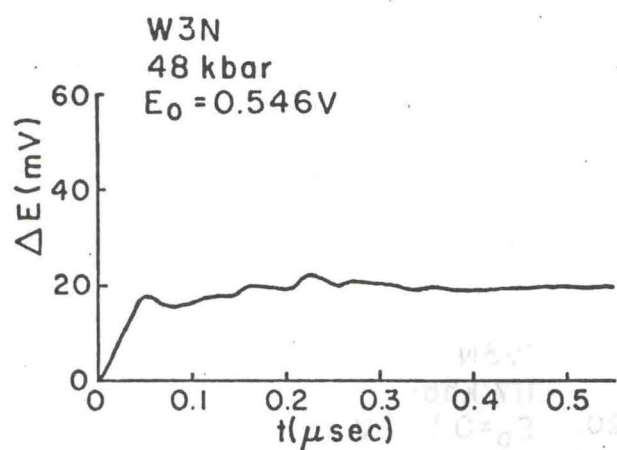
(a)   73-028
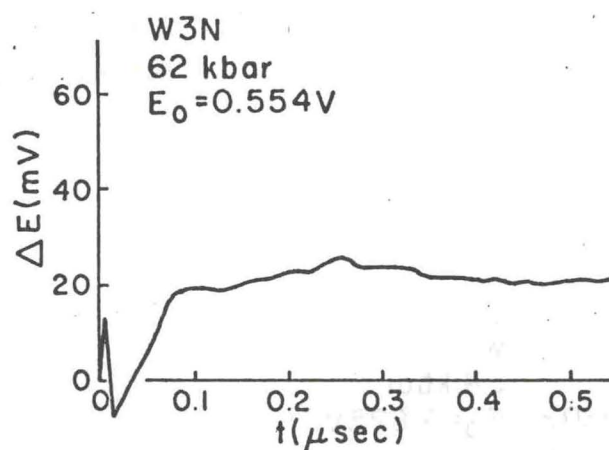
(b)   73-040

(c) 73-036

(d) 73-044

128
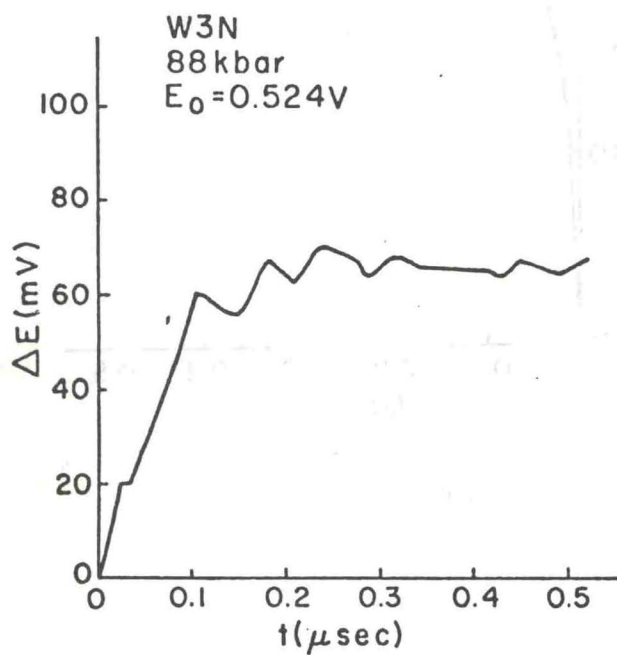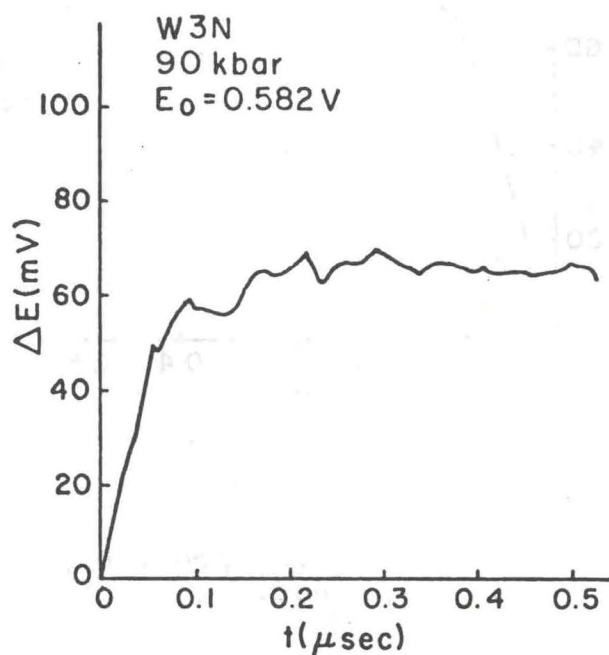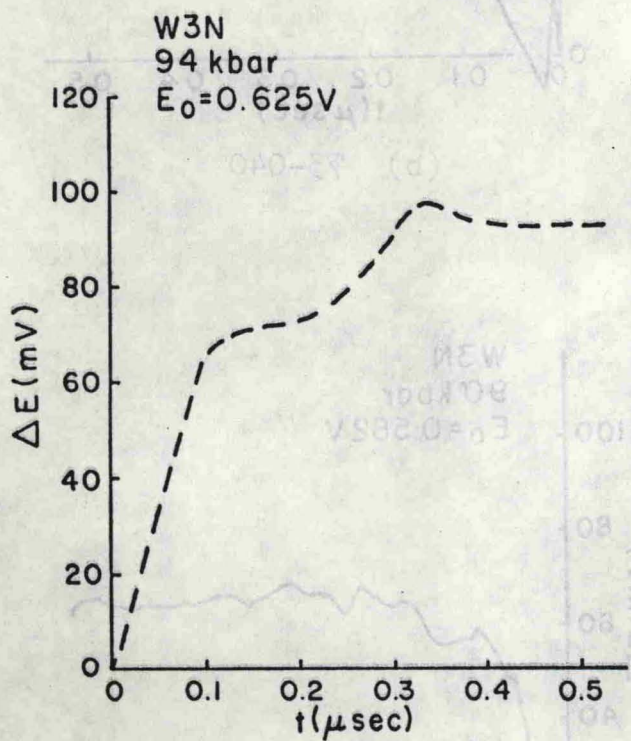
(e) 73-047

Only a coarse profile was obtained.

(f) 73-050

MRC-A
27 kbar
$E_0 = 0.734V$

(g)   73-013

MRC-A
60 kbar
$E_0 = 0.768V$

(h)   73-011
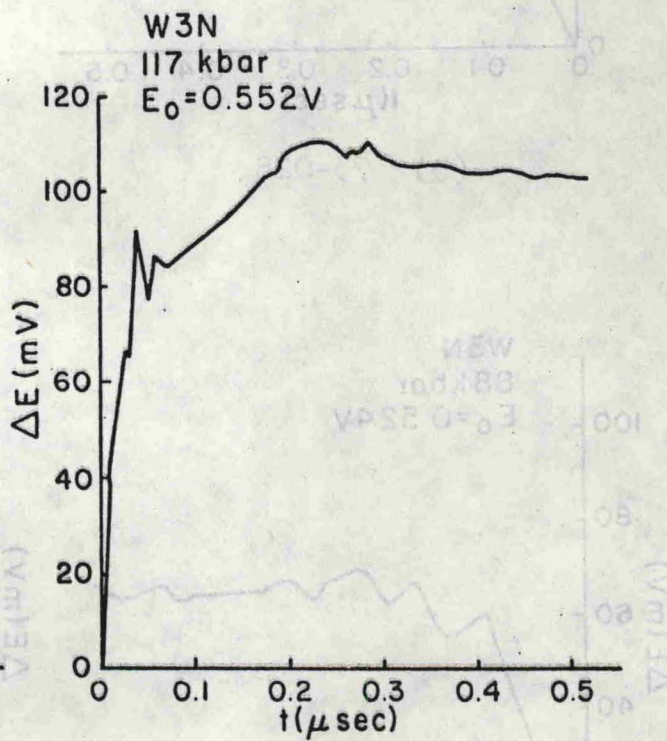
MRC-A
87 kbar
$E_0 = 0.797V$
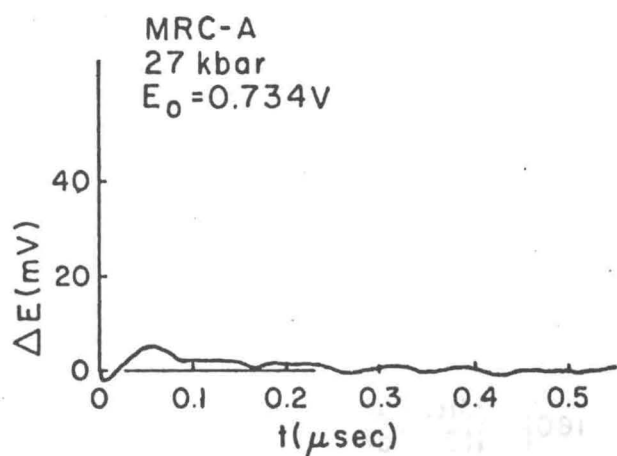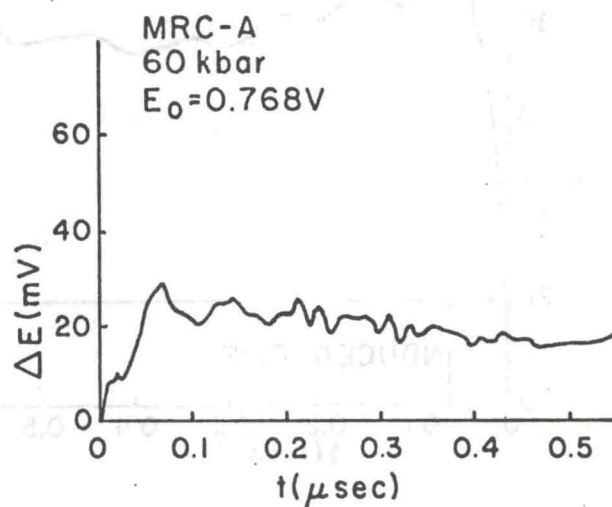
(i)   73-009
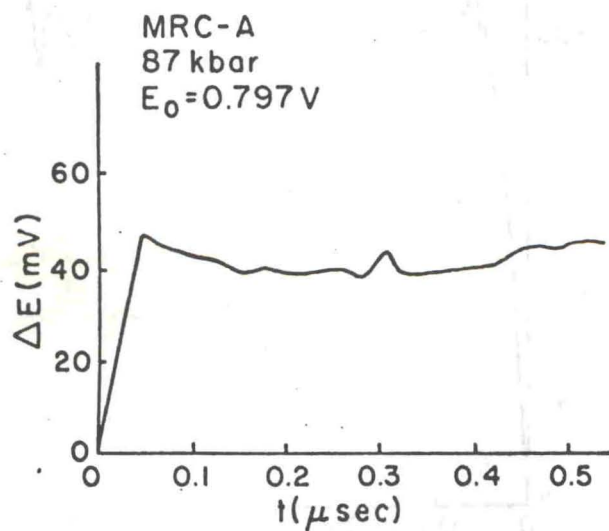
MRC-A
88 kbar
$E_0 = 0.861V$
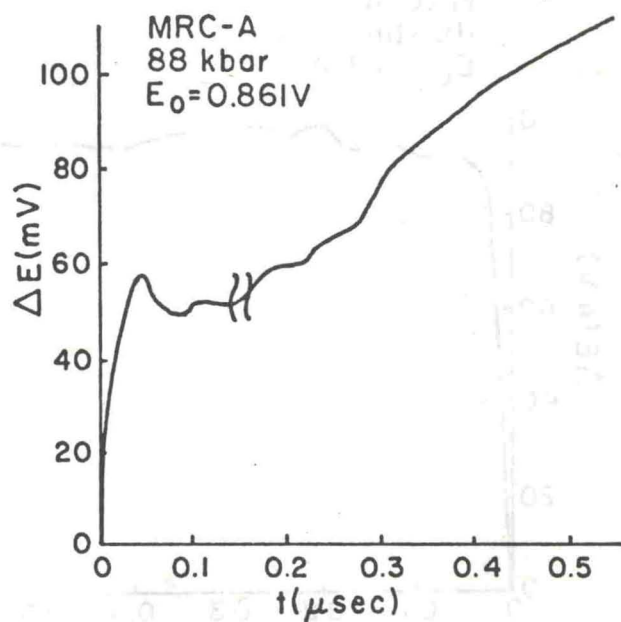
(j)   73-010

MRC-A
104 kbar
$E_0 = 0.713 V$

INDUCED EMF
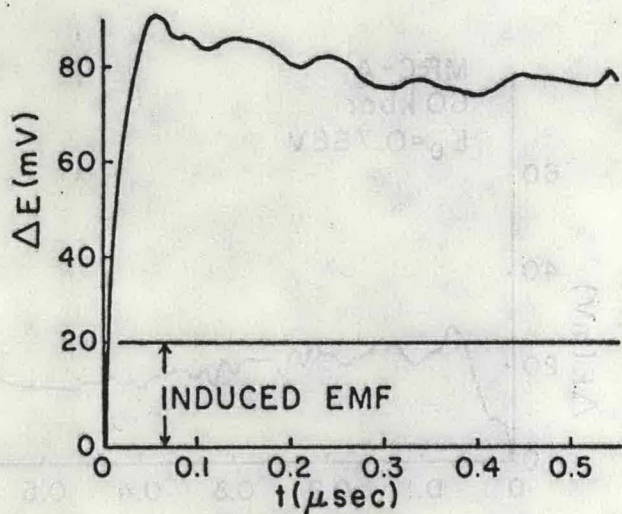
(k)   72-069

MRC-A
116 kbar
$E_0 = 0.839 V$
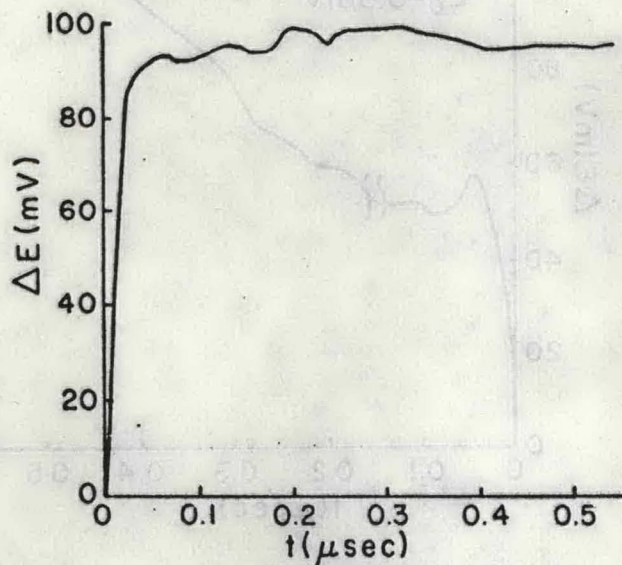
(1)   73-027

MRC-A
119 kbar
$E_0 = 0.742 V$
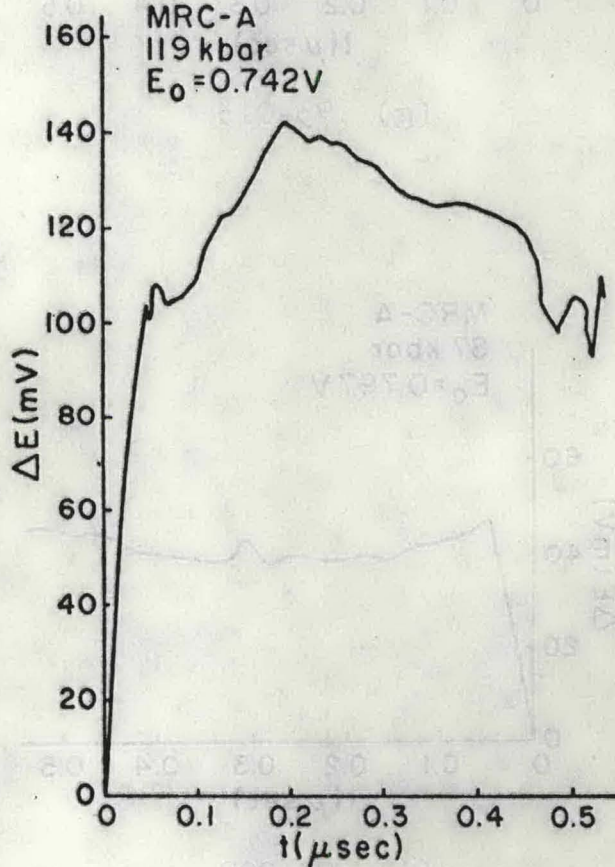
(m)   73-059
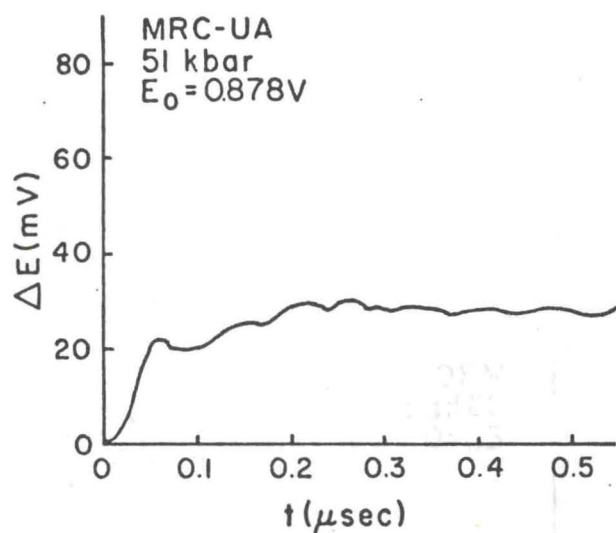
(n)   73-029

(o)   73-034

(p)   72-065

(q)   72-068

MRC-A
118 kbar
$E_0 = 0.800V$

(r)   73-051

MRC-A
83 kbar
$E_0 = 0.74V$
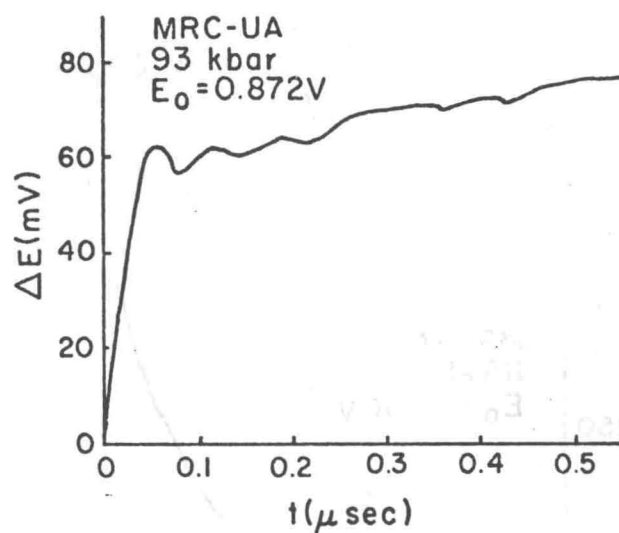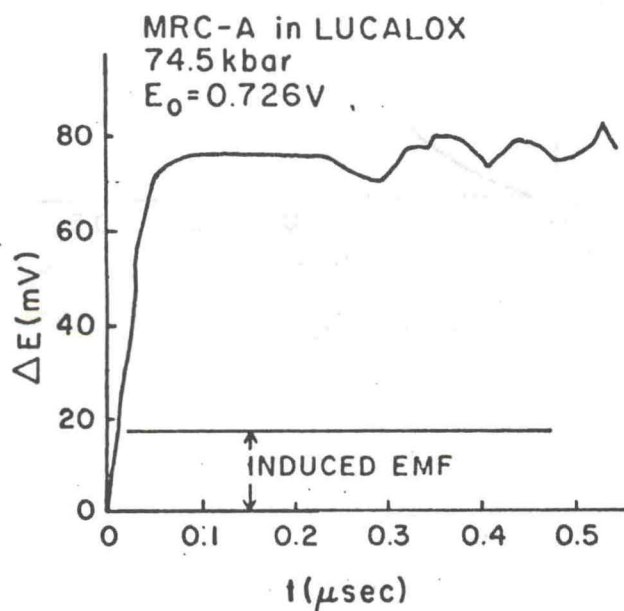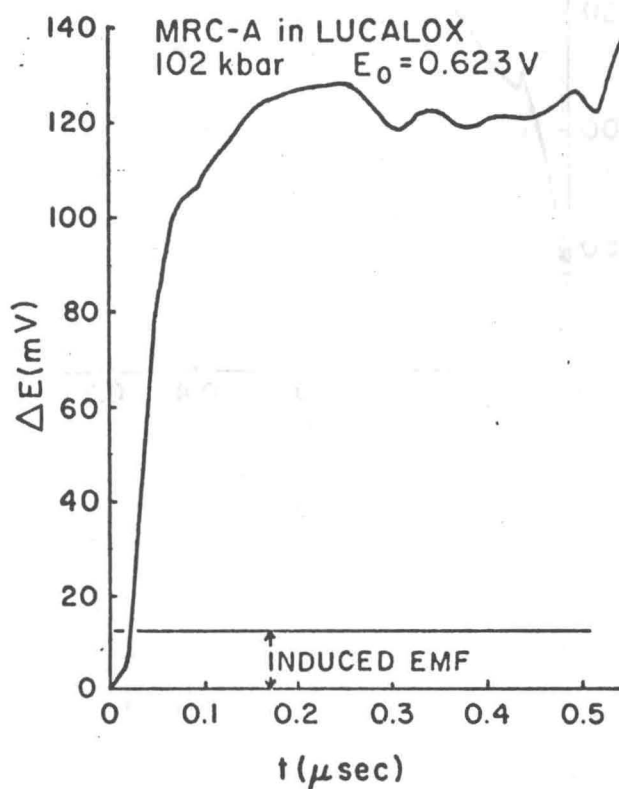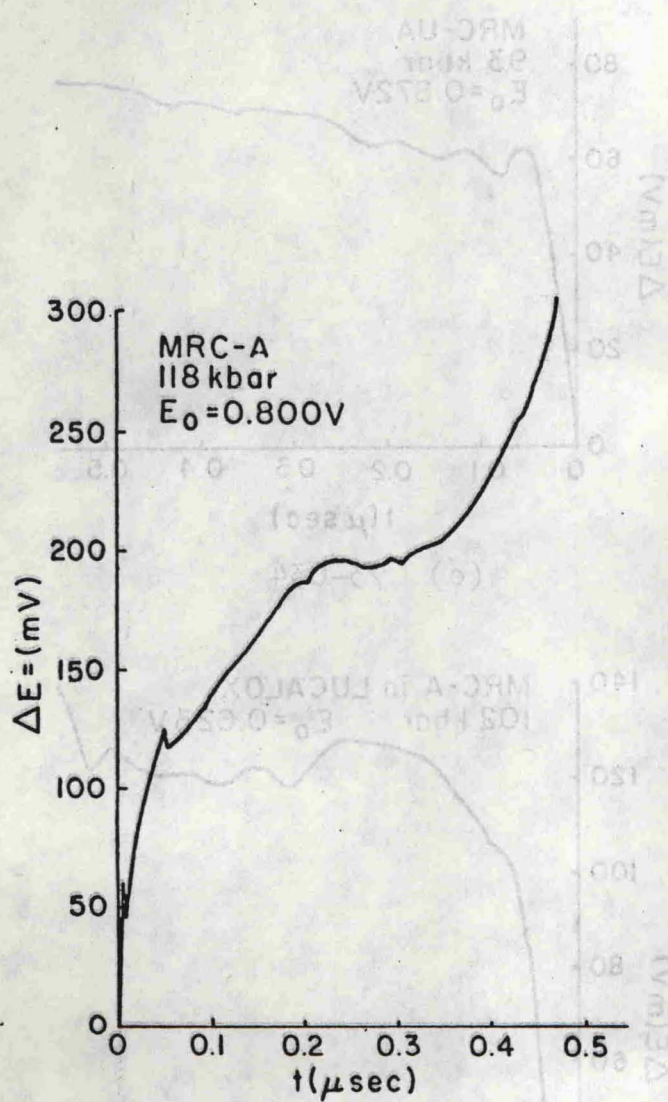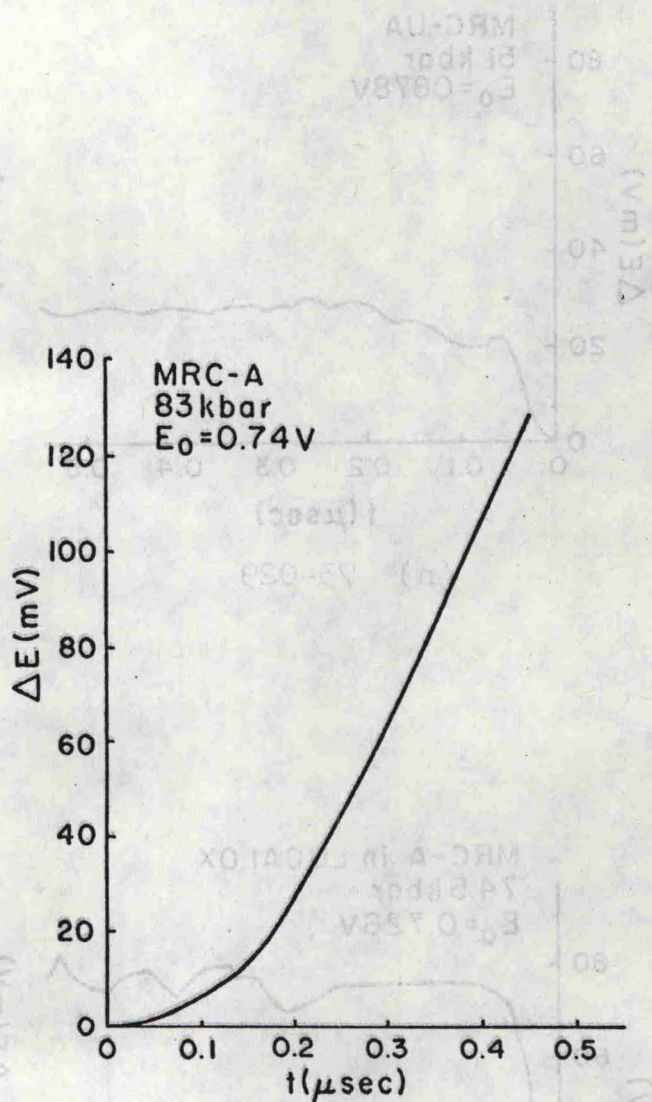
(s)   73-056

APPENDIX B

FOIL STRETCHING

APPENDIX B

FOIL STRETCHING

One possible source of anomalous resistance changes observed in records from shots 73-051 and 73-056 is deviations from uniaxial compression by lateral deformation. Lateral deformation will cause resistance changes due to changes in specimen dimensions and due to lattice imperfections generated by plastic deformation.

Stretching of the foil could be caused by a shock wave which is partly tilted with respect to the foil plane. The high shock speed, 11.4 mm/μsec, in sapphire causes especially high magnification of the relative tilt between impactor and target. For an impactor approaching at 0.4 mm/μsec, a 0.3 milliradian tilt would become $0.3 \times (\frac{11.4}{0.4}) = 8.6$ milliradians in sapphire. This means that the lateral particle velocity is $8.6 \times 10^{-3} \, u_p$. Stretching requires relative lateral motion in opposite directions of adjacent segments of the foil; so either one segment must be accelerated while the other is still at rest or the shock must be non-planar in order for stretching to take place.

Consider a slab element whose length L and cross-sectional area A are being altered by stretching. Conservation of mass requires $DA_o L_o = DAL$ where D is the mass density.

The relative resistance is

$$\frac{R}{R_o} = \frac{\rho}{\rho_o} \frac{L}{A} \frac{A_o}{L_o} = \frac{\rho}{\rho_o} \left(\frac{L}{L_o}\right)^2 \quad .$$

Consider a uniform stretch $L = L_o + u_y(t - t_o)$ where u_y is the relative lateral particle velocity of the slab ends; then R/R_o has a quadratic dependence on time. Let $u_y = \alpha u_x$ where $\alpha = 10$ milliradians, $u_x = 0.5$ mm/μsec, $L_o = 1$ mm, $\frac{\rho}{\rho_o} = 1$. Then $R/R_o = (1.005)^2 = 1.01$ in 1 microsecond of stretch. This is not enough to account for observed effects in 73-051 and 73-056.

Stretching will also cause plastic deformation and hence additional resistance changes due to defect generation. Suppose $\Delta\rho/\rho_o$ is proportional to work of plastic deformation according to Saada's relation (Sec. IV.E); and that tensile stress is linearly related to strain ϵ. Then $\rho \propto W_{PD} = a\epsilon + b\epsilon^2$; for tensile deformation $\epsilon = (1-2\nu)\Delta L/L$ where ν is Poisson's ratio. This implies that again the resistance would have quadratic time dependence. Since magnitude of resistivity change generated by deformation at these strain rates is not known, the mechanism proposed here represents only a possible source of the anomalous signals in shots 73-051 and 73-056.

APPENDIX C

DETAILS OF VARIATIONS IN EXPERIMENTAL PROCEDURE

APPENDIX C

DETAILS OF VARIATIONS IN EXPERIMENTAL PROCEDURE

Variations in target preparation are not believed to have affected the experimental results in any significant way, but for completeness some of the variations which occurred will be recorded.

A number of air bubbles in the epoxy near the active foil edges were observed in target 73-011. There were 10 bubbles with diameters from 0.01 to 0.02 cm; some bubbles were as close as 0.03 cm from the foil, and a couple were touching the foil. For a short time during the impact experiment these bubbles would be a source of rarefaction waves, disturbing the state of uniaxial compression. After shock arrival the pressure in bubble volumes would remain near one atmosphere until the bubbles collapse as the free surface at the sapphire accelerates, collapsing in about 60 nanoseconds. In 60 nanoseconds the waves would travel 0.03 cm, so a small but not serious effect on the foil response might be expected. The voltage-time profile on that shot was noisier than other shots but otherwise normal.

There were some variations in the procedure for making electrical connections to the specimen. In shots 73-027 and 73-028 mercury amalgam was put in the electrical-lead holes in

the sapphire backing piece while the epoxy was still soft.
This resulted in mercury stain on the foil (mercury embrittles
silver), but the voltage-time profiles showed nothing unusual.
Beginning with shot 73-013 silver wire was spot-welded to the
foil leads; previously copper wire had been used. Electrical
signals have been observed from shocked metallic junctions
(Crosnier, Jacquesson, and Migault, 1965). Even if present,
the symmetry of the two potential leads implies that no net
signal would be observed. No change in response was noted in
changing from copper to silver.

Beginning with shot 73-029 the screw clamping the sand-
wich together was tightened just once instead of twice.
Previous to that shot the screw was tightened a second time
after the excess epoxy had a chance to flow out of the sandwich.
No noticeable change in the thickness of the epoxy layer re-
sulted from this change of procedure. If the clamping were
deforming the foil, the change of procedure might have affected
shot results; no effect was noted.

In impact experiments up to 73-010 there were some
problems with erratic shifts in the reference voltage level
during preshot pulsing. The problem was eliminated by removing
all intermediate ground connections to points on cable outer
conductors from the target assembly to the power supply and
oscilloscopes. Apparently the problem was caused by ground
loops.

APPENDIX D

THREE-SLAB HEAT FLOW DERIVATION

APPENDIX D

THREE-SLAB HEAT FLOW DERIVATION

In principle the heat flow equation, $u_t = ku_{xx}$, can be solved for any number of slabs for any initial and boundary conditions (Carlslaw and Jaeger, 1959). But the solution for a particular set of initial and boundary conditions and number of slabs involves considerable labor.[3] The problem to be solved was for three slabs, a single slab of one material surrounded by identical slabs of a second material (Fig. D.1). From symmetry $u(x,t) = u(-x,t)$. Initial and boundary conditions are $u(x,a) = T_1$ for $x\epsilon(o,a)$, $u(x,o) = T_2$ for $x\epsilon(a,b)$ and $u(b,t) = 0$. At slab interfaces, jump conditions of continuity of temperature and heat flux apply.

The problem can be solved using the Laplace transformation. For regions numbered as in Fig. D.1, the problem is as follows:

$$\text{Region 1,} \quad \varphi_t = k\varphi_{xx}$$
$$\text{Region 2,} \quad \Psi_t = \varkappa\Psi_{xx}$$
$$\text{Region 3,} \quad \eta_T = \varkappa\eta_{xx}$$

Initial conditions

$$\varphi(x,o) = T_1 \quad x\epsilon(-a,a)$$
$$\Psi(x,o) = T_2 \quad x\epsilon(a,b)$$
$$\eta(x,o) = T_2 \quad x\epsilon(-b,-a)$$

---

[3]The solution to the present problem was obtained in cooperation with G. Swan, Department of Applied Mathematics, Washington State University.
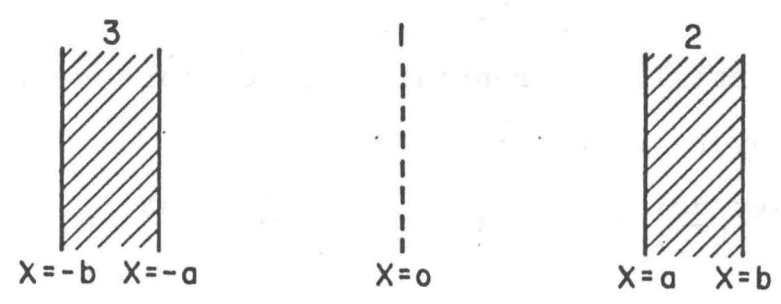
HEAT FLOW GEOMETRY

Fig. D.1.   Three-slab heat flow geometry.

Boundary conditions

$$\Psi(b,t) = 0, \quad \eta(-b,t) = 0$$

Jump conditions

$$\varphi(a,t) = \Psi(a,t) \quad \varphi(-a,t) = \eta(-a,t)$$

$$\lambda\varphi_x(a,t) = \Lambda\,\Psi_x(a,t) \quad \lambda\varphi_x(-a,t) = \Lambda\eta_x(-a,t).$$

$(\lambda, \Lambda$ are thermal conductivities.$)$

Define the Laplace transform of φ by

$$\Phi(s,x) = \int_0^\infty \varphi(x,t)\, e^{-st}\, \partial t$$

Multiply the partial differential equation for φ by e^{-st} and integrate over all time:

$$\int_0^\infty e^{-st}\left(\frac{\partial\varphi}{\partial t}\right)_x \partial t = k \int_0^\infty \left(\frac{\partial^2\varphi}{\partial x^2}\right)_t e^{-st}\, dt$$

Integration by parts gives $-\varphi(x,o) + s\Phi = k\dfrac{d^2\Phi}{dx^2}$.

We now have an ordinary differential equation for Φ ,

$\left(\dfrac{d^2}{dx^2} - \dfrac{s}{k}\right)\Phi = -\dfrac{T_1}{k}$. Similar results are obtained for the other regions. The solutions to the differential equations for the Laplace transforms can be expressed:

Region 1, $\quad \Phi(s,x) = A\cosh(\mu x) + B\sinh(\mu x) + \dfrac{T_1}{s}$, $\mu \equiv \left(\dfrac{s}{k}\right)^{1/2}$

Region 2, $\quad \mp(s,x) = C\cosh(\mu px) + D\sinh(\mu px) + \dfrac{T_2}{s}$, $p \equiv \left(\dfrac{k}{\varkappa}\right)^{1/2}$

Region 3, $\quad H = E\cosh(\mu px) + F\sinh(\mu px) + \dfrac{T_2}{s}$.

After some effort, the coefficients can be found by applying the several conditions of the problem. Then the inversion

integral,

$$\varphi(x,t) = \frac{1}{2\pi i} \int_{\gamma-i\infty}^{\gamma+i\infty} \Phi(x,s) \, e^{st} \, ds$$

in the complex s-plane can be used to complete the solution.
The integral is evaluated by the method of residues. There is
a first-order pole at the origin; other poles are the solution
of the transcendental equation

$$\sigma \cos(\ell z_n) \cos(z_n) - \sin(\ell z_n) \sin(z_n) = 0$$

($\sigma \equiv \frac{\Lambda}{\lambda} p$, $\ell \equiv p(\frac{b}{a} - 1)$, $z_n \equiv ia\mu$). There are an infinite number
of roots to this equation. For each positive root there is an
equal and opposite negative root, however the physical solution
corresponds to just positive roots. The result is

$$\varphi(x,t) = 2\sigma \sum_{n=1}^{\infty} \frac{1}{z_n} \frac{[(T_1-T_2)\cos(\ell z_n)+T_2] \cos(z_n \frac{x}{a}) \exp\left(- \frac{kz_n^2 t}{a^2}\right)}{(\lambda+\sigma)\sin(z_n)\cos(\ell z_n)+(1+\lambda\sigma)\sin(\ell z_n)\cos(z_n)}$$

which can be rearranged to

$$\varphi(x,t) =$$

$$2 \sum_{n=1}^{\infty} \frac{1}{z_n} \frac{\sin(z_n)\sin(\ell z_n)[(T_1-T_2)\cos(\ell z_n)+T_2]\cos(z_n \frac{x}{a})\exp\left(- \frac{kz_n^2 t}{a^2}\right)}{\sin(\ell z_n)\cos(\ell z_n) + \ell \sin(z_n) \cos(z_n)}$$

using the eigenvalue equation. The transcendental equation
for eigenvalues was solved numerically using the Newton-
Raphson method (Booth, 1957). Results were checked graphically
to be sure no eigenvalues were missed. For typical computations,

50 terms in the series were computed; convergence of the
series is slower for earlier times than later times.

APPENDIX E

LIST OF SYMBOLS

APPENDIX E

LIST OF SYMBOLS

A parameter in temperature coefficient of resistance

A_1, A_2, A_F Fermi surface cross-sectional areas

b Burgers vector, coefficient in equation of state (Sec. III.B)

B $\left(\dfrac{d \ln A}{d \ln V}\right)_{V=V_o}$

C_V constant volume heat capacity per gram

c_S, c_L shear and longitudinal sound speeds

$^\circ C$ Centigrade temperature

D Debye function, diffusion coefficient (Sec. IV.I)

E voltage, internal energy per gram (Sec. III.B)

E_F electron Fermi energy

E_H internal energy per gram on Hugoniot path

E_o internal energy per gram in initial state

E_p potential internal energy per gram

E_T thermal part of internal energy per gram

e electron charge

e_K strain deviator

F Helmholtz energy

F_k intensive parameter in entropy representation

f frequency

G γ/V

H	work-hardening coefficient
H'	coefficient in Saada's relation
HEL	Hugoniot elastic limit
h	number in Gruneisen-Borelius relation
$\hbar$	Planck's constant
I	electrical current, an integral (Sec. III.B)
J	integral in Bloch resistivity theory
K	several constants
$^\circ$K	absolute temperature
K_T	isothermal compressibility
k	electron wave number, material diffusivity (Sec. IV.J)
k_B	Boltzmann's constant
k_F	electron wave number at the Fermi surface
ℓ	electron mean free path, parameter in heat flow calculation (Appendix D)
MRC	Materials Research Corporation
M	gram molecular weight
m	electron mass
N	quantity of defects
n	conduction electron density
P	pressure
P_p	potential pressure
P_x	negative of longitudinal stress
$\overline{P}$	mean pressure
p	parameter in heat flow calculation
p_F	electron momentum at Fermi surface
R	resistance, gas constant (Sec. III.B)

r	$(\sigma_I/\sigma_F - 1)$
S	entropy, Fermi surface area (Sec. III.A.2)
s	stress relaxation time
s_j	stress deviator
T	temperature
t	time
U_s	shock-wave speed
u	particle speed, temperature in heat flow equation (Sec. IV.J).
V	volume per gram, potential energy (Sec. III.A.1)
v	vacancies
W_P	work of pore collapse
W_{PD}	work of plastic deformation
W3N	Wilkinson three nine
X	V/V_o
X_k	extensive parameter in entropy representation
x	position coordinate
Y	quasi-static yield stress in tension
z_n	eigenvalues of heat flow problem
α	temperature coefficient of resistivity
α'	volume coefficient of thermal expansion
β	$\rho(V,T) - \alpha(V)T$
β_T	isothermal bulk modulus
γ	Gruneisen parameter
Δ	finite change in following parameter
δ	parameter in equation of state
ϵ	strain

H	Laplace transform of η
η	regional temperature in heat flow problem
θ	characteristic temperatures
$\theta_E, \theta_R, \theta_D$	characteristic temperatures of Einstein, resistivity, and Debye, respectively
$\varkappa$	material diffusivity
Λ	dislocation density, thermal conductivity (Appendix D)
λ	thermal conductivity
μ	shear modulus or Lame constant, parameter in heat flow calculation (Appendix D)
ν	Poisson's ratio
ρ	electrical resistivity
$\Delta\rho_D$	resistivity difference or deviation between shock and hydrostatic results
ρ_i	impurity resistivity
ρ_L	perfect lattice resistivity
ρ_o	$\rho(V_o, T_o)$
ρ_T	thermal resistivity
ρ_v	resistivity per vacancy
$\rho(HF)$	resistivity change due to heat flow
σ	stress, conductivity (Sec. IV.G)
σ_x	longitudinal stress (in shock direction)
σ_y	lateral stress
τ	maximum shear stress, relaxation time (Sec. IV.G)
φ	regional temperature
Φ	Laplace transform of φ
χ_{pd}	point defect concentration
χ_v	vacancy concentration

Ψ   regional temperature

Ψ̄   Laplace transform of Ψ

Ω   ohm

ω   angular frequency